OPTICAL ROGUE WAVES AND NONLINEAR EFFECTS IN HOLLOW-CORE PHOTONIC CRYSTAL FIBERS

by

Yashar Esfahani Monfared

Submitted in partial fulfillment of the requirements
for the degree of Doctor of Philosophy

at

Dalhousie University
Halifax, Nova Scotia
April 2018

This thesis is dedicated to my wife, Raha, who has always been a constant source of support and encouragement during the challenges of my whole academic life. This thesis is also dedicated to my parents who have always loved me unconditionally and have taught me to work hard for the things that I aspire to achieve.

Table of Contents

List of Tables

List of Figures

Abstract

In this dissertation, we theoretically study nonlinear optical effects inside hollow core photonic crystal fibers (HCPCFs). In particular, we explore the formation of optical rogue waves near resonance in stimulated Raman scattering inside HCPCF. We further examine the role of coherence time, coherent memory and source noise in the formation of a long-tailed probability density function (PDF) as a signature of ORWs. We also investigate the design of highly nonlinear liquid-filled PCFs for different nonlinear applications. The research performed throughout this thesis leads to the following results.

1. In the case of noisy Stokes pulses, we show that the degree to which the PDF deviates from Gaussian, sharply increases as the source coherence time decreases. Our results establish a clear link between optical coherence and rogue wave theories.

2. In the case of noisy pump pulses, we demonstrate that Stokes power PDF tail increases as the system coherent memory is enhanced. We show that the maximum attainable power level strongly depends on the pump noise level. We develop the analytical theory of noise transfer in the system in the initial stage of SRS within the undepleted pump approximation.

3. We demonstrate that RWs can be excited in a self-similar asymptotic regime of integrable turbulence and they appear as giant fluctuations away from the average (self-similar) evolution of the system.

4. We design a highly nonlinear liquid-filled PCF with a nonlinear coefficient of 7700 $W^{-1}km^{-1}$ and a total loss lower than 0.3 dB/m. Using the proposed PCF, we theoretically show the possibility of slowing down the group velocity of light to $c/50$ with a required power of only 25 mW via stimulated Brillouin scattering.

5. We design a carbon-disulfide-filled PCF with nearly-zero dispersion of 0.00007 ps/(nm km) and a dispersion slope of 0.0000018 near 1550 nm. We demonstrate theoretically widely tunable wavelength conversion based on four-wave mixing using the proposed PCF. A 3-dB tunable wavelength conversion bandwidth is about 108 nm and the conversion efficiency is about -10.6 dB.

List of Abbreviations and Symbols Used

A_{eff}	Effective area
Di	Dispersion parameter
$E_{p,s}$	Pump and Stokes amplitudes
G_{th}	Exponential Brillouin gain threshold of fiber
$H_n(x)$	Hermite polynomial of order n
L_{eff}	Effective fiber length
P_{pump}	Pump power
P_{th}	Threshold pump power
T_c	Coherence time
Γ^{-1}	Coherence memory of the system
Ω_B	Brillouin frequency
α	Loss coefficient of fiber
β_1	Inverse group velocity
β_2	Group velocity dispersion
γ	SRS medium relaxation rate
γ^{-1}	Relaxation time
γ_{NL}	Nonlinear coefficient
ω_p	Pump pulse frequency
ω_s	Stokes frequency
c_n	Complex Gaussian random variable
l_{SRS}	Raman characteristic length
n_2	Nonlinear refractive index
$n_{p,s}$	Refractive indices of pump and Stokes pulses
r_{eff}	Raman transition dipole matrix element
t_{SRS}	Raman characteristic time
$t_{p,s}$	Pump and Stokes pulse durations
FWM	Four-wave mixing

GSM	Gaussian Schell model
GVD	Group velocity dispersion
HC-PCF	Hollow-core photonic crystal fiber
MI	Modulation instability
NA	Numerical aperture
NLSE	Nonlinear Schrodinger equation
ORW	Optical Rogue Wave
PDF	Probability density function
RW	Rogue wave
SBS	Stimulated Brillouin scattering
SRS	Stimulated Raman scattering
TIR	Total internal reflection
TLA	Two level amplification
UPA	Undepleted pump approximation

Acknowledgements

I would like to express my deepest appreciation to my supervisor Dr. Sergey Ponomarenko for his excellent scientific guidance, continuous support and motivation during my Ph.D program. I would also like to thank my committee members, Dr. Zhizhang (David) Chen and Dr. William Phillips for their support and recommendations

Chapter 1

Introduction

1.1 Preface

In this thesis, we focus on rogue waves and nonlinear effects inside hollow-core photonic crystal fibers. This chapter starts with an introduction to the general theme of our thesis. Thesis objectives, contributions, and organization are then presented.

1.2 Thesis theme

The development of laser technology, initiated by the invention of ruby lasers in the late 1950s [1], has paved the way for the generation of short and high intensity pulses at optical frequencies. The generation of high intensity laser pulses opened new prospects in different fields in optics and, especially, in the field of nonlinear optics [2, 3]. The generation of such pulses sparked ever growing interest in studying resonant light-matter and light-light interactions. Resonance occurs when a pulse carrier frequency coincides with a particular optical transition frequency of the medium. The importance of near resonance optical studies arises from the fact that there are many significant optical phenomena that occur only near optical resonance [4]. Such near resonant phenomena include enhanced absorption, amplification and self-induced transparency effects.

In the first few chapters of this thesis, our research focuses on resonant and near resonant regimes of pulse propagation in the medium with random input fields. Stimulated Raman scattering (SRS) is used to describe the characteristics of light-matter interactions inside a hollow-core photonic crystal fiber (HCPCF). HCPCFs has two

major benefits for realizing near-resonance pulses in SRS: first, it increases the interaction length between the laser and the medium significantly. Second, it isolates the fundamental Raman mode from higher-order ones by suppressing the latter with an appropriate fiber design. [5]. One of the interesting near resonance phenomena is formation of unusually large amplitude statistical waves with a non-Gaussian probability distribution [6, 7]. These giant waves are called optical rogue waves (ORWs) and they have attracted a lot of attention in academia in the recent years [6-8]. Even though the ORWs in various media have been explored, no study has yet, to the best of our knowledge, investigated the ORW formation near optical resonances. Therefore, explorations into the near resonance behaviour of extreme waves are of great importance.

Furtheremore, light guidance through liquids in HCPCFs rather than glass in conventional fibers, can result in dramatic increase in the nonlinear coefficient of a fiber which opens new prospects in various fields, especially in low threshold nonlinear optics. In the second part to this thesis we investigate design of highly nonlinear liquid-filled PCFs for various applications including slow light generation and wavelength conversion based on different nonlinear processes inside the fiber.

1.3 Thesis objectives

Our overarching goal throughout this thesis is to explore nonlinear processes such as stimulated Raman scattering (SRS), stimulated Brillouin scattering (SBS)and four-wave mixing (FWM) inside hollow-core photonic crystal fibers (HCPCF). We have also studied statistical properties of optical rogue waves (ORWs) in SRS in the vicinity of an optical resonance. More specifically, the objectives of this study are summarized as follows:

1. We aim to numerically explore the possibility of having extreme events in the vicinity of optical resonance in SRS with noisy Stokes pulses.

2. We intend to examine ORW formation near optical resonance in SRS with noisy pump pulses.

3. We propose to explore the extreme wave excitation dynamics in a self-similar regime of SRS in HCPCF, employing different source noise models.

4. We plan to explore the possibility of design of a highly nonlinear liquid-filled HCPCFs as a medium for slow light generation based on SBS.

5. Our aim is to study wavelength conversion based on FWM in a dispersion-flattened highly nonlinear liquid-filled HCPCF.

1.4 Thesis contributions

This thesis explores ORW formation in SRS and also nonlinear processes such as SBS and FWM inside a hollow-core photonic crystal fiber. Gaussian-Schell model pulses are employed as a generic model to simulate realistic partially coherent pulses in the study of ORWs.

The research performed throughout this thesis is divided into into five interrelated projects which are published (or submitted) as journal papers [9-14]. Contributions to each research project are summarized as follows:

1. We explored ORW formation in SRS inside HCPCF in the case of the noisy Stokes pulses. We showed that the degree to which the probability density function (PDF) deviates from Gaussian, sharply increases as the source coherence time decreases. This tail dependence on source coherence time can be explained by the concept of statistical granularity in time. As coherence time decreases, the number of uncorrelated modes (statistical granules) increases. These uncorrelated modes all compete for energy supply from the pump, resulting in a selective amplification and leading to a giant amplitude granule formation within the Stokes pulse profile during the SRS amplification process. The results of this project are already published as a journal paper [9].

2. We studied the formation of ORWs in near-resonance SRS with noisy pump pulses. We showed the Stokes power PDF tail becomes longer as the system coherent memory enhanced. This is because the enhanced coherent memory implies efficient noise

transfer from the pump to the Stokes pulses. We further showed that the maximum attainable power level strongly depends on the pump noise level. The results of this project are already published as a journal paper [10].

3. Using various source noise models, we investigated the formation of ORWs in a self-similar regime of SRS. We demonstrated that RWs can be excited in the asymptotic self-similar regime of integrable turbulence. We further showed that the RW appearance is independent of a particular source model, thereby representing a universal signature of the self-similar regime of integrable turbulence. The results of this project are submitted for publication as a journal paper [11].

4. We studied liquid-filled PCFs and their nonlinear characteristics. We designed a highly nonlinear carbon-disulfide-filled PCF with nonlinear coefficient of more than 7700 $W^{-1}km^{-1}$ and a moderate loss. Using the proposed PCF, we show the possibility of slowing down the light to $c/50$ via the SBS process. The results of this project are already published as a journal paper [12].

5. We investigated the possible dispersion engineering methods in a CS_2-PCF. We obtained an ultra-flattened nearly-zero dispersion fiber near 1550 nm with a high nonlinear coefficient. Using the proposed fiber, we demonstrated the possibility of a broadband wavelength conversion based on FWM with a conversion bandwidth of 108 nm and a maximum conversion efficiency of -10 dB. The results of this project are submitted for publication as a journal paper [12].

1.5 Thesis organization

This dissertation is in a paper-based format and is composed of a brief introduction to the physical concepts of the theories used throughout the thesis along with the results of our research as published or submitted journal papers.

Chapter 1 presents the introduction to a general theme of this research, along with the objectives and contributions. The remainder of this thesis is organized as follows.

Chapter 2 briefly reviews the hollow-core photonic crystal fibers and the theory behind nonlinear processes such as SRS, SBS and FWM. The basic concepts of SRS and SBS,

and some parameters like Raman threshold and Brillouin threshold are also presented in this chapter.

Chapter 3 discusses some background theories on the physics of RWs. In this chapter, the importance of the study of ORWs near resonance is stressed.

In Chapter 4, ORW formation in SRS when the noise exists in the Stokes pulses is explored. The role of coherence time and source noise in the formation of a long-tailed probability distribution function as a signature of ORW is investigated.

Chapter 5 studies the formation of ORWs in SRS with noisy pump pulses. We explore the role of coherence memory and source noise in this process and also present the differences between this case and the noisy Stokes case.

In chapter 6 the formation of ORWs in the self-similar regime of SRS is investigated using various noise models in the source is investigated. Our results hold irrespective of a specific source correlation model, suggesting the universality of the proposed scenario.

Chapter 7 presents liquid-filled PCFs and their nonlinear characteristics. We design a highly nonlinear carbon-disulfide-filled PCF with the nonlinear coefficient of more than 7700 $W^{-1}km^{-1}$ and moderate losses. Using the proposed PCF, we show the possibility of slowing the group velocity of light down to the $c/50$ via the SBS process.

Chapter 8 shows possible dispersion engineering methods in a CS_2-PCF. We obtain an ultra-flattened nearly-zero dispersion fiber near 1550 nm with a large nonlinear coefficient. Using the proposed fiber, we show the possibility of a broadband wavelength conversion based on FWM with a conversion bandwidth of 108 nm and a maximum conversion efficiency of -10 dB.

Chapter 9 provides a brief summary of the main results of this thesis along with suggestions for future work.

Bibliography

[1] F. P. Schfer, F. P. W. Schmidt, and J. Volze, Organic dye solution laser, Appl. Phys. Lett. 9, 306309 (1966).

[2] M. Born and E. Wolf, Principles of Optics, 7th ed. (Cambridge University Press,1999).

[3] M. E. Fermann, A. Galvanauskas, and G. Sucha, Ultrafast Lasers. Technology and Applications, (Marcel Dekker, New York, 2003).

[4] L. Allen and J. H. Eberly, Optical Resonance and Two-level Atoms, (Dover Publications Inc., New York, 1975).

[5] A. Nazarkin, A. Abdolvand, A.V. Chugreev, and P. St.J. Russell, Direct Observation of Self-Similarity in Evolution of Transient Stimulated Raman Scattering in Gas-Filled Photonic Crystal Fibers, Phys. Rev. Lett. 105, 173902 (2010).

[6] P. Walczak, S. Randoux, and P. Surret, Optical Rogue Waves in Integrable Turbulence, Phys. Rev. Lett. 114, 143903 (2015).

[7] J. M.Dudley, F. Dias, M. Erkintalo and G. Genty, Instabilities, breathers, and rogue waves in optics, Nature Photon. 8, 755764 (2014).

[8] D. R. Solli, C. Ropers, P. Koonath and B. Jalali, Optical rogue waves, Nature (London) 450, 10541057 (2007).

[9] Yashar E. Monfared and Sergey A. Ponomarenko, Non-Gaussian statics and optical rogue waves in stimulated Raman scattering , Opt. Express 25, 5941-5950O, (2017).

[10] Yashar E. Monfared and Sergey A. Ponomarenko, Non-Gaussian statistics of extreme events in stimulated Raman scattering: The role of coherent memory and source noise, Phys. Rev. A, 96, 043817, (2017).

[11] Yashar E. Monfared and Sergey A. Ponomarenko, Rogue Waves, Self-similarity, Integrable Turbulence, Submitted to Phys. Rev. Lett., (2018).

[12] Yashar E. Monfared and Sergey A. Ponomarenko, Slow light generation in liquid-filled photonic crystal fibers via stimulated Brillouin scattering, Optik - Int. J. Light Electron Opt., 127 (15), pp. 5800-5805, (2016).

[13] Yashar E. Monfared and Sergey A. Ponomarenko, Design of a dispersion-flattened highly nonlinear carbon-disulfide-filled photonic crystal fiber for broadband wavelength conversion based on four-wave mixing, Submitted to Optik - Int. J. Light Electron Opt., (2018).

Chapter 2

Hollow-core photonic crystal fibers

2.1 Hollow-core photonic crystal fibers

Since the major breakthroughs in the 1970s [1, 2], optical fibers have evolved into many forms over time. Conventional fibers have been used for different important applications such as fiber-optic telecommunications [3], fiber-optic sensors [4, 5], optical imaging [6, 7] and fiber-based lasers [8]. Conventional optical fibers consist of a solid core with the refractive index n_1 surrounded by a cladding of slightly lower refractive index $n_2 < n_1$ [9]. Light can be completely confined inside the fibre core if the incidence angle (on the boundary) is smaller than the critical angle for total internal reflection $\theta < \theta_{cr} = arcsin(n_2/n_1)$. This mechanism of light confinement in the core of conventional optical fibers is called total internal reflection (TIR) [9] which is illustrated in the Fig. 2.1.

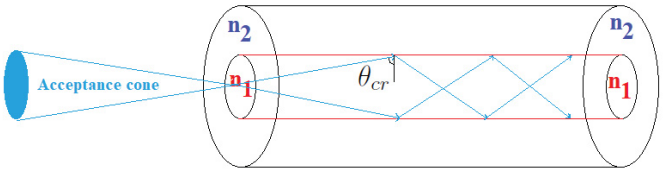

Figure 2.1: Guiding the light through TIR in a conventional optical fiber.

However, conventional optical fibres have some limitations for specific applications because the fiber geometry and refractive index deviation of the core and cladding are restricted and we cannot use a low index material in the core. Furthermore, silica glass does not exhibit a high nonlinearity [10] and therefore there is little incentive for considering silica fibers for nonlinear applications.

Photonic crystal fibers (PCFs) is another class of optical fibers [11]. PCFs consist

of a core which is surrounded by a periodic array of air holes (cladding) [11]. In recent years, PCFs have attracted much attention of the scientists and engineers due to numerous unique features such as ultra flattened dispersion, endlessly single mode operation, low propagation loss, high nonlinearity and small effective mode area [12-14]. There are two main classes of PCFs: solid-core PCFs and hollow-core PCFs. In solid-core PCFs the guiding mechanism is based on TIR similar to conventional optical fibers whereas in hollow-core PCFs (HCPCFs) the guiding mechanism strongly depends on the core material. If we fill the core of the HCPCF with a high index material such as a high index liquid, the guiding mechanism is still TIR. However if we fill the core with a low index material such as gas, the guiding mechanism cannot be TIR as the core has a lower refractive index than the cladding. The light guidance is possible via photonic bandgap with extremely low loss over a narrow bandwidth [15]. The photonic bandgap can be described as a situation where a given photonic structure exhibits forbidden frequencies for optical waves (stop bands) [15]. The photonic bandgaps in HCPCFs are formed by the periodic lattice of air holes running along the entire length of fiber. The cross section of a solid-core PCF and a hollow-core PCF is illustrated in Fig. 2.2.

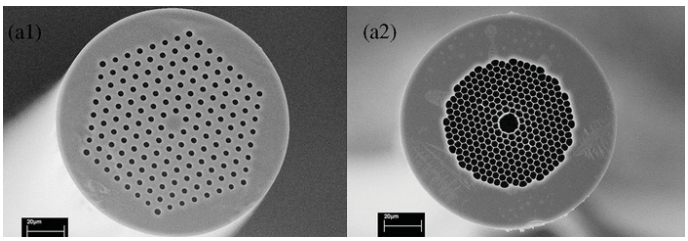

Figure 2.2: Cross section of a solid core PCF (left) and a hollow-core PCF (right), reprinted, with permission, from ref. 42, IEEE 2007.

In HCPCFs the light propagates in a diffractionless fashion, in contrast to the intrinsic diffractive nature of free space laser beams [15]. Therefore light guidance through liquids or gasses in HCPCFs can result in dramatic increase in the effective interaction length which opens new prospects in various fields, especially in low threshold nonlinear optics [15, 16]. The schematic cross-section of a regular hexagonal lattice hollow-core PCF is shown in Fig. 2.3.

One of the most important characteristics of a fiber is its nonlinear coefficient which

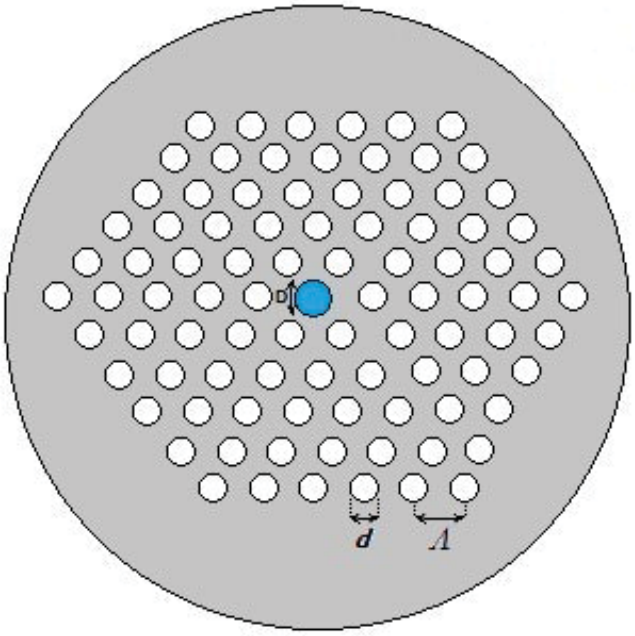

Figure 2.3: Cross section of a regular hexagonal lattice hollow-core PCF.

contains information about both mode confinement (effective mode area) and the nonlinear refractive index of the fiber material. The nonlinear coefficient γ_{NL} is defined as [17]

$$\gamma_{NL} = \frac{2\pi n_2}{\lambda A_{eff}}, \tag{2.1}$$

where n_2 is a nonlinear refractive index, λ is the wavelength and A_{eff} is an effective area of the fundamental fiber mode, defined as [18, 19]

$$A_{eff} = \frac{\int\int(|\mathbf{E}|^2 dA)^2}{\int\int(|\mathbf{E}|^4 dA)}. \tag{2.2}$$

where $\mathbf{E}$ is transverse electric field vector and A is the fiber cross section. Due to the high refractive index contrast between silica and air, the PCFs offer a much tighter mode confinement over a wide range of wavelengths and thereby a lower effective mode area than do conventional optical fibers. Another important characteristic of a fiber is the fiber group velocity dispersion (GVD). In some nonlinear processes such as four-wave mixing (FWM), fiber GVD will determine the efficiency of the process through a phase matching condition. The GVD parameter of a fiber is usually calculated in

terms of the dispersion parameter Di, defined as [20]

$$Di = -\frac{\lambda}{c}\frac{d^2 n_{eff}}{d\lambda^2}. \tag{2.3}$$

where c is the velocity of light in free space and n_{eff} is the effective index of the propagating mode. The dispersion parameter Di and GVD parameter β_2 are related to each other as

$$Di = -\frac{2\pi c}{\lambda^2}\beta_2. \tag{2.4}$$

The total dispersion is calculated as the sum of waveguide and material dispersion [20, 21]. In our calculations, the material dispersion has been taken into account.

2.2 Stimulated Raman scattering in HCPCFs

Raman scattering was first observed in 1928. It is named after the Indian physicist Chandrasekhara Raman, who discovered this phenomenon in the laboratory [22]. Raman discovered the existence of a frequency-shifted wave during the investigations of light scattering in different media. The vibrational oscillations that occur within the molecules of the material determine the frequency shift of the scattered light [22]. Spontaneous Raman scattering is a result of the weak molecular resonance excitation due to the presence of an input field (pump wave). As the pump wave intensity increases, the scattering process eventually becomes stimulated. In the stimulated regime, the resonances will be further excited due to a coherent interaction of the scattered field with the pump field, which dramatically enhances the transfer of power between the two waves [22]. The process of Raman scattering is schematically depicted in Fig. 2.4. According to Fig. 2.4 and considering the quantum mechanical picture, the stimulated Raman scattering (SRS) process can be viewed as absorption of a photon from the pump pulse at frequency ω_p and the emission of a photon at Stokes frequency ω_s. The difference in energy is taken up by molecular vibrations at frequency Ω. Thus, SRS provides energy gain at the Stokes frequency at the expense of the pump.

Through the Raman scattering process, both downshifted (Stokes) and upshifted

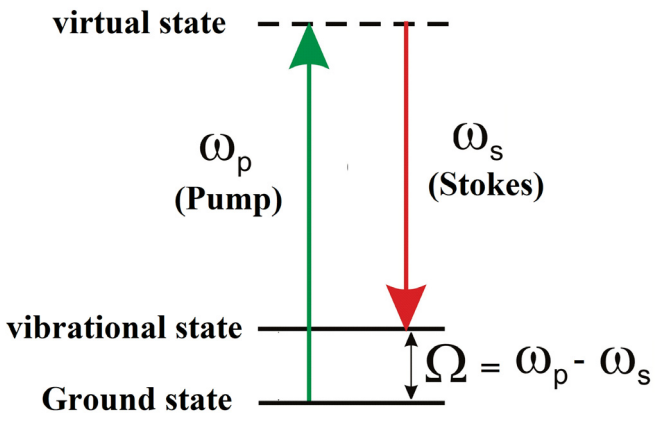

Figure 2.4: Illustrating SRS process using a photon picture.

(anti-Stokes) waves can be generated. However, in the optical fibers, the Stokes radiation is generally much stronger than the anti-Stokes radiation [22]. SRS has two feasible regimes: the co-propagating regime where the pump and Stokes pulses propagate in the same direction and counter-propagating regime in which the pump pulse propagates in the direction opposite to the Stokes pulse. We usually try to maximize the pulse profile overlap in order to increase the Raman interaction efficiency. In the co-propagating regime, this can be achieved with nearly identical temporal profiles of the pump and Stokes pulses. In the counter-propagating regime, we usually use a long pump pulse in order to enable the short Stokes pulse to extract as much energy from it as possible. The two SRS propagation regimes are shown in Fig. 2.5. Note that in this thesis, we use the co-propagating regime for SRS excitation.

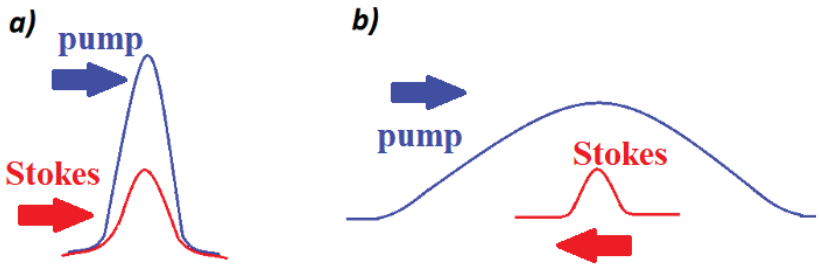

Figure 2.5: Two different SRS excitation regimes : a) co-propagating regime and b) counter-propagating regime.

SRS has some remarkable characteristics: high conversion efficiency to scattered frequency, explicit excitation threshold and quite narrow linewidth compared with the

spontaneous regime [22]. These characteristics make SRS an excellent tool with a wide range of applications in the areas such as high-resolution spectroscopy, optical communications, frequency shifting applications, pulse compression and comb frequency generation [23-25]. HCPCFs can enhance the interaction length significantly and they can suppress higher order Raman modes in specific applications due to the fiber stop bands. Compared to free-space systems, gas-filled HCPCFs provide huge advantages for SRS applications, including pressure-controllable and structure-controllable dispersion and low SRS thresholds [16, 27]. One important parameter in SRS is Raman threshold [36]. The threshold for stimulated Raman scattering is defined as the input pump power at which the output power for the pump and Stokes waves become equal. The SRS threshold formula for a fiber is usually given by [22, 26]

$$P_{th} = \frac{16A_{eff}}{g_R L_{eff}} \tag{2.5}$$

where A_{eff} is an effective mode area of the fiber, g_R is a Raman gain coefficient, $L_{eff} = (1 - exp(-\alpha_p L))/\alpha_p$ is an effective length of the fiber and α_p is a propagation loss rate. Since Raman threshold is dependent on the fiber characteristics, several improved fiber designs have been recently proposed [27, 29]. Many of these designs are based either on modifying certain guiding properties of the fiber or on scaling up the core area. HCPCFs can reduce Raman threshold significantly where conventional techniques require high power lasers (1 MW) to reach Raman threshold. The unique characteristics of gas-filled HCPCFs have opened new opportunities in the field of gas nonlinear optics [30]. The reduction in threshold power for SRS in gases should allow the use of low-power lasers as pumps and should extend the wavelengths of sources into new spectral regions [30]. The ability to load HCPCFs at high pressure without damage could also be of great importance for SRS in the transient regime (that is, when the pulse duration is much shorter than the dephasing time), where Raman gain is proportional to gas pressure [30].

2.3 Stimulated Brillouin scattering in HCPCFs

Brillouin scattering is an interaction of light and sound waves within a medium [22]. The scattered part of the optical field remains weak for the low input intensities. However, the process becomes powerful and stimulated as we increase the input intensities which is possible with powerful lasers [22]. Stimulated Brillouin scattering (SBS) is similar to SRS in that a Stokes wave is also generated in this case. However, instead of internal material resonances, an acoustic wave causes the interaction between the pump and Stokes waves in the SBS process [22]. The acoustic wave will be generated if the frequency and linear momentum matching conditions are satisfied, $\Omega_B = \Omega_p$ - Ω_s, where Ω_B is the Brillouin frequency, Ω_p is a pump frequency and Ω_s is a probe frequency. We can describe the SBS process using the classical picture where the pump wave creates a pressure wave in the medium through electrostriction [22]. A material density wave propagates at the velocity of sound in the medium. Thus, a moving refractive index grating appears due to the periodic changes in material density. The input pump generates the acoustic wave that scatters the pump, and the scattering creates a Stokes wave [22]. The Stokes wave is shifted to a lower frequency because of the Doppler shift and a large portion of the pump power will be converted into the Stokes wave (travels in the backward direction). The process of SBS is schematically shown in Fig. 2.6.

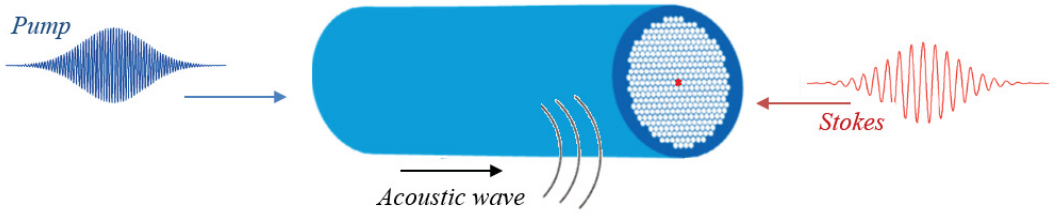

Figure 2.6: SBS process which includes counterpropagating pump and Stokes pulses and a generated acoustic wave.

The Brillouin gain bandwidth is usually very small (about 30 MHz) in optical fibers [22, 31]. Thus, we can view SBS as a narrowband amplification process in which a strong pump wave produces a narrowband gain region in a spectral region around $\Omega_p - \Omega_B$ and a loss region around $\Omega_p + \Omega_B$ [31]. The process of forming gain and loss regions via SBS is schematically shown in Fig. 2.7.

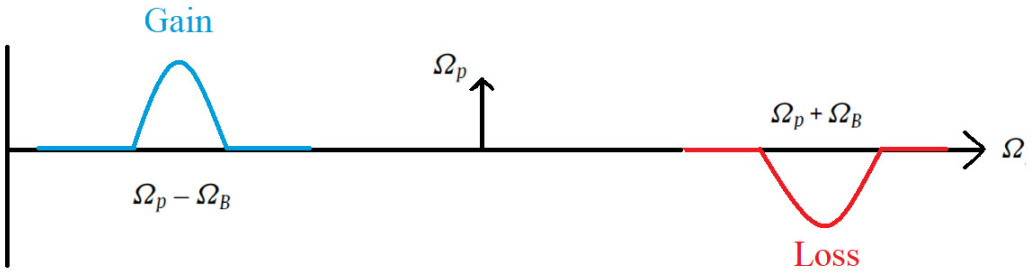

Figure 2.7: Spectral manifestation of SBS: a narrow band gain and a narrow band loss.

SBS and SRS have five major differences. First, SBS only occurs when the pump and Stokes counterpropagate inside the fiber. Second, a Stokes frequency shift for SBS is smaller by three orders of magnitude compared to that of SRS. Third, the Stokes component generation mechanism of SBS is totally different from that of SRS. Fourth, the Brillouin gain spectrum is extremely narrow. Finally, the peak of the Brillouin gain coefficient is over 100 times greater than the Raman gain peak [22], which makes SBS the dominant nonlinear process in solid core optical fibers. One of the important parameters when we deal with Brillouin scattering is the Brillouin threshold. We may estimate the pump power Brillouin threshold as [22]

$$P_{th} = \frac{G_{th} K_B A_{eff}}{g_B L_{eff}}, \tag{2.6}$$

where G_{th} is an exponential gain threshold of the fiber which depends on the experimental parameters such as input pulse, material, length and numerical aperture (NA) of the fiber; K_B is a constant depending on the polarization property of the fiber which is equal to 1 if the fiber is polarization maintaining and 1.5 otherwise, A_{eff} is the effective fiber area and L_{eff} is the effective fiber length, $L_{eff} = 1 - e^{\alpha L}/\alpha$, where L is a physical length of the fiber and α is a loss coefficient of the fiber.

As the Brillouin gain of high-index liquids is large and we can control the effective area of the fiber, SBS process in liquid-filled HCPCFs can be efficient and useful for a number of applications including optical amplification, optical phase conjugation, temperature and strain sensing, slow and fast light generation, optical storage and many others [32-36].

2.4 Four-wave mixing in HCPCFs

Four-wave mixing (FWM) is a parametric process in which waves interact with each other due to the third-order nonlinearity of a material [22]. FWM can occur if at least two frequency components propagate together in a nonlinear medium such as a PCF. The occurrence of the FWM phenomenon in optical fibers was observed for the first time by Stolen et al. [37] using a 9 cm long multimode fiber pumped by a double-pulsed YAG laser at 532 nm. When three frequencies ω_i, ω_j and ω_k interact in a nonlinear medium, they give rise to a fourth wavelength ω_{ijk} which is formed by the scattering of the incident photons, producing the fourth photon. The nonlinear medium will produce $\pm\omega_i \pm \omega_j \pm \omega_k$ frequency components, one of these components is given by $\omega_{ijk} = \omega_i + \omega_j - \omega_k$ as we illustrate in the Fig. 2.8. FWM is a phase-sensitive process and the interaction depends on the relative phases of all waves [22]. Thus if the frequencies involved are close to each other, or if the dispersion profile has a suitable shape, FWM can be efficient in the fiber [40]. On the other hand, FWM is effectively suppressed if there is a strong phase mismatch. FWM is also present if

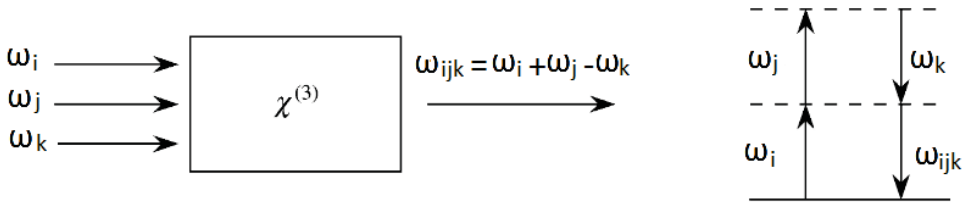

Figure 2.8: Possible mixing processes which can occur when three input waves interact in a nonlinear medium.

only two frequency components interact. Therefore, FWM can cause the generation of new frequency components as we show in the Fig. 2.9. Suppose we have a pump wave at frequency ω_p and a signal at frequency ω_s. If we mix these waves and transmit them together along a highly nonlinear HCPCF, we will obtain two new frequency components $\omega_{converted} = 2\omega_p - \omega_s$ and $\omega_{idler} = 2\omega_s - \omega_p$ if a phase-matching condition is satisfied [38]. As stated above, the efficiency of this phenomenon strongly depends on the phase matching condition as well as fiber dispersion and even dispersion slope [39, 40]. Finite phase mismatch in the degenerate case of FWM when we only have a strong

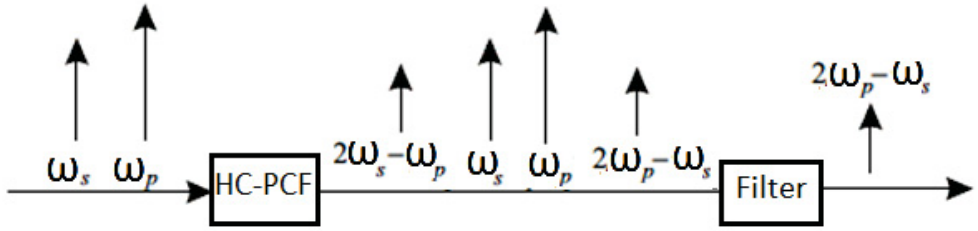

Figure 2.9: Generation of new frequency components in HCPCF via FWM.

pump, a signal and an idler can be calculated from [40] $\Delta k = \beta_s + \beta_i - 2\beta_p$, where β_i, β_p and β_s are idler, pump and signal wave vectors. Δk is usually approximated by a Taylor expansion around the pump frequency as $\Delta k = \beta_2 \Omega^2$, where β_2 is the GVD parameter at the pump wavelength and Ω is the optical frequency shift between signal and pump waves [41]. When β_2 is small, we must take into account the fourth-order term in the expansion of Δk since the odd-order terms (such as β_3) exactly cancel out due to the opposite signs of the frequency detuning of the signal from the pump and that of the idler from the pump [42]. Thus the finite phase mismatch parameter becomes [22, 42]

$$\Delta k = \beta_2 \Omega^2 + (\beta_4/12)\Omega^4 \tag{2.7}$$

where β_4 is the fourth order dispersion defined as $\beta_4 = d^4\beta/d\omega^4$. As we can shorten the fiber and control the dispersion slope and nonlinearity in liquid-filled HCPCFs, FWM in HCPCFs can have important applications to all-optical signal amplification and all-optical wavelength conversion systems where the fiber length, pump power and, at the same time, dispersion controllability are important [40, 41].

Bibliography

[1] F. P. Kapron, D. B. Keck and R. D. Maurer, Radiation losses in glass optical waveguides, Appl. Phys. Lett. 17, 423425 (1970).

[2] R. H. Stolen and A. Ashkin, Optical Kerr effect in glass waveguide, Appl. Phys. Lett. 22, 294296 (1973).

[3] S. Jiang, B. Bristiel, Y. Jaouen, P. Gallion, E. Pincemin, and S. Capouilliet, Full characterization of modern transmission fibers for Raman amplified-based communication systems, Opt. Express 15, 4883-4892 (2007).

[4] S. D. Dyer, M. G. Tanner, B. Baek, R. H. Hadfield, and S. . Nam, Analysis of a distributed fiber-optic temperature sensor using single-photon detectors, Opt. Express 20, 3456-3466 (2012).

[5] H. E Limodehi and F. Legare, Fiber optic humidity sensor using water vapor condensation, Opt. Express 25, 15313-15321 (2017).

[6] T. J. Muldoon, M. C. Pierce, D. L. Nida, M. D. Williams, A. Gillenwater, and R. Richards-Kortum, Subcellular-resolution molecular imaging within living tissue by fiber microendoscopy, Opt. Express 15, 16413-16423 (2007).

[7] Y. Wu, Y. Leng, J. Xi, and X. Li, Scanning all-fiber-optic endomicroscopy system for 3D nonlinear optical imaging of biological tissues, Opt. Express 17, 7907-7915 (2009).

[8] Y. Xu, L. Zhang, L. Chen, and X. Bao, Single-mode SOA-based 1kHz-linewidth dual-wavelength random fiber laser, Opt. Express 25, 15828-15837 (2017).

[9] N. M. Thang, Stimulated Raman Scattering in Gas Filled Hollow-Core Photonic Crystal Fibres, Max-Planck-Institut thesis, (2013).

[10] G. P. Agrawal, Nonlinear fiber optics: its history and recent progress [Invited], J. Opt. Soc. Am. B 28, A1-A10 (2011).

[11] P. Russell, Photonic-crystal fibers, J. Lightwave Technol, 24, 47294749, (2006).

[12] K. Saitoh, M. Koshiba, T. Hasegawa, and E. Sasaoka, Chromatic dispersion control in photonic crystal fibers: application to ultra-flattened dispersion, Opt. Express, 11, 843-852, (2003).

[13] R. Hubbard, Y. B. Ovchinnikov, J. Hayes, D. J. Richardson, Y. J. Fu, S.D. Lin, P. See, and A.G. Sinclair, Wide spectral range confocal microscope based on endlessly single-mode fiber, Opt. Express 18, 18811-18819 (2010).

[14] J. C. Knight and D. V. Skryabin, Nonlinear waveguide optics and photonic crystal fibers, Opt. Express 15, 15365-15376 (2007).

[15] F. Benabid, P. St. J. Russell, Hollow-core photonic crystal fibers: progress and prospects, Proc. SPIE, 5733, 5733-5733, (2005).

[16] R. Jamier, F. Gerome, G. Humbert, J. L. Auguste, J. M. Blondy and F. Benabid, Prospects on Hollow-core Photonic Crystal Fibers for unconventional fibered laser sources, 2011 13th International Conference on Transparent Optical Networks, Stockholm, 1-5, (2011).

[17] J. Kanka, Design of photonic crystal fibers with highly nonlinear glasses for four-wave-mixing based telecom applications, Opt. Express 16, 20395-20408 (2008).

[18] M. Koshiba and K. Saitoh, Structural dependence of effective area and mode field diameter for holey fibers, Opt. Express 11, 1746-1756 (2003).

[19] S. Yang, Y. Zhang, X. Peng, Y. Lu, S. Xie, J. Li, W. Chen, Z. Jiang, J. Peng, and H. Li, Theoretical study and experimental fabrication of high negative dispersion photonic crystal fiber with large area mode field, Opt. Express 14, 3015-3023 (2006).

[20] K. Saitoh and M. Koshiba, Empirical relations for simple design of photonic crystal fibers, Opt. Express 13, 267-274 (2005).

[21] J. Wang, C. Jiang, W. Hu, M. Gao, Modified design of photonic crystal fibers with flattened dispersion, Opt Laser Technol, 38, 169-172, (2006).

[22] M. F. Ferreira, Nonlinear effects in optical fibers, Wiley-OSA, US, (2011).

[23] F. Saltarelli, V. Kumar, D. Viola, F. Crisafi, F. Preda, G. Cerullo, and D. Polli, Broadband stimulated Raman scattering spectroscopy by a photonic time stretcher, Opt. Express 24, 21264-21275 (2016).

[24] A. G. Griffith, M. Yu, Y. Okawachi, J. Cardenas, A. Mohanty, A. L. Gaeta, and M. Lipson, Coherent mid-infrared frequency combs in silicon-microresonators in the presence of Raman effects, Opt. Express 24, 13044-13050 (2016).

[25] Y. Kida, T. Nagahara, S. Zaitsu, M. Matsuse, and T. Imasaka, Pulse compression based on coherent molecular motion induced by transient stimulated Raman scattering, Opt. Express 14, 3083-3092 (2006).

[26] S. Im, A. Husakou, and J. Herrmann, Guiding properties and dispersion control of kagome lattice hollow-core photonic crystal fibers, Opt. Express 17, 13050-13058 (2009).

[27] Y. Chen, Z. Wang, Z. Li, W. Huang, X. Xi, and Q. Lu, Ultra-efficient Raman amplifier in methane-filled hollow-core fiber operating at 1.5 m, Opt. Express 25, 20944-20949 (2017).

[28] C. Jauregui, J. Limpert, and A. Tunnermann, Derivation of Raman threshold formulas for CW double-clad fiber amplifiers, Opt. Express 17, 8476-8490 (2009).

[29] F. Benabid,G. Bouwmans, J. C. Knight, P. St. J. Russell,and F. Couny, Efficiency Laser Wavelength Conversion in a Gas-Filled Hollow Core Photonic Crystal Fiber by Pure Stimulated Rotational Raman Scattering in Molecular Hydrogen, Phys. Rev. Lett., 93, 12, 123903, (2004).

[30] F. Benabid, J. C. Knight, G. Antonopoulos, and P. St. J. Russell, Stimulated Raman Scattering in Hydrogen-Filled Hollow-Core Photonic Crystal Fiber, Science, 298, 5592, 399-402, (2002).

[31] W. Fu, F. Shu, Y. Zhang, C. Dong, C. Zou, and G. Guo, Integrated optical circulator by stimulated Brillouin scattering induced non-reciprocal phase shift, Opt. Express 23, 25118-25127 (2015).

[32] R. Pant, M. D. Stenner, M. A. Neifeld, and D. J. Gauthier, Optimal pump profile designs for broadband SBS slow-light systems, Opt. Express 16, 2764-2777 (2008).

[33] W. Gao, X. Hu, D. Sun, and J. Li, Simultaneous generation and Brillouin amplification of a dark hollow beam with a liquid-core optical fiber, Opt. Express 20, 20715-20720 (2012).

[34] A. Zadok, A. Eyal, and M. Tur, Stimulated Brillouin scattering slow light in optical fibers [Invited], Appl. Opt. 50, E38-E49 (2011).

[35] Y. Cao, P. Lu, Z. Yang, and W. Chen, An efficient method of all-optical buffering with ultra-small core photonic crystal fibers, Opt. Express 16, 14142-14150 (2008).

[36] L. Xing, L. Zhan, L. Yi, and Y. Xia, Storage capacity of slow-light tunable optical buffers based on fiber Brillouin amplifiers for real signal bit streams, Opt. Express 15, 10189-10195 (2007).

[37] R. Stolen, Phase-matched-stimulated four-photon mixing in silica-fiber waveguides, in IEEE Journal of Quantum Electronics, v11, 3, 100-103, (1975).

[38] R. Stolen and J. Bjorkholm, Parametric amplification and frequency conversion in optical fibers, in IEEE Journal of Quantum Electronics, 18, 7, 1062-1072, (1982).

[39] P. D. Rasmussen, J. Laesgaard, and O. Bang, Degenerate four wave mixing in solid core photonic bandgap fibers, Opt. Express 16, 4059-4068 (2008).

[40] A. Zhang and M. S. Demokan, Broadband wavelength converter based on four-wave mixing in a highly nonlinear photonic crystal fiber, Opt. Lett. 30, 2375-2377, (2005).

[41] K. K. Chow, K. Kikuchi, T. Nagashima, T. Hasegawa, S. Ohara, and N. Sugimoto, Four-wave mixing based widely tunable wavelength conversion using 1-m dispersion-shifted bismuth-oxide photonic crystal fiber, Opt. Express 15, 15418-15423 (2007).

[42] M. Ebnali-Heidari, C. Monat, C. Grillet, and M. K Moravvej-Farshi, A proposal for enhancing four-wave mixing in slow light engineered photonic crystal waveguides and its application to optical regeneration, Opt. Express 17, 18340-18353 (2009).

Chapter 3

Rogue waves

3.1 Oceanic rogue waves

Rogue waves (RWs) are rare and unusually large amplitude statistical waves that appear more frequently than predicted by Gaussian statistics [1]. The terminology was first coined in the context of oceanography as oceanic RWs [2], but has since been generalized to describe huge waves in different physical media [3]. Unexpectedly, large surface waves at high seas is a real threat to maritime activities and offshore structures. Intensive research efforts are conducted to understand the physics of RWs and to develop measures to predict or detect such waves [2, 4]. There are several definitions for such surprisingly huge waves. In oceanography, RWs are usually defined as waves whose height satisfies the following criteria [5]

$$AI = H/H_S \geq 2, \tag{3.1}$$

where AI is an abnormality index, H is the wave height defined as the vertical distance between the highest and the lowest surface elevation of a wave and H_S is a significant wave height. The significant wave height can be defined as the mean of the largest third of waves in a wave train using the following formula [6]

$$H_S = \frac{1}{N/3} \sum_{j=1}^{N/3} H_j \tag{3.2}$$

where j is the rank number of the waves based on the wave height (i.e., j=1 is the tallest wave, j=2 is the second tallest wave, etc.). Some authors suggest a more simplified formula for calculating the significant wave height: $H_S = 4\sigma$ where σ is the

standard deviation of the wave height [5]. The statistical distribution of ocean wave heights and the concept of significant wave height are illustrated in Fig. 3.1. When the latter convention is accepted, the AI is the only parameter defining whether the wave is rogue or not. However the RW definition is not always consistent and it actually varies from study to study. For example, in Louis Majesty incident [7], the estimated maximum wave amplitude is between 8.4 and 9.4 m, while the significant wave height was 5 m and it is still considered a RW in some literature. Therefore, RWs are not

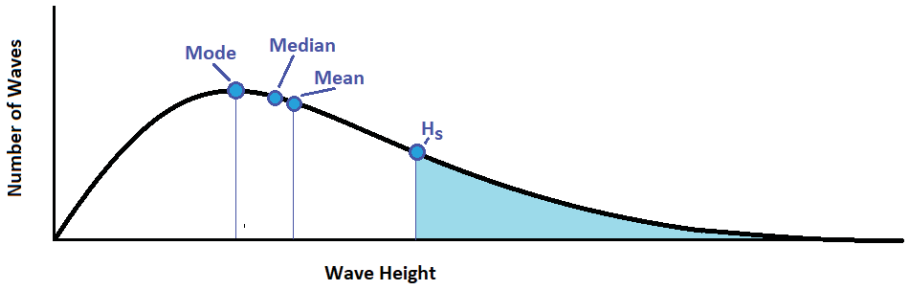

Figure 3.1: Statistical distribution of ocean wave heights and the concept of significant wave height (H_S).

necessarily huge, they are rather unusually large for a given sea state. The emergence of giant waves involves the physics different from that generating a usual population of ocean waves. However, the existence of a universal RW generation mechanism appears highly unlikely. [1, 8]. Oceanic RWs arise at arbitrary water depths (in deep as well as shallow water), with or without currents. Moreover, oceanic RWs have been shown to form due to different mechanisms—from linear effects such as random superposition of independent wave trains and geometrical focusing to nonlinear effects associated with the growth of surface noise [1, 8].

3.2 Optical rogue waves

As stated above, RWs exist in media other than water. The analogous physics of nonlinear wave propagation in optics and hydrodynamics has triggered a flurry of theoretical and experimental research in optics aimed at understanding RW generating mechanisms [9, 10]. The common property heralding RW formation in the diverse systems is the observation of large deviations from Gaussian statistics of the wave

amplitude (or wave power/intensity), with a heavy tail (or long tail) probability density function (PDF) which predicts the occurrence of high amplitude events with the probability greater than that allowed by Gaussian statistics [11, 12].

Optical rogue wave (ORW) formation can be influenced by a number of factors. In other words, the statistics of the giant waves can be affected by changing incident conditions [13]. For example, Dudley et al. [14] showed that RW formation can be enhanced or suppressed through a small modulation across the input pulse envelope or using a sliding frequency filter. Furthermore, Buccoliero et al. [15] demonstrated that rogue waves will not occur in any supercontinuum (SC) spectrum that is limited by fiber loss, such as commercial silica fiber based SC sources. There are also a few papers exploring how to generate high intensity RW in a more controlled manner. For example, using the generalized nonlinear Schrödinger equation (GNLSE), K. Hammani et al. [16] investigated the emergence of RWs from turbulent fluctuations. As another example, A. Mathis et al. [17] proposed some particular conditions leading to the extended tails in the associated PDF of optical RWs. Recently, H. Yang et al. [18] studied the induced modulation instability in the process of SC generation and showed the possibility of ORW formation regardless of noise effects.

There have been a number of theoretical or experimental studies of ORWs after the pioneer work of Solli et al. in 2007 [19] when measurements of optical fiber supercontinuum spectra yielded long-tailed histograms for intensity fluctuations. ORWs have been demonstrated in different systems such as optical cavities, passively mode-locked fiber lasers, erbium-doped fiber systems, parametric processes, in microwave settings and even in linear light propagation inside multimode fibers [20-23]. However, most studies have focused on the nonlinear Schrödinger equation (NLSE) which applies to both optics and hydrodynamics systems in certain limits. The modulation instability (MI) is believed to be the mechanism for optical rogue wave (ORW) formation in such systems where noise-induced fluctuations can modify the dynamics and generate rare but extreme events [13]. In other words, MI is causing broadband noise amplification through phase-matched four-wave mixing (FWM) [13]. MI is usually investigated within NLSE which studies weakly nonlinear and dispersive waves.

There exists a class of NLSE solutions known as breathers [1]. Most breathers are

localized in space and oscillate (breathe) in time or vice versa [15]. Breathers form because small amplitude fluctuations are susceptible to MI which causes them to grow to large amplitude modulations on top of a finite-amplitude background [24]. Breather solutions of NLSE, especially a limiting case which is called the Peregrine soliton, are presently well accepted as potential prototypes for the rogue waves in the ocean and optics [25]. The Peregrine soliton shows a double spatio-temporal localization and therefore, presents a progressive increase of its amplitude and a narrowing of its temporal duration [26]. At the maximum compression, the amplitude is three times larger than that of the level of the continuous background (or the intensity is nine times larger than the background) [27]. This feature of the Peregrine soliton is in agreement with the criteria usually applied to identify a wave as rogue. Therefore, Peregrine soliton formation is one the most attractive hypotheses to explain the formation of RWs.

Another possible driver mechanism behind ORW generation is solition collisions. The fundamental solitons have different peak intensities and durations and therefore multiple collisions occur between them due to different group velocities. Noise-induced MI results in soliton fission which ,in turn, leads to a number of solitons that interact and transfer energy during multiple collisions. The interaction will increase the noise level which strongly depends on the phases and amplitudes of solitons. This energy transfer can result in the formation of ORWs with large amplitudes (at least two times larger than that of the average wave amplitude). As an example, Eberhard et. al. [32] demonstrated a cascade model with an energy-exchange mechanism that drives the formation of ORWs in GNLSE with the third-order dispersion via quasi-solition collisions. These explorations have motivated much research to gain analytic insight into conditions favouring rogue wave emergence [25-32].

3.3 Optical rogue waves near resonance

As we mentioned in the previous section, RW excitation in the NLSE model with random input fields has been studied both numerically and experimentally. These studies show the emergence of heavy-tailed probability density distributions (PDF)

Table 3.1: NLSE and near-resonance models

Property	NLSE	Near-resonance
Nonlinearity	weak	strong
Medium response	instantaneous	long memory
Amplification/absorption	no	yes

of field intensities which indicate the RW excitation in the system. However, the work on ORW excitation with random sources has so far been limited to optical waves far away from internal medium resonances. The NLSE model cannot accurately describe the dynamics of nonlinear waves in the vicinity of wave-wave or wave-matter resonances [33, 34]. The NLSE model implies instantaneous medium response and weak nonlinearity. However strong nonlinearity, long coherent memory of the system, and strong amplification/absorption near resonance are the main characteristics of a resonant wave-wave or wave-matter interaction regime [33]. Thus the two models differ profoundly in many respects. We point out the differences between these two models in table 3.1.

In optical physics, we usually model the resonant RW excitation through either two level amplification (TLA) or SRS-like process. The energy transfer to an optical wave from either medium atoms (TLA) or from another wave via two-photon resonance (SRS) serves as a resonant amplification mechanism. The ORW emergence in resonant nonlinear media is of fundamental interest. The level diagram for SRS and TLA processes is schematically depicted in Fig. 3.2.

We propose to study ORW generation through SRS in optical fibers as an ideal model for near resonant ORW excitation because of the existence of the natural noise transfer and amplification mechanisms. The noise can be transferred from the pump to amplified Stokes waves (noisy pump case) or the noise present in a seeded Stokes wave is amplified as the Stokes amplitude is amplified (noisy Stokes case). Both of these mechanisms in SRS can lead to a heavy-tailed probability distribution of the Stokes wave peak power which is a signature of the ORW formation in the system. As we said above, one of the fundamental differences between NLSE and

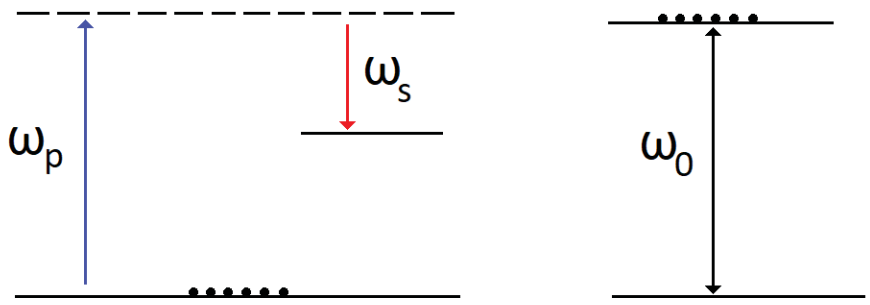

Figure 3.2: Level diagram for SRS (left) and TLA (right); the black dots denote initial atomic population.

near-resonance models is coherent memory of the medium in the case of resonance interactions. In SRS, the coherent memory (Γ^{-1}) is controlled by relative magnitudes of a characteristic SRS interaction time (T_{SRS}) and the Raman medium relaxation time, $T_2 = \gamma^{-1}$. Thus we can define the coherent memory parameter as

$$\Gamma = \gamma T_{SRS} \tag{3.3}$$

where γ is a medium dipole relaxation rate. Γ determines the extent of system memory and the system proximity to the integrability limit. If $\Gamma \ll 1$ the SRS is highly transient with an extremely long memory time. Another important aspect of near resonant interaction studies is the effect of the source noise. Optical pulses are generally assumed to be fully deterministic or fully coherent [35]. However, experimental evidence shows that we cannot accurately simulate and study optical pulses in purely deterministic terms [35]. In fact, optical pulses are intrinsically stochastic or partially coherent [35, 36]. It means realistic laser sources generate pulses with random fluctuations in their amplitude and phase. These amplitude and phase fluctuations should be taken into account in simulation of realistic optical sources and optical systems. Optical coherence theory investigates optical phenomena as stochastic processes and therefore, considers pulses to be partially coherent. To this end, we use partially coherent pulses to study the effect of source noise and coherence time of the source on the formation of large amplitude waves with non-Gaussian statistics in the output of the system.

Bibliography

[1] J. M.Dudley, F. Dias, M. Erkintalo and G. Genty, Instabilities, breathers, and rogue waves in optics, Nature Photon. 8, 755764 (2014).

[2] C. Kharif, E. Pelinovsky, and A. Slunyaev, Rogue Waves in the Ocean, (Springer, Berlin, 2009).

[3] M. Onorato, S. Residori, U. Bertolozzo, A. Montina, and F. T. Arecchi, Rogue waves and their generating mechanisms in different physical contexts, Phys. Rep. 528, 47 (2013).

[4] K. Dysthe, H.E Krogstad and P. Muller, Oceanic rogue waves, Annu. Rev. Fluid Mech. 40, 287-310 (2008).

[5] A. Chabchoub, Tracking Breather Dynamics in Irregular Sea State Conditions, Phys. Rev. Lett., 117, 14, 144103, 2016.

[6] L. H. Holthuijsen, Waves in Oceanic and Coastal Waters, Cambridge University Press, 1st edition, UK, (2010).

[7] L. Cavaleri, L. Bertotti, L. Torrisi, E. Bitner-Gregersen, M. Serio, and M. Onorato, Rogue waves in crossing seas: The Louis Majesty accident, J. Geophys. Res., 117, C00J10, (2012).

[8] C. Kharif, and E. Pelinovsky, Physical mechanisms of the rogue wave phenomenon, Eur. J. Mech. B/Fluids 22, 603-634 (2003).

[9] N. Akhmediev, J. M. Dudley, D. R. Solli, and S. K. Turitsyn, Recent progress in invesitgating optical rogue waves, J. Opt. 15, 060201 (2013).

[10] N. Akhmediev, B. Kibler, F. Baronio, M. Belic, W-P Zhong, Y. Zhang, W. Chang, J. M. Soto-Crespo, P. Vouzas, P. Grelu, C. Lecaplain, K. Hammani, S. Rica, A. Picozzi, M. Tlidi, K. Panajotov, A. Mussot, A. Bendahmane, P. Szriftgiser, G. Genty, J. Dudley, A. Kudlinski, A. Demircan, U. Morgner, S. Amiranashvili, C. Bree, G. Steinmeyer, C. Masoller, N. G. R. Broderick, A. F. J. Runge, M. Erkintalo, S. Residori, U. Bortolozzo, F. T. Arecchi, S. Wabnitz, C. G. Tiofack, S. Coulibaly and M. Taki, Roadmap on optical rogue waves and extreme events, J. Opt. 18, 063001 (2016).

[11] A. I. Dyachenko and V. E. Zaklharov, Modulation instability of Stokes waves to freak wave, JETP Lett. 81, 255 (2005).

[12] V. E. Zakharov, A. I. Dyachenko, and A. O. Prokofiev, Freak waves as nonlinear stage of Stokes wave modulation instability, Eur. J. Mech. B 25, 677 (2006).

[13] S. Zhao, H. Yang, N. Chen and C. Zhao, Controlled generation of high-intensity optical rogue waves by induced modulation instability, Scientific Reports, 7, 39926, (2017).

[14] J. M. Dudley, G. Genty, G. and B. J. Eggleton, Harnessing and control of optical rogue waves in supercontinuum generation, Opt. Express, 16, 36443651 (2008).

[15] D. Buccoliero, H. Steffensen, H. Ebendorff-Heidepriem, T. M. Monro, O. Bang, Midinfrared optical rogue waves in soft glass photonic crystal fiber, Opt. Express 19, 1797317978 (2011).

[16] K. Hammani, B. Kibler, C. Finot, and A. Picozzi, Emergence of rogue waves from optical turbulence, Phys. Lett. A, 374, 35853589,(2010).

[17] A. Mathis, L. Froehly, S. Toenger, F. Dias, G. Genty and J. M. Dudley Caustics and rogue waves in an optical sea, Sci. Rep. 5, 12822 (2015).

[18] H. Yang, N. Chen, N., B. Wang, P. Tang, Q. Zeng, Supercontinuum and rogue soliton generation by induced modulation instability in photonic crystal fiber, Jour. of Mod. Opt. 63, 13701377 (2016).

[19] D. R. Solli, C. Ropers, P. Koonath and B. Jalali, Optical rogue waves, Nature (London) 450, 10541057 (2007).

[20] A. Montina, U. Bertolozzo, S. Residori, and F. T. Arecchi, Non-Gaussian statistics and extreme waves in a nonlinear optical cavity, Phys. Rev. Lett. 103, 173901 (2009).

[21] J.M. Soto-Crespo, Ph. Grelu and N. Akhmediev, Dissipative rogue waves: extreme pulses generated by passively mode-locked lasers, Phys. Rev. E 84, 016604 (2011).

[22] J. He, S. Xu and K. Porsezian, New types of rogue wave in an erbium-doped fiber system, J. Phys. Soc. Japan 81, 033002 (2012).

[23] R. Hohmann, U. Kuhl, H-J. Stockmann, L. Kaplan and E. J. Heller, Freak waves in the linear regime: a microwave study, Phys. Rev. Lett. 104, 093901 (2010).

[24] N. Akhmediev, V. Eleonskii, N. Kulagin, Exact first-order solutions of the nonlinear Schrdinger equation, Theoretical and Mathematical Physics, 72, 2, 809818, (1987).

[25] A. Chowdury, W. Krolikowski, and N. Akhmediev, Breather solutions of a fourth-order nonlinear Schrodinger equation in the degenerate, soliton, and rogue wave limits, Phys. Rev. E, 96, 4, 042209, (2017).

[26] P. Dubard, P. Gaillard, C. Klein, and V. B. Matveev, On multi-rogue wave solutions of the NLS equation and positon solutions of the KdV equation, Eur. Phys. J. Special Topics 185, 247-258 (2010).

[27] M. J. Ablowitz, D. J. Kaup, A. C. Newell, and H. Segur, Method for Solving the Sine-Gordon Equation, Phys. Rev. Lett., 30, 25, 1262-1264, (1973).

[28] N. Akhmediev, A. Ankiewicz, and M. Taki, Waves that appear from nowhere and disappear without a trace, Phys. Lett. A 373, 675-678 (2009).

[29] V. I. Shrira, and V. V. Geogjaev, What makes the Peregrine soliton so special as a prototype of freak waves? Journal of Engineering Mathematics, 67, 1, 11-22, (2010).

[30] S. Toenger, T. Godin, C. Billet, F. Dias, M. Erkintalo, G. Genty, G., and J. M. Dudley, Emergent rogue wave structures and statistics in spontaneous modulation instability, Scientific Reports, 5, 10380, (2015).

[31] H. Bailung, S. K. Sharma, and Y. Nakamura, Observation of Peregrine Solitons in a Multicomponent Plasma with Negative Ions, 107, 25, 255005, (2011).

[32] M. Eberhard, A. Savojardo, A. Maruta, and R. A. Rmer, Rogue wave generation by inelastic quasi-soliton collisions in optical fibres, Opt. Express 25, 28086-28099 (2017).

[33] L. Allen and J. H. Eberly, Optical resonance and two-level atoms, Dover Publications Inc., New York, (1975).

[34] Byoung S. Ham, Reversible quantum optical data storage based on resonant Raman optical field excited spin coherence, Opt. Express 16, 14304-14313 (2008).

[35] L. Mandel and E. Wolf, Optical Coherence and Quantum Optics, Cambridge University Press, (1995).

[36] J. W. Goodman , Statistical Optics, John Willy and Sons INC, (2000).

Chapter 4

Non-Gaussian statistics and optical rogue waves in stimulated Raman scattering

Yashar E. Monfared and Sergey A. Ponomarenko
Published in: Optics Express, 2017, Vol. 25, No. 6, pp. 5941-5950
URL: https://www.osapublishing.org/oe/abstract.cfm?uri=oe-25-6-5941

4.1 Abstract

We explore theoretically and numerically optical rogue wave formation in stimulated Raman scattering inside a hydrogen filled hollow core photonic crystal fiber. We assume a weak noisy Stokes pulse input and explicitly construct the input Stokes pulse ensemble using the coherent mode representation of optical coherence theory, thereby providing a link between optical coherence and rogue wave theories. We show that the Stokes pulse peak power probability distribution function (PDF) acquires a long tail in the limit of nearly incoherent input Stokes pulses. We demonstrate a clear link between the PDF tail magnitude and the source coherence time. Thus, the latter can serve as a convenient parameter to control the former. We explain our findings qualitatively using the concepts of statistical granularity and global degree of coherence.

4.2 Introduction

Optical rogue waves (ORWs) are rare and uncommonly large amplitude statistical optical waves with heavy-tailed probability distributions [91]. The pioneering work of

Solli *et.al* on ORW excitation in supercontinuum generation in optical fibers [7] has triggered a tsunami of publications on ORWs in various contexts [137, 135, 5]. The vast majority of ORW research has so far focused on the modulation instability excitation scenario within the framework of integrable nonlinear Schr odinger equation [135]. Yet, optical rogue waves have also been theoretically predicted and/or experimentally demonstrated in such diverse systems as optical cavities [140, 141], passively mode-locked fiber lasers [142, 143, 144], erbium-doped fiber systems [145] , Raman fiber amplifiers [98], spatiotemporal structures and laser filamentation [147, 148], parametric processes [101] and even in linear light propagation inside multimode fibers [150] as well as in microwave settings [103]. To date, several coherent structures such as the Peregrine soliton [91, 104, 19, 106], solitons on finite background [91, 19, 105, 152], and superregular breathers [108] have been conjectured to serve as ORW prototypes in weakly dispersive, weakly nonlinear wave systems described by the integrable 1D nonlinear Schr odinger equation. These predictions have prompted elegant experiments aiming to realize such coherent ORW prototypes in highly controlled environments in fiber optics [109, 110] .

On the other hand, the role played by source coherence in shaping emergent nonlinear wave structures is a fundamental issue in nonlinear statistical optics [151]. In this context, the ORW generation with random sources has lately triggered growing interest. In particular, the source coherence influence on the ORW emergence has been examined both numerically [24, 181, 113, 154, 115] and experimentally [24, 181] and a pronounced sensitivity of the peak wave power probability density function (PDF) shape to random initial conditions was established. The above results were obtained for 1D wave turbulence described by the nonlinear Schrdinger equation within the framework of integrable turbulence [116]. The ORW excitation in nearly integrable, Hamiltonian nonlinear systems with noisy input waves was also studied [117, 25, 118]

To our knowledge however, the work on ORW excitation with random sources has so far been limited to optical waves far away from internal medium resonances. Yet, resonant light-matter interactions are known to strongly enhance media nonlinearity, dispersion and absorption, giving rise to a host of new nonlinear phenomena such as electromagnetically- and self-induced transparency [182]. Lately, self-induced

transparency and the ensuing random phase soliton formation with statistical light has been explored in resonant nonlinear media in the two-level approximation [120]. Thus, the ORW emergence in resonant nonlinear media is of fundamental interest. In this context, we anticipate stimulated Raman scattering (SRS) in optical fibers to be a fertile ground for ORW exploration. The latter arise naturally in SRS as either noise is irreversibly transferred from the pump to amplified Stokes waves or the noise present in a seeded Stokes wave is amplified as the Stokes amplitude is amplified, leading to a heavy-tailed probability distribution of the Stokes wave peak power. The first mechanism was explored in SRS generation in highly nonlinear solid-core fibers in the picosecond pulse regime [98]. Although the influence of pump noise on the Stokes pulse characteristics in SRS generation from quantum noise in the nanosecond regime was examined in detail [121, 122, 123], no explicit connection to rogue waves was made. Moreover, the ORW excitation in the SRS amplification regime with a noisy Stokes input present has not, to our knowledge, been addressed. A related fundamental issue concerns rogue wave control in the nanosecond SRS regime. The issue has also a practical dimension in light of recent efforts to realize novel SRS and supercontinuum generation regimes, controllable over long interaction lengths inside hollow core photonic crystal fibers [124, 32, 125].

In this work, we numerically study SRS in the amplification regime of a weak noisy probe Stokes pulse, mediated by a strong coherent Raman pump pulse inside a hydrogen filled hollow core photonic crystal fiber (HC PCF). We show that nonlinear noise amplification, concurrent with the Stokes pulse amplitude growth, skews the Stokes pulse peak power statistics, converting it to a heavy-tailed non-Gaussian one which is a statistical signature of rogue wave excitation. We model fluctuating input Stokes pulses as a Gaussian random process. We explicitly construct the input Stokes pulse ensemble using the coherent mode representation of optical coherence theory. Our approach has two major benefits. First, we establish a link between fundamental concepts of optical coherence theory such as coherence time and global degree of coherence of the source and the generated rogue wave statistics. Second, we show that the source coherence time can serve as a versatile control parameter for ORW excitation in the system. In particular, we show how the Stokes power distribution tail can be enlarged or shortened by simply adjusting the Stokes input coherence time.

We explain our findings qualitatively using the concepts of statistical granularity and global degree of coherence.

4.3 Theoretical formulation and statistical source description

We start by considering the standard SRS equations, written in a moving reference frame, $\tau = t - \beta_1 z$, where β_1 is an inverse group velocity assumed to be the same for co-propagating pump and Stokes pulses. The wave equations for the slowly-varying pump E_p and Stokes E_s amplitudes read

$$\partial_\zeta E_p = \left(\frac{i\omega_p N r_{eff}}{2\epsilon_0 c n_p} \right) \sigma E_s \tag{4.1}$$

and

$$\partial_\zeta E_s = \left(\frac{i\omega_s N r_{eff}}{2\epsilon_0 c n_s} \right) \sigma^* E_p, \tag{4.2}$$

and the Schr odinger equation for the medium dipole matrix element σ can be written in the weak excitation limit as

$$\partial_\tau \sigma = -\gamma\sigma + \left(\frac{i r_{eff}}{4\hbar} \right) E_s^* E_p. \tag{4.3}$$

Here $\omega_{p,s}$ and $n_{p,s}$ are the carrier frequencies and refractive indices of the pump and Stokes pulses, respectively, N is a medium density, γ is an SRS medium relaxation rate, and $r_{eff} = \frac{1}{\hbar} \sum_i \frac{d_{3i} d_{i1}}{\omega_{i3} + \omega_{i1} - \omega_p - \omega_s}$ is a Raman transition dipole matrix element [32, 125, 158]. We also assumed that the fiber is designed to suppress all but the pump and fundamental Stokes modes of molecular hydrogen [32].

Next, suppose all hydrogen molecules are in their ground states prior to interaction with the pulses and take the strong input pump pulse to be a Gaussian such that $E_p(t,0) = |E_{p0}|\, e^{-t^2/2t_p^2}$, where t_p is a pump pulse duration. At the same time, we assume a weak probe Stokes pulse to be fluctuating such that at the fiber input, $E_s(t,0) = |E_{s0}|\, a_s(t) e^{-t^2/2t_s^2}$, where t_s is a Stokes pulse duration and $a_s(t)$ is a dimensionless statistically stationary random amplitude. Introducing peak optical intensities of the pulses $I_{s0,p0} = \epsilon_0 n_{s,p} c\, |E_{s0,p0}|^2 /2$ we scale the pulse fields to the peak

pump intensity at the source, $E_p = \sqrt{2I_{p0}/\epsilon_0 c n_p}\mathcal{E}_p$ and $E_s = \sqrt{2I_{p0}/\epsilon_0 c n_p}\mathcal{E}_s$. Next, we introduce dimensionless distance and time, $Z = \zeta/l_{SRS}$ and $T = \tau/t_{SRS}$ where $l_{SRS} = (2\epsilon_0 c/N r_{eff})\sqrt{n_p n_s/\omega_p\omega_s}$ and $t_{SRS} = 2\hbar\epsilon_0 c n_p/r_{eff} I_{p0}$ are characteristic length and time over which energy exchange between pulses and the medium unfolds. The SRS equations can then be cast into a dimensionless form as

$$\partial_Z \mathcal{E}_p = ik\sigma\mathcal{E}_s, \tag{4.4}$$

$$\partial_Z \mathcal{E}_s = ik^{-1}\sigma^*\mathcal{E}_p, \tag{4.5}$$

and

$$\partial_T \sigma = -\Gamma\sigma + i\mathcal{E}_p\mathcal{E}_s^* \tag{4.6}$$

Here $k = \sqrt{\omega_p n_s/\omega_s n_p}$ and $\Gamma = \gamma t_{SRS}$ is a key dimensionless parameter governing the SRS process. Further, the dimensionless initial conditions read

$$\mathcal{E}_p(T,0) = e^{-T^2/2T_p^2}, \tag{4.7}$$

and

$$\mathcal{E}_s(T,0) = \sqrt{\frac{n_p I_{s0}}{n_s I_{p0}}}a_s(T)e^{-T^2/2T_s^2} \tag{4.8}$$

Let us now construct an input Stokes pulse ensemble. To enhance the SRS efficiency we want to maximize the pump and Stokes pulse intensity overlap. To this end, we assume that Stokes and pump pulses have the same durations, $t_p = t_s = t_0$. We model Stokes pulses as a Gaussian random process, which is completely specified by its second-order correlation function, the mutual coherence function. The latter is assumed to be Gaussian; this is a celebrated Gaussian Schell model (GSM) of optical coherence theory [232]. With the help of Eqs. (4.7) and (4.8), the GSM mutual intensity can be expressed as

$$\begin{aligned}\Gamma(T_1,T_2,0) \equiv \langle\mathcal{E}_s^*(T_1,0)\mathcal{E}_s(T_2,0)\rangle = \left(\frac{n_p\langle W_s\rangle}{n_s W_p}\right)\\ \times\exp\left(-\frac{T_1^2+T_2^2}{2T_0^2}\right)\exp\left[-\frac{(T_1-T_2)^2}{2T_c^2}\right].\end{aligned} \tag{4.9}$$

Here the angle brackets denote ensemble averaging; $T_p = T_s = T_0 = t_0/t_{SRS}$ and $T_c = t_c/t_{SRS}$, where t_c is a Stokes pulse coherence time and we eliminated the pump and Stokes peak intensities in favor of the pulse energies, W_p and $\langle W_s \rangle$.

To construct the random pulse ensemble, we employ the Karhunen-Loève expansion [231]

$$\mathcal{E}_s(T,0) = \sum_n c_n \psi_n(T), \tag{4.10}$$

where the random coefficients $\{c_n\}$ are orthogonal such that

$$\langle c_n^* c_m \rangle = \lambda_n \delta_{mn}, \tag{4.11}$$

and the coherent modes are orthonormal, implying that

$$\int_{-\infty}^{\infty} dT \psi_n^*(T) \psi_m(T) = \delta_{mn}. \tag{4.12}$$

The mutual coherence function is then represented as a Mercer-type series in coherent modes as [232]

$$\Gamma(T_1, T_2, 0) = \sum_n \lambda_n \psi_n^*(T_1) \psi_n(T_2). \tag{4.13}$$

Next, the complex random amplitudes $\{c_n\}$ can be expressed in the polar form as

$$c_n = \sqrt{i_n} e^{i\phi_n}. \tag{4.14}$$

We stress that Eqs. (3) through (12) describe any statistical source. Thus, we must spell out a concrete model for the random amplitudes and phases, adequately describing a given physical source. In our case, we assume random phases $\{\phi_n\}$ to be uniformly distributed in the interval $0 \leq \phi_n \leq 2\pi$, and random amplitudes $\{|c_n|\}$ to obey the Rayleigh distribution such that $\{i_n\}$'s are governed by the exponential distribution as

$$\mathcal{P}(i_n) = \frac{1}{\lambda_n} e^{-i_n/\lambda_n}. \tag{4.15}$$

Thus c_n is a complex Gaussian random variable. It follows that the incident Stokes pulse ensemble $\{\mathcal{E}_s(T,0)\}$ is Gaussian as a sum of independent Gaussian random variables [231]. We stress that the mode power distribution of the form (4.15) is sufficient

to guarantee Gaussian statistics of the source regardless of its temporal coherence. On the one hand, in the low-coherence limit when many coherent modes in the expansion (6) are required to faithfully reproduce the source mutual intensity, Gaussian statistics of the pulse ensemble can be ensured for any mode power distribution $P(i_n)$ by virtue of the central limit theorem [231, 157]. On the other hand, however, as the source becomes sufficiently coherent such that only a few coherent modes enter Eq. (6), the central limit theorem no longer applies. Yet, the input source ensemble is Gaussian, provided it is a sum of independent modes each obeying Gaussian statistics. We note in passing that the present source ensemble is drastically different from previously considered non-Gaussian stochastic input pulses, generating random phase solitons in resonant media [120]. We also note that we focus on noise effects due to strongly fluctuating input Stokes pulses. In other words, we ignore spontaneous Raman scattering (quantum) noise which is dwarfed by thermal-like fluctuations of the incident Stokes pulses.

To complete our source modelling, we observe that the GSM eigenvalues and coherent mode profiles are given by [232]

$$\lambda_n = \sqrt{\pi} T_0 \left(\frac{n_p W_s}{n_s W_p} \right) \frac{(\alpha + \xi)\beta^n}{(\alpha + \beta + \xi)^{n+1}}, \tag{4.16}$$

and

$$\psi_n(T) = \left(\frac{2\xi}{\pi} \right)^{1/4} \left(\frac{1}{2^n n!} \right)^{1/2} H_n(T\sqrt{2\xi}) e^{-\xi T^2}, \tag{4.17}$$

where $H_n(x)$ is a Hermite polynomial of the order n and we introduced the notations $\alpha = (2T_0^2)^{-1}$, $\beta = (2T_c^2)^{-1}$, and $\xi = \sqrt{\alpha^2 + 2\alpha\beta}$.

4.4 Numerical results

As a practical realization of the system, we consider a meter long hydrogen-filled HC PCF with typical parameters representative of the HC PCFs previously designed for SRS experiments [124, 32]. The HC PCF has a low-loss transmission window between 1030 and 1150 nm. As a result, only the pump and first Stokes modes, interacting with the J=1 to J=3 rotational transition, can co-propagate in the HC PCF. We

choose a narrow linewidth laser delivering 10 ns pulses of a 20 μJ energy at 1064 nm as the pump. The Stokes pulses with the mean peak power of 10 W operate at 1134 nm. Such Stokes pulses can be excited by time modulating (chopping) an output of a cw partially coherent source using, for instance, electro-optical modulators [161]. We take the relaxation time of hydrogen in the HC PCF to be $\gamma^{-1} = 5$ ns [158]; the effective Raman interaction length and time are estimated to be $l_{SRS} = 1$ mm and $t_{SRS} = 6$ ns, respectively.

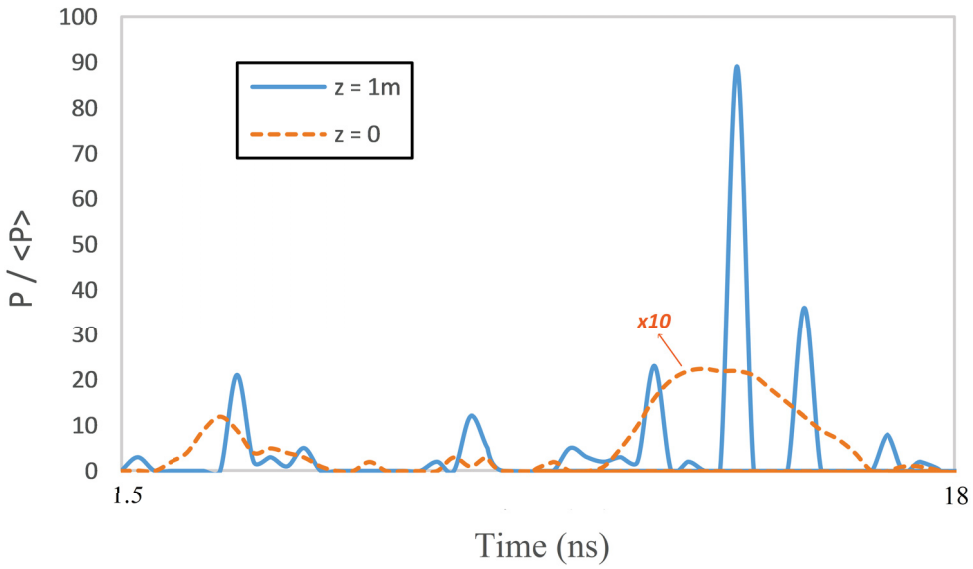

Figure 4.1: Normalized (to the average power at the source) peak power fluctuations of a random Stokes pulse with $T_c = 0.1\ T_0$ at the fiber output (blue) and input (orange). To facilitate the visualization, the orange curve is scaled by the factor of 10.

We use the same numerical Monte Carlo simulation procedure as the one described in [120] in the context of random phase soliton excitation in two-level media to generate a random Stokes pulse ensemble of 2×10^4 realizations and examine its power fluctuations on pulse propagation inside the fiber. Our extensive numerical simulations indicate that power fluctuations 90 times greater than the mean power–nearly 900 W compared to the mean power of 10 W–can occur at the fiber output. We illustrate this point by exhibiting a time series of the normalized Stokes pulse powers at the fiber input and output in Fig. 4.1. We checked that giant power fluctuations can take place even for shorter fiber lengths. For instance, power fluctuations greater than 50 times the mean power (around 500 W) occur in 1 cm long fibers. These

observations are reflected in the presence of a very long probability distribution tail in Fig. 4.2 where we display the normalized Stokes peak power PDF for three cases: $T_c = 10T_p$ (rather coherent input pulses), $T_c = T_p$, and $T_c = 0.1T_p$ (nearly incoherent Stokes input). All powers are normalized to the average power of the input Stokes pulse ensemble. It is seen in Fig. 4.2 that as the Stokes source coherence time progressively increases, the probability distribution tail gradually depopulates. The

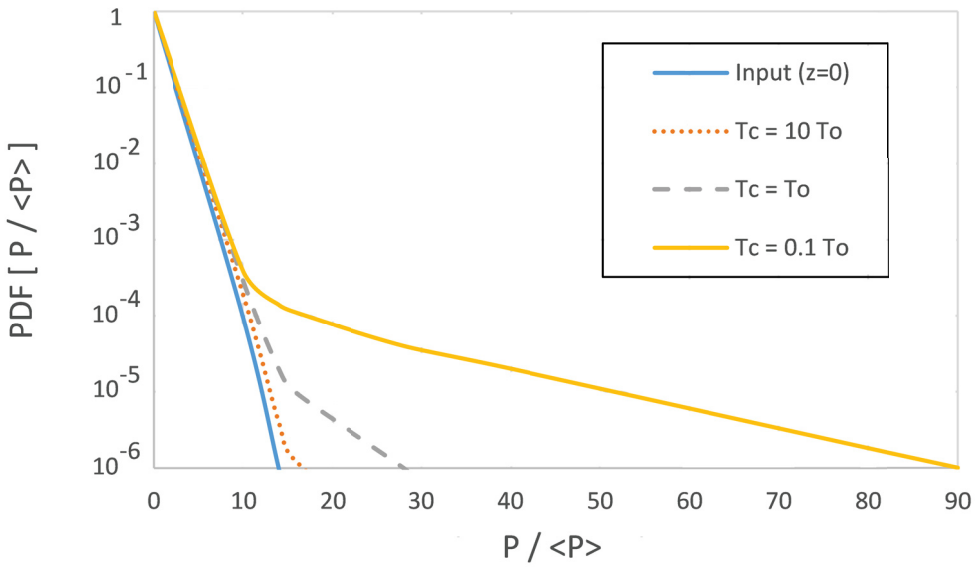

Figure 4.2: Normalized Stokes pulse peak power PDF at the entrance (blue) and exit to the HC PCF. The input/output pulse power is normalized to the average power at the source. The Stokes source coherence time takes on values $T_c = 0.1\ T_0$, $T_c = T_0$ and $T_c = 10T_0$.

exponential power distribution of the input Stokes ensemble is also displayed for comparison. It can be inferred from the figure that in all three cases, the PDF, exhibited in the logarithmic scale, nearly coincides with the exponential input distribution for sufficiently low powers, but it sharply deviates from the exponential distribution in the high Stokes power limit. Thus, the PDF is strongly non-Gaussian. Moreover, the output PDF appearance–including the magnitude of its tail–can be controlled by adjusting the Stokes source coherence time.

We notice that the degree to which the peak power statistics deviates from Gaussian, sharply increases as the source coherence time shrinks. This trend is opposite to the one recently encountered for integrable turbulence governed by the nonlinear Schr

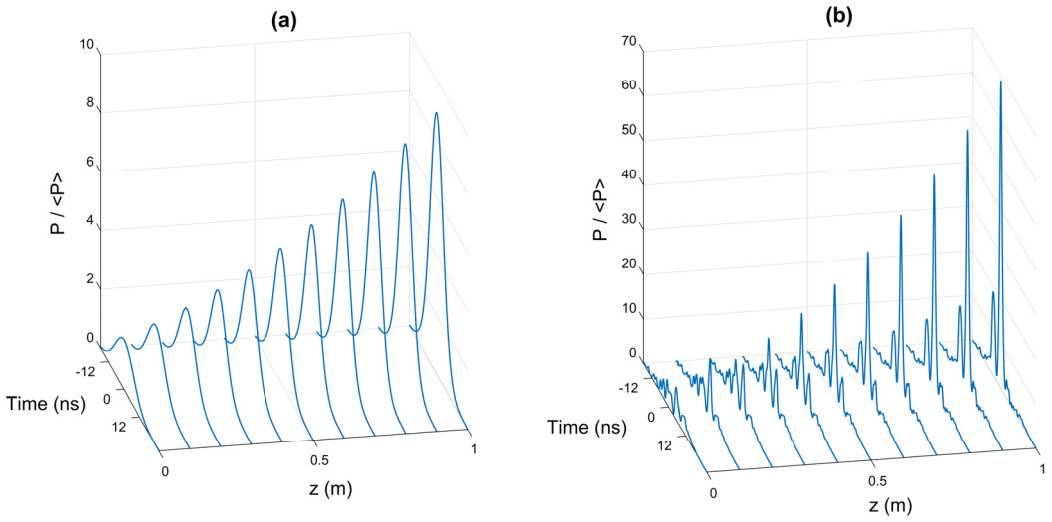

Figure 4.3: Normalized (to the average power at the source) peak power fluctuations of a random Stokes pulse for (a) very coherent, $T_c = 10T_0$ and (b) nearly incoherent, $T_c = 0.1T_0$ Stokes ensemble at the source as functions of time and propagation distance.

odinger equation [113]. This circumstance should not be surprising as SRS is fundamentally different from the system studied in [113]. While the former unfolds as a noinstantaneous resonant light-matter interaction, described, in general, by nonintegrable nonlinear equations, the latter is essentially a weakly dispersive wave system with a weak instantaneous nonlinearity. The ORW emergence in [113] is linked by the authors to soliton and breather collisions, the frequency of which is enhanced with the source coherence time increase. The ORW generation in SRS cannot be explained by this mechanism because, even in the coherent transient limit when the input pulse duration is much shorter than the SRS medium relaxation time and the SRS equations are integrable [185], solitons are known to be transient in SRS, giving way to self-similar waves as fundamental asymptotics of the system in the long-term limit [32, 132]. Furthermore, SRS soliton lifetimes are expected to shrink as the input pulse duration becomes comparable to the SRS medium relaxation time which is the case here.

To explain the PDF tail dependence on the source coherence time in SRS, we employ the concept of statistical granularity in time. Statistical granularity implies that the SRS interaction is coherent within a time interval of t_c and Stokes pulses

outside these time intervals are uncorrelated. The number of statistical granules corresponds to the effective number of coherent modes entering the Karhunen-Loève representation, Eq. (3), of the Stokes pulse ensemble. As t_c decreases, the number of uncorrelated modes (statistical granules) representing each Stokes ensemble member increases, making the Stokes source noisier. As the statistical granules are uncorrelated, they all compete for energy supply from the pump, resulting in a selective granule amplification and, eventually, leading to a giant amplitude granule formation within the Stokes pulse profile during the SRS amplification process. We stress that the long memory of the system plays an important role in facilitating selective amplification of large amplitude Stokes granules, leading to champion pulses of enormous amplitudes. This situation is vividly illustrated in Fig. 4.3 where we display, side by side, the Stokes ensemble member evolution as the pulse propagates along the fiber for a very coherent source, $T_c = 10T_0$, and a nearly incoherent one, $T_c = 0.1T_0$. The formation of a large amplitude statistical granule within the incoherent Stokes pulse is manifest in the figure. On the contrary, amplification is coherently distributed across the pulse profile in the coherent case, resulting in fairly uniform amplification.

The characteristic number of statistical granules present at the source is related to the source coherence time. We can estimate the number of statistical (time) granules N as an inverse of the global degree of coherence of the source. The latter is defined as $\nu = \lambda_0 / \sum_n \lambda_n$ [232]. It follows at once from Eq. (4.16) that for a nearly incoherent Stokes source, $T_c \ll T_p$, the number of time granules can be estimated as $N \simeq \nu^{-1} \propto T_c^{-1}$. Thus, the number of statistical granules grows in inverse proportion to shrinking source coherence time, augmenting the probability of rogue-wave events, and hence the emergence of a non-Gaussian, heavy-tail statistics of the Stokes pulse power. We note that statistical time granules are temporal analogs of spatial speckles, hypothesized to give rise to rogue waves in spatially extended systems [140, 141].

To confirm the crucial role played by the source coherence time and rule out the source nonstationarity influence, we carried out a series of simulations with highly coherent input Stokes pulse ensemble with $T_c = 200\ T_0$ for different values of T_0. The results are displayed in Fig. 4.4. It can readily be inferred from the figure that source nonstationarity has a negligible effect on the ensemble PDF shape at the fiber exit.

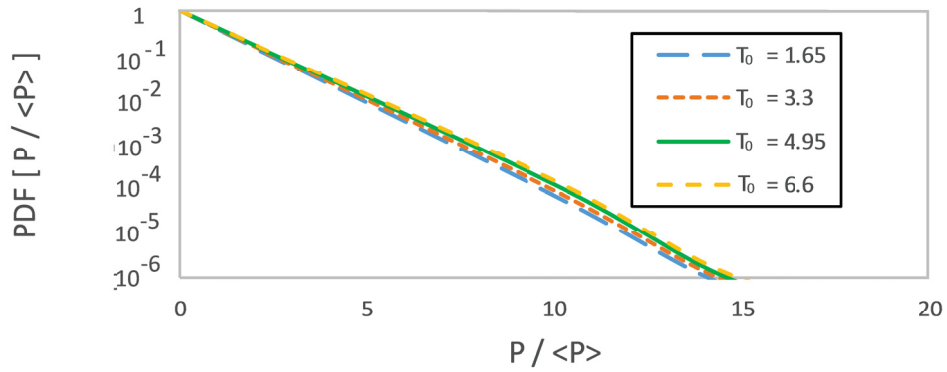

Figure 4.4: Normalized (to the average power at the source) peak power PDF of the Stokes pulse ensemble at the fiber exit for highly coherent Stokes input ensemble with $T_c = 200\ T_0$ for different T_0 values.

Finally, we show that a heavy-tail Stokes output statistics can be generated with not too incoherent ($T_c = T_0$) and even rather coherent ($T_c = 10T_0$) Stokes input if we increase the pump pulse energy. As we illustrate in Fig. 4.5, by increasing the pump pulse energy (W_p) from 20μJ to 80μJ the statistical behaviour of the Stokes pulses begins to shift from Gaussian to highly non-Gaussian, heavy-tail statistics. This deviation is more pronounced for the less coherent case of $T_c = T_0$ in complete agreement with the just outlined qualitative picture of ORW formation in the SRS in HC PCFs.

4.5 Conclusion

In conclusion, we have explored a Stokes power statistics in SRS inside hydrogen filled HC PCFs. We have shown that the statistics significantly deviates from the normal distribution, exhibiting heavy tails indicative of anomalously high probabilities of extremely large amplitude output pulses. We have shown that the extreme-value output statistics strongly depends on the initial noise level of the source Stokes pulses. The latter can be conveniently controlled by adjusting the source Stokes coherence time. Thus our findings establish a clear link between optical coherence and rogue wave theories. We explain our results invoking the concepts of statistical granularity and global degree of coherence. The former emerges as a crucial driving factor behind optical rogue wave formation in transient SRS. We observe that while the medium

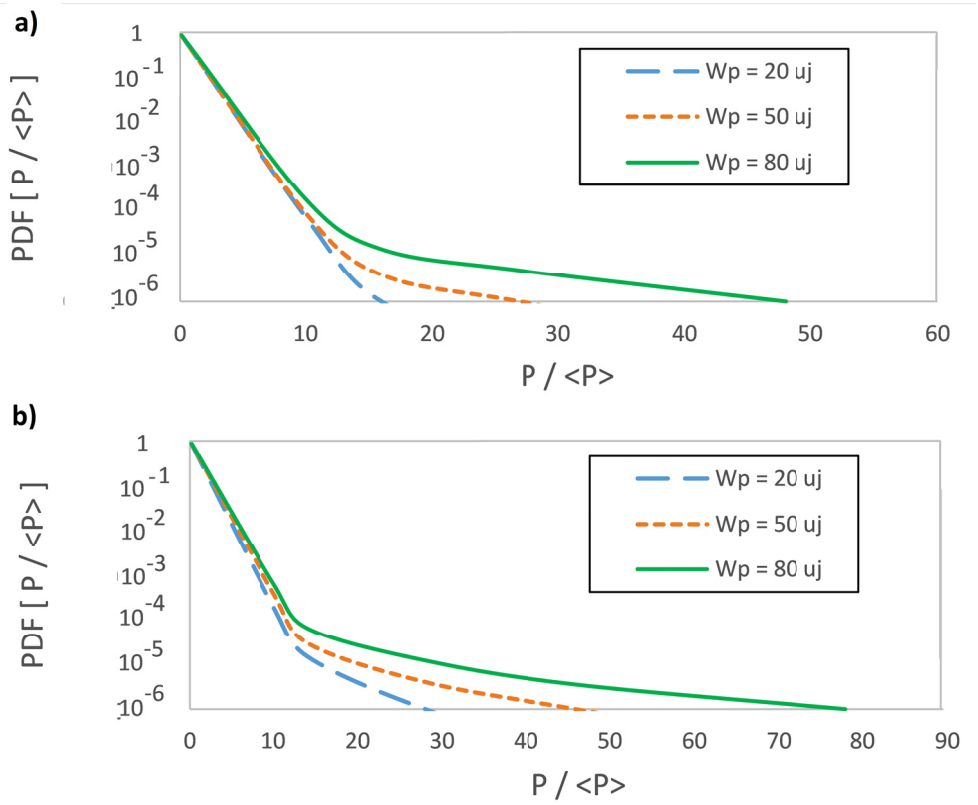

Figure 4.5: Normalized (to the average power at the source) Stokes pulse peak power PDF at the HC PCF exit for different input pump pulse energies and Stokes input coherence times: a) $T_c = 10\ T_0$ and b) $T_c = T_0$.

relaxation time in solid-core fibers is so short, $\Gamma \gg 1$, that the SRS interaction is virtually instantaneous, the SRS in HC PCFs has a finite relaxation time, $\Gamma \sim 1$, and hence a non-instantaneous character. This circumstance makes the latter especially conducive to ORW formation because the noninstantaneous nonlinear light-matter interaction leads to an efficient energy redistribution to higher-energy realizations of the Stokes pulse ensemble. We anticipate our work to stimulate further theoretical and experimental investigations into rogue wave formation in nonlinear wave systems in the vicinity of optical resonances.

Bibliography

[1] J. M.Dudley, F. Dias, M. Erkintalo and G. Genty, Instabilities, breathers, and rogue waves in optics, Nature Photon., **8**, 755-764 (2014).

[2] D. R. Solli, C. Ropers, P. Koonath and B. Jalali, Optical rogue waves, Nature (London) **450**, 1054–1057 (2007).

[3] N. Akhmediev, B. Kibler, F. Baronio, M. Belic, W-P Zhong, Y. Zhang, W. Chang, J. M. Soto-Crespo, P. Vouzas, P. Grelu, C. Lecaplain, K. Hammani, S. Rica, A. Picozzi, M. Tlidi, K. Panajotov, A. Mussot, A. Bendahmane, P. Szriftgiser, G. Genty, J. Dudley, A. Kudlinski, A. Demircan, U. Morgner, S. Amiranashvili, C. Bree, G. Steinmeyer, C. Masoller, N. G. R. Broderick, A. F. J. Runge, M. Erkintalo, S. Residori, U. Bortolozzo, F. T. Arecchi, S. Wabnitz, C. G. Tiofack, S. Coulibaly and M. Taki, Roadmap on optical rogue waves and extreme events, J. Opt., **18**, 063001 (2016).

[4] M. Onorato, S. Residori, U. Bertolozzo, A. Montina and F. T. Arecchi, "Rogue waves and their generating mechanisms in different physical contexts, Phys. Rep. **528**, 47–89 (2013).

[5] N. Akhmediev, J. M. Dudley, D. R. Solli, and S. K. Turitsyn, Recent progress in invesitgating optical rogue waves, J. Opt., **15**, 060201 (2013).

[6] A. Montina, U. Bertolozzo, S. Residori, and F. T. Arecchi, Non-Gaussian statistics and extreme waves in a nonlinear optical cavity, Phys. Rev. Lett., **103**, 173901 (2009).

[7] S. Residori, U. Bertolozzo, A. Montina, F. Lenzini and F. T. Arecchi, Rogue waves in spatially extended optical systems, Fluctuat. Noise Lett., **11**, 1240014 (2009).

[8] J.M. Soto-Crespo, Ph. Grelu and N. Akhmediev, Dissipative rogue waves: extreme pulses generated by passively mode-locked lasers, Phys. Rev. E, **84**, 016604, (2011).

[9] A. Zavyalov, O. Egorov, R. Iliew and F. Lederer, Rogue waves in mode-locked fiber lasers, Phys. Rev. A, **85**, 013828 (2012).

[10] A. F. J. Runge, N. G. R. Broderick, and M. Erkintalo, Observation of soliton explosions in a passively mode-locked fiber laser, Optica **2**, 36-39 (2015).

[11] J. He, S. Xu and K. Porsezian, New types of rogue wave in an erbium-doped fiber system, J. Phys. Soc. Japan, **81**, 033002 (2012).

[12] K. Hammani, C. Finot, J. M. Dudley and G. Millot, Optical rogue-wave-like extreme value fluctuations in fiber Raman amplifiers, Opt. Express **16**, 16467–16473 (2008).

[13] J. Kasparian, P. Béjot, J..-P. Wolf, and J. M. Dudley, Optical rogue wave statistics in laser filamentation, Opt. Express **17**, 12070-12075 (2009).

[14] D. Majus, V. Jukhna, G. Valiulis, D. Faccaio and A. Dubietis, Spatiotemporal rogue events in femtosecond filamentation, Phys. Rev A, **83**, 025802 (2011).

[15] K. Hammani, C. Finot and G. Millot, Emergence of extreme events in fiber-based parametric processes driven by a partially incoherent pump wave, Opt. Lett., **34**, 1138–1140 (2009).

[16] F. T. Arecchi, U. Bertolozzo, A. Montina and S. Residori, Granularity and inhomogeneity are joint generators of optical rogue waves, Phys. Rev. Lett., **106**, 153901 (2011).

[17] R. H ohmann, U. Kuhl, H-J. St ockmann, L. Kaplan and E. J. Heller, Freak waves in the linear regime: a microwave study, Phys. Rev. Lett., **104**, 093901 (2010).

[18] D. H. Peregine, "Water waves nonlinear Schr odinger equations and their solutions, J. Aust. Math. Soc. Ser. B, **25**, 16-43 (1983).

[19] N. Akhmediev, A. Ankiewicz, and M. Taki, Waves that appear from nowhere and disappear without a trace, Phys. Lett., A, **373**, 675-678 (2009).

[20] N. Akhmediev, J. M. Soto-Crespo, and A. Ankiewicz, How to excite a rogue wave, Phys. Rev. A, **80**, 043818 (2009).

[21] V. I. Shrira and V. V. Geogjaev, What makes Peregrine soliton so special as a prototype of freak waves?, J. Eng. Math., **67**, 11-12 (2010).

[22] S. Toenger, T. Godin, C. Billet, F. Dias, M. Erkintalo, G. Genty, and J. M. Dudley, Emergent rogue wave structures and statistics in spontaneous modulation instability, Sci. Rep., **5**, 10380 (2015).

[23] B. Kibler, A. Chabchoub, A. Gelash, N. Akhmediev, and V. E. Zakharov, Superregular Breathers in Optics and Hydrodynamics: Omnipresent Modulation Instability beyond Simple Periodicity, Phys. Rev. X, **5**, 041026 (2015).

[24] B. Kibler, J. Fatome, C. Finot, G. Millot, F. Dias, G. Genty, N. Akhmediev, and J. M. Dudley, The Peregrine soliton in nonlinear fiber optics, Nat. Phys., **6**, 790-795 (2010).

[25] B. Kibler, J. Fatome, C. Finot, G. Millot, G. Genty, B. Wetzel, N. Akhmediev, F. Dias, and J. M. Dudley, Observation of Kuznetsov-Ma soliton dynamics in optical fiber, Sci. Rep., **2**, 463 (2012).

[26] A. Picozzi, J. Garnier, T. Hanson, P. Suret, S. Randoux, G. Millot, and D. N. Christodoulides,Optical wave turbulence: toward a unified thermodynamic formulation of statistical nonlinear optics, Phys. Rep. **542**, 1-132 (2014).

[27] P. Walczak, S. Randoux, and P. Surret, Optical Rogue Waves in Integrable Turbulence, Phys. Rev. Lett., **114**, 143903 (2015).

[28] P. Surret, R. El Koussaifi, A. Tikan, C. Evain, S. Randoux, C. Szwaj, and S. Bielawski, Single-shot observation of optical rogue waves in integrable turbulence using microscopy, Nat. Commun., **7**, 13136 (2016).

[29] J. M. Soto-Crespo, N. Devine, and N. Akhmediev, Integrable Turbulence and Rogue Waves: Breathers or Solitons? Phys. Rev. Lett., **116**, 103901 (2016).

[30] N. Akhmediev, J. M. Soto-Crespo, and N. Devine, Rogue waves, probability density functions and spectral features, Phys. Rev. E, **94**, 022212 (2016).

[31] D. Agafontsev and V. E. Zakharov, Integrable turbulence and formation of rogue waves, Nonlinearity, **28**, 2791 (2015).

[32] V. E. Zakharov, Turbulence in integrable systems, Stud. Appl. Math., **122**, 219-234 (2010).

[33] M. Taki, A. Mussot, A. Kudlinski, E. Louvergneaux, M. Kolobov, and M. Douay, Phys. Lett. A, "Third-order dispersion for generating optical solitons, **374**, 691-695 (2010).

[34] K. Hammani, B. Kibler, C. Finot, and A. Picozzi, Emergence of rogue waves from optical turbulence, Phys. Lett. A, **374**, 3585-3589 (2010).

[35] B. Kibler, K. Hammani, C. Michel, C. Finot, and A. Picozzi, Rogue waves, rational solitons and wave turbulence theory, Phys. Lett. A, **375**, 3149-3155 (2011).

[36] L. Allen and J. H. Eberly, *Optical resonance and two-level atoms,* (Dover Publications Inc., New York, 1975).

[37] L. Mokhtarpour and S. A. Ponomarenko, Fluctuating pulse propagation in resonant nonlinear media: self-induced transparency random phase soliton formation, Opt. Express **23**, 30270- 30282 (2015).

[38] A.Betlej, P. Schmitt, P. Sidereas, R. Tracy, C. G. Goedde, and J. R. Thompson, Increased Stokes pulse energy variation from amplified classical noise in a fiber Raman generator, Opt. Express, **13**, 2948–2960 (2005).

[39] E. Landahl, D. Baiocchi, and J. R. Thompson, A simple analytical model for noise shaping by an optical fiber generator, Opt. Commun., **150**, 339–347 (1998).

[40] A. S. Grabtchikov, A. I. Vodtchits, and V. A. Orlovich, Pulse-energy statistics in the linear regine of stimulated Raman scattering with a broad-band pump, Phys. Rev. A., **56**, 1666–1669 (1997).

[41] F. Benabid, G. Bouwmans, J. C. Knight, and P. St. J. Russell, Ultrahigh Efficiency Laser Wavelength Conversion in a Gas-Filled Hollow Core Photonic Crystal Fiber by Pure Stimulated Rotational Raman Scattering in Molecular Hydrogen, Phys. Rev. Lett. **93**, 123903 (2004).

[42] A. Nazarkin, A. Abdolvand, A.V. Chugreev, and P. St.J. Russell, Direct Observation of Self-Similarity in Evolution of Transient Stimulated Raman Scattering in Gas-Filled Photonic Crystal Fibers, Phys. Rev. Lett. **105**, 173902 (2010).

[43] F. Belli, A. Abdolvand, W. Chang, J. C. Travers, and P. St.J. Russell, Vacuum-ultraviolet to infrared supercontinuum in hydrogen-filled photonic crystal fiber, Optica **2**, 292–300 (2015).

[44] F. Flora and L. Giudicotti, Complete calibration of a Thomson scattering spectrometer system by rotational Raman scattering in H_2, Appl. Opt. **26**, 4001–4008 (1987).

[45] L. Mandel and E. Wolf, *Optical Coherence and Quantum Optics* (Cambridge University Press, Cambridge, 1995).

[46] A. Papoulis, *Probability Random Variables, and Stochastic Processes* (McGraw Hill, New York, 1991) 3rd Ed.

[47] J. W. Goodman, *Statistical Optics* (Wiley, New York, 1985).

[48] M. Qasymeh, M. Cada and S. A. Ponomarenko, Quadratic Electro-Optical Kerr Effect: Application to Photonic Devices, IEEE J. Quant. Electron., **44**, 740–746 (2008).

[49] F. Y,. F. Chu and A. C. Scott, "Inverse scattering transform for wave-wave scattering, Phys. Rev. A, **12**, 2060–2064 (1975).

[50] C. R. Menyuk, "Transient solitons in stimulated Raman scattering, Phys. Rev. Lett., **62**, 2937–2940 (1989).

Chapter 5

Non-Gaussian statistics of extreme events in stimulated Raman scattering: the role of coherent memory and source noise

Yashar E. Monfared and Sergey A. Ponomarenko
Published in: Physical Review A, October 2017, Vol. 96, No. 4, 043817
URL: https://journals.aps.org/pra/abstract/10.1103/PhysRevA.96.043817

5.1 Abstract

We explore theoretically and numerically extreme event excitation in stimulated Raman scattering in gases. We consider gas filled hollow core photonic crystal fibers as a particular system realization. We show that moderate amplitude pump fluctuations obeying Gaussian statistics lead to the emergence of heavy-tailed non-Gaussian statistics as coherent seed Stokes pulses are amplified on propagation along the fiber. We reveal the crucial role that coherent memory effects play in causing non-Gaussian statistics of the system. We discover that extreme events can occur even at the initial stage of stimulated Raman scattering when one can neglect energy depletion of an intense, strongly fluctuating Gaussian pump source. Our analytical results in the undepleted pump approximation explicitly illustrate power-law probability density generation as the input pump noise is transferred to the output Stokes pulses.

5.2 Introduction

Rogue waves were originally observed as giant amplitude waves occurring in high seas more frequently than predicted by Gaussian statistics [133, 4, 134]. The concept has subsequently been extended from oceanography to other areas of physics to describe waves of enormous amplitudes, or, in general, extreme statistical events obeying heavy-tailed probability distributions [135]. Optics has proven to be an especially fertile ground for extreme event and, in particular, optical rogue wave (ORW) exploration [136, 137]. To date, ORWs have been discovered theoretically and/or experimentally in supercontinuum generating optical fibers [7, 138, 139], optical cavities [140, 141], passively mode-locked fiber lasers [142, 143, 144], erbium-doped fiber systems [145], Raman fiber amplifiers [98, 146], spatiotemporal structures and laser filamentation [147, 148, 149], parametric processes [101], stimulated Raman scattering (SRS) [17] and even in linear light propagation inside multimode fibers [150].

As ORWs are inherently statistical structures, their universal statistical signature is encapsulated in heavy-tailed non-Gaussian statistics of their amplitudes and/or powers. Non-Gaussian statistics emergence in nonlinear media has been a central theme of the burgeoning field of nonlinear statistical optics [151]. Specifically, non-Gaussian statistics generation and ORW excitation with a source field comprised of a coherent (cw) condensate component mixed with Gaussian noise has been extensively examined numerically [25, 118, 152, 24, 181, 115, 154] and experimentally [24, 181] within the framework of the 1D nonlinear Schr odinger equation (NLSE) [116]. The particulars of system statistics were shown to be very sensitive to initial conditions, strongly depending on the ratio of the condensate to random component amplitudes and the coherence time of the source [25, 118, 154]. Lately, the generation of highly non-Gaussian, heavy-tailed probability distributions has been numerically discovered and explored in stimulated Raman scattering (SRS) [17].

The just mentioned two models profoundly differ in many respects. While the first encompasses a class of weakly nonlinear wave systems with instantaneous response (no memory), governed by the integrable 1D NLSE, the second features a strong nonlinearity, long memory, and is, in general, nonintegrable. In this context, it is

instructive to explore the role of coherent memory in causing non-Gaussian statistics of nonlinear systems. SRS appears to be a suitable candidate to address this question because its coherent memory is controlled by relative magnitudes of a characteristic SRS interaction and the Raman medium relaxation times. In the limit of an infinitely long Raman relaxation time, the system has extremely long memory and the SRS equations are integrable [185, 186]. Another fundamental issue concerns the source noise modelling in rogue-wave generating systems.

In our previous work on statistical SRS [17], we examined the case of noisy Stokes input pulses, amplified by a coherent pump in a gas filled hollow-core photonic crystal fiber (HC PCF). In this work, we study the same system under the condition that seed Stokes pulses are perfectly coherent, but pump pulses carry fluctuations obeying thermal statistics. This type of noisy pump can be implemented with amplitude-modulated statistically stationary sources or with multimode lasers operating at a large number of uncorrelated modes, yielding thermal-like source statistics [157]. We show, in particular, that SRS with a noisy pump is conducive to non-Gaussian statistics generation. We demonstrate that the Stokes pulse power PDF acquires a long tail at the fiber exit. The PDF tail extent strongly increases as the system approaches the long-memory integrability limit. In sharp contrast to the previously studied SRS with noisy input Stokes pulses, the Stokes pulse statistics is virtually unaffected by the source coherence time. We examine separately the Stokes pulse area PDF behaviour in the undepleted pump approximation regime. We analytically demonstrate that the PDF exhibits power-like behaviour, failing to attain finite moments over fairly short propagation distances. This behaviour points to the feasibility of ORW excitation over remarkably short distances in this SRS regime. We stress that this conclusion is independent of the initial Stokes pulse profile because our analytical theory gives a universal PDF in the undepleted pump approximation.

This work is organized as follows. In the next section, we introduce our theoretical model, including key dimensionless parameters describing the SRS physics. We formulate the statistical ensemble of fluctuating pump pulses in Section III. We then present our analytical theory in the undepleted pump approximation in Section IV. Next, we present the results of our numerical simulations in Section V. Finally, we

summarize our findings in Section VI.

5.3 Theoretical model and key dimensionless parameters

We consider stimulated Raman scattering in a gas sample of molecular hydrogen, filling the core of a hollow core photonic crystal fiber (HC PCF). The fiber is assumed to be designed such that only pump and the first Stokes modes lie within the fiber transparency window. In the usual weak excitation limit, the governing SRS equations in the co-propagating geometry can be written in the dimensionless variables as [17]

$$\partial_Z \mathcal{E}_p = i\kappa\sigma\mathcal{E}_s, \tag{5.1}$$

$$\partial_Z \mathcal{E}_s = i\kappa^{-1}\sigma^*\mathcal{E}_p, \tag{5.2}$$

and

$$\partial_T \sigma = -\Gamma\sigma + i\mathcal{E}_p\mathcal{E}_s^* \tag{5.3}$$

Here we introduced dimensionless pump and Stokes pulse amplitudes, $\mathcal{E}_p$ and $\mathcal{E}_s$; the distance and time are scaled to the characteristic SRS interaction length and time, respectively, $Z = z/L_{\mathrm{SRS}}$ and $T = \tau/T_{\mathrm{SRS}}$, where $\tau = t - z/v_g$ is a time coordinate in the reference frame moving with the pulse group velocity v_g.

The characteristic SRS interaction length and time scales are defined as

$$L_{\mathrm{SRS}} = \left(\frac{2\epsilon_0 c}{N r_{eff}}\right)\sqrt{\frac{n_p n_s}{\omega_p \omega_s}}, \tag{5.4}$$

and

$$T_{\mathrm{SRS}} = \left(\frac{2\hbar\epsilon_0 c n_p}{r_{eff}\langle I_{p0}\rangle}\right). \tag{5.5}$$

Here $\omega_{p,s}$ and $n_{p,s}$ are the carrier frequencies and refractive indices of the pump and Stokes pulses, respectively, N is a medium density, $\langle I_{p0}\rangle$ is a peak average pump intensity at the source, the angle brackets denoting ensemble averaging, and $r_{eff} = \frac{1}{\hbar}\sum_i \frac{d_{3i}d_{i1}}{\omega_{i3}+\omega_{i1}-\omega_p-\omega_s}$ is a Raman transition dipole matrix element at the exact Raman resonance [124, 158].

Further, we introduced $\kappa = \sqrt{\omega_p n_s/\omega_s n_p}$ and a coherent memory parameter Γ. The latter, defined as

$$\Gamma = \gamma\, T_{\rm SRS}, \tag{5.6}$$

where γ is a medium dipole phase relaxation rate, determines the extent of system memory and the system proximity to the integrability limit. Indeed, whenever $\Gamma \ll 1$, the SRS is highly transient with an extremely long memory time and its governing equations approach the mathematical integrability limit, $\Gamma = 0$, first discussed in Refs. [185, 186]. Thus, Γ is a key dimensionless parameter of the system as its magnitude distinguishes quasi-cw, $\Gamma \gg 1$, from transient, $\Gamma \ll 1$, SRS regimes. While SRS in the former regime has a relatively short memory, it is described by nearly integrable equations with long memory in the transient regime.

We stress that the magnitude of Γ demarcates the boundary between quasi-cw and transient SRS regimes in the nonlinear domain where pump depletion is no longer negligible. One should then exercise caution employing the usual "rule-of-thumb criterion classifying SRS with pump pulses much shorter than the Raman relaxation time as transient [159]. The latter criterion, based on quantum SRS theory in the undepleted pump approximation [160], can prove too restrictive in the nonlinear domain. Indeed, coherent oscillations of pump and Stokes pulse profiles, which are unambiguous signatures of the transient dynamics, have been vividly displayed in the recent SRS experiments with pulses as long as, or even longer than the Raman relaxation time [40] . A typical period of such oscillations in Ref. [40] was of the order of $T_{\rm SRS} \ll \gamma^{-1}$, implying that $\Gamma \ll 1$.

5.4 Input pump and Stokes pulses and statistical ensemble formulation

We consider a pump source pulse composed of a coherent Gaussian and a random component such that

$$\mathcal{E}_p(T,0) = e^{-(T-T_0)^2/2T_*^2} + \Delta\mathcal{E}_p(T), \tag{5.7}$$

where T_0 is a (dimensionless) pulse peak time. Such a source pulse can be experimentally realized by coherently combining a Gaussian pulse with a partially coherent one at a beam splitter, for example. The partially coherent (random) component can be generated by time modulating a statistically stationary source employing an electro-optical modulator, operating on the basis of either linear [6] or quadratic [161] electro-optical effect. All this is readily achievable in the nanosecond pulse range, adequate for SRS in gas-filled HC PCFs. The input Stokes pulse field reads

$$\mathcal{E}_s(T,0) = \sqrt{\frac{n_p P_s}{n_s P_p}}\, e^{-(T-T_0)^2/2T_*^2}, \tag{5.8}$$

where $P_{p,s}$ are peak powers of the (coherent components of) pump and Stokes pulses and $n_{p,s}$ are the refractive indices at the pump ω_p and Stokes ω_s frequencies, respectively. Further, we assume the pump and Stokes pulses to have the same duration (in dimensionless units) T_* at the source. Such a Stokes source can be produced in a separate fiber using the pump coherent component and quantum noise as inputs. A coherent macroscopic Stokes pulse is then formed as quantum noise is "cleaned up [162]. This Stokes input can then be transported back into the original fiber to study ORW formation in the amplification regime of SRS.

We express the mutual intensity of the random component $\Delta\mathcal{E}_p$ using a celebrated Gaussian Schell model (GSM) of statistical optics [232]. The GSM presumes that both the intensity and the temporal degree of coherence of the fluctuating part have Gaussian profiles. We assume, for simplicity, that the fluctuating and coherent components have the same width T_p at the source. The mutual intensity of the random component, defined as

$$\Gamma(T_1,T_2,0) \equiv \langle \Delta\mathcal{E}_p^*(T_1,0)\Delta\mathcal{E}_p(T_2,0)\rangle, \tag{5.9}$$

can then be written as

$$\begin{aligned}\Gamma(T_1,T_2,0) &= \left(\frac{\Delta P_p}{P_p}\right)\exp\left[-\frac{(T_1-T_0)^2+(T_2-T_0)^2}{2T_*^2}\right] \\ &\quad\times\exp\left[-\frac{(T_1-T_2)^2}{2T_c^2}\right].\end{aligned} \tag{5.10}$$

Here $\Delta P_p/P_p$ is a ratio of the random to coherent component peak powers, and T_c is a coherence time of the random component. It follows from Eq. (2) that the correlation spectrum of GSM is also Gaussian. The GSM is a generic statistical source model, widely used in statistical optics [232]. For instance, a Gaussian correlation spectrum was shown to better approximate statistical properties of supercontinuum sources than does another commonly used model featuring a one-photon-per-mode spectrum [164].

We can now represent the random component of the source using the Karhunen-Loève expansion [231, 120]

$$\Delta\mathcal{E}_p(T,0) = \sum_n c_n\psi_n(T), \tag{5.11}$$

where the random coefficients $\{c_n\}$ are statistically orthogonal such that

$$\langle c_n^* c_m\rangle = \lambda_n\delta_{mn}, \tag{5.12}$$

and the coherent modes are orthonormal, implying that

$$\int_{-\infty}^{\infty} dT\,\psi_n^*(T)\psi_m(T) = \delta_{mn}. \tag{5.13}$$

The mutual coherence function is then represented as a Mercer-type series in coherent modes as [232]

$$\Gamma(T_1,T_2,0) = \sum_n \lambda_n\psi_n^*(T_1)\psi_n(T_2). \tag{5.14}$$

The coherent modes $\{\psi_n\}$ are determined by solving the following Fredholm integral equation

$$\int_{-\infty}^{\infty} dT_1\,\Gamma(T_1,T_2,0)\psi_n(T_1) = \lambda_n\psi_n(T_2). \tag{5.15}$$

In the GSM case, Eq. (7) can be analytically solved and all modes and the eigenvalues $\{\lambda_n\}$ determined such that [232]

$$\psi_n(T) = \left(\frac{2\xi}{\pi}\right)^{1/4}\left(\frac{1}{2^n n!}\right)^{1/2} H_n[\sqrt{2\xi}(T-T_0)]e^{-\xi(T-T_0)^2}, \tag{5.16}$$

where $H_n(x)$ is a Hermite polynomial of the order n, and

$$\lambda_n = \sqrt{\pi} T_* \left(\frac{\Delta P_p}{P_p} \right) \frac{(\alpha + \xi)\beta^n}{(\alpha + \beta + \xi)^{n+1}}. \tag{5.17}$$

Here we introduced the notations

$$\alpha = \frac{1}{2T_*^2}, \quad \beta = \frac{1}{2T_c^2}, \tag{5.18}$$

and

$$\xi = \sqrt{\alpha^2 + 2\alpha\beta}. \tag{5.19}$$

We note that the mode powers, Eq. (9), are normalized such that they add up to the total power of the random component (relative to the coherent component power).

To complete the ensemble description, we must specify the random amplitude statistics to any order such that it is consistent with Eq. (4). Expressing the complex random amplitudes $\{c_n\}$ in the polar form as

$$c_n = \sqrt{i_n} e^{i\phi_n}, \tag{5.20}$$

we stipulate that the complex amplitudes be independent random variables; the phases are assumed to be uniformly distributed in the interval $-\pi \leq \phi_n \leq \pi$, while $\{i_n\}$'s obey the exponential distribution such that

$$\mathcal{P}(i_n) = \frac{1}{\lambda_n} e^{-i_n/\lambda_n}; \quad i_n \geq 0. \tag{5.21}$$

If coherent modes correspond to natural oscillation modes of the source, such a source can be interpreted as a multimode laser source with each mode having a random phase and a strongly fluctuating power. The overall field at the source is a superposition of uncorrelated mode fields. As each mode obeys Gaussian statistics, the overall source PDF is guaranteed to be Gaussian (thermal-like) for any source coherence time T_c [17].

5.5 Undepleted pump approximation

We first focus on the case of a very long, high-power pump pulse, $t_p \gg t_s$ and $P_p \gg P_s$ such that the pump pulse can be treated as a plane wave. In the undepleted pump approximation (UPA), $\mathcal{E}_p = const$ and the SRS equations linearize. They can then be solved by a Fourier transform technique. Introducing a Fourier transform of the Stokes field,

$$\tilde{\mathcal{E}}_s(\Omega, Z) = \int_{-\infty}^{\infty} dT\, e^{-i\Omega T} \mathcal{E}_s(T, Z), \tag{5.22}$$

where Ω is a frequency shift from the Stokes carrier and the Stokes pulse area,

$$\mathcal{A}_s(Z) = \int_{-\infty}^{\infty} dT\, \mathcal{E}_s(T, Z), \tag{5.23}$$

we can conclude at once that the latter is a component of the former at the carrier frequency, i. e.,

$$\mathcal{A}_s(Z) = \tilde{\mathcal{E}}_s(0, Z). \tag{5.24}$$

This observation allows to quickly solve linearized Eqs. (5.1) through (5.3) to obtain for the area the expression

$$\mathcal{A}_s(Z) = \mathcal{A}_{s0} \exp\left(\frac{|\mathcal{E}_p|^2 Z}{\kappa\Gamma}\right). \tag{5.25}$$

The area describes a universal dynamics of Stokes pulses: whatever the initial pulse shape, the area grows exponentially.

Next, we can determine the PDF of the area magnitude under the UPA. We assume a strong coherent pump with small intensity fluctuations such that the (dimensionless) intensity can be written as

$$|\mathcal{E}_p|^2 = 1 + i_p - \langle i_p \rangle \simeq 1 + i_p, \quad \langle i_p \rangle \ll 1. \tag{5.26}$$

This model is in sync with our general ensemble construct of Sec. III. The intensity fluctuations are specified by the PDF

$$\mathcal{P}(i_p) = \frac{1}{\langle i_p \rangle}\, e^{-i_p/\langle i_p \rangle}. \tag{5.27}$$

The area PDF is then given by the expression

$$\mathcal{P}(|\mathcal{A}_s|, Z) = \langle \delta \left[|\mathcal{A}_s| - |\mathcal{A}_s(Z)| \right] \rangle. \tag{5.28}$$

A straightforward calculation using the $\delta-$function property

$$\delta[f(x)] = \sum_n \frac{1}{|f'(x_n)|} \delta(x - x_n), \tag{5.29}$$

where x_n is an nth root of $f(x)$, $f(x_n) = 0$, yields

$$\begin{aligned} \mathcal{P}(|\mathcal{A}_s|, Z) &= \frac{\kappa\Gamma\, e^{1/\langle i_p \rangle}}{\langle i_p \rangle Z |\mathcal{A}_{s0}|} \left| \frac{\mathcal{A}_s}{\mathcal{A}_{s0}} \right|^{-1-\frac{\kappa\Gamma}{\langle i_p \rangle Z}} \\ &\quad \times \theta\left(|\mathcal{A}_s| - |\mathcal{A}_{s0}| e^{Z/\kappa\Gamma} \right). \end{aligned} \tag{5.30}$$

Here $\theta(x)$ is a unit step function. It can be easily verified that the PDF is normalized to unity at any $Z = const$ and Eq. (5.30) works for any $Z \neq 0$; it is singular at $Z = 0$ because $\mathcal{P}$ is a δ-function at the source. We note in passing that a qualitatively similar form of PDF was derived for Stokes wave statistics in silica glass Raman amplifiers [146]. However, the long coherent memory of SRS in gases makes our system fundamentally different from silica glass Raman amplifiers with an instantaneous medium response. Further, we consider pump pulses with a strong coherent component superimposed with weak fluctuations whereas the authors of [146] discuss the opposite regime of incoherent pump input.

The PDF of Eq. (5.30) is displayed in Fig. 5.1 in a logarithmic scale at several propagation distances. It can be inferred from Eq. (5.30) that the PDF shape is determined by two factors. First, the unit step-function describes a shift toward larger areas upon propagation due to the Stokes pulse amplification. Second, the power-law dependence is brought about by the noise transfer from the pump to the Stokes pulse in the course of SRS. Qualitatively, the interplay of these two trends fixes the Stokes area PDF shape. Further analysis of Eq. (5.30) reveals that the area PDF becomes so broad-tailed, it ceases to attain finite moments at the distances

$$Z \geq Z_* = \kappa\Gamma / \langle i_p \rangle, \tag{5.31}$$

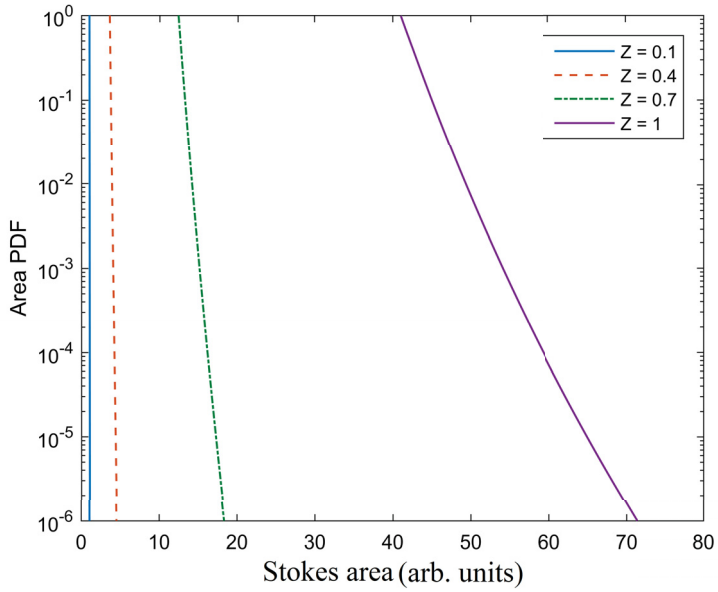

Figure 5.1: Analytics: Stokes Area PDF in the logarithmic scale at several propagation distances Z. Numerical values of the parameters are: $T_p = 10^2 T_s$, $P_s = 10^{-3} P_p$ and $\Gamma = 0.24$.

estimating for our regime $\kappa \simeq 1$, $\Gamma \sim 1$, $\langle i_p \rangle \sim 10^{-2}$, corresponding to 10% amplitude noise in the pump, $z_* \sim 100 L_{\rm SRS} \simeq 10$ cm. It follows from Eq. (5.31) that z_* is controlled by the pump noise intensity and coherent memory of the system; it can drop to a fraction of $L_{\rm SRS}$ for sufficiently long coherent memory times (small Γ) or noisy enough pump. Thus, rogue-wave like phenomena can potentially unfold at very short propagation distances and be quantitatively described by our analytical theory. We stress that this conclusion is applicable to input Stokes pulses of any shape.

To test our UPA predictions, we carried out numerical simulations for the long intense pump case such that $T_p = 10^2 T_s$ and $P_s = 10^{-3} P_p$. We use $i_p = 10^{-2}$ and $\Gamma = 0.24$ in our numerical simulations. In Fig. 5.2 we display the average pump and Stokes pulse profiles at $Z = 0.3$ indicating that the UPA still holds at this propagation distance. We then exhibit the Stokes area PDF at several propagation distances and compare it with the corresponding analytical results in Fig. 5.3. It can be seen in the figure that while the theory and simulation agree very well up to $Z = 0.3$ for our pump noise level and coherent memory time, the two start deviating at $Z = 0.5$ and differ substantially at $Z = 0.7$. Thus the UPA breaks down rather quickly in this

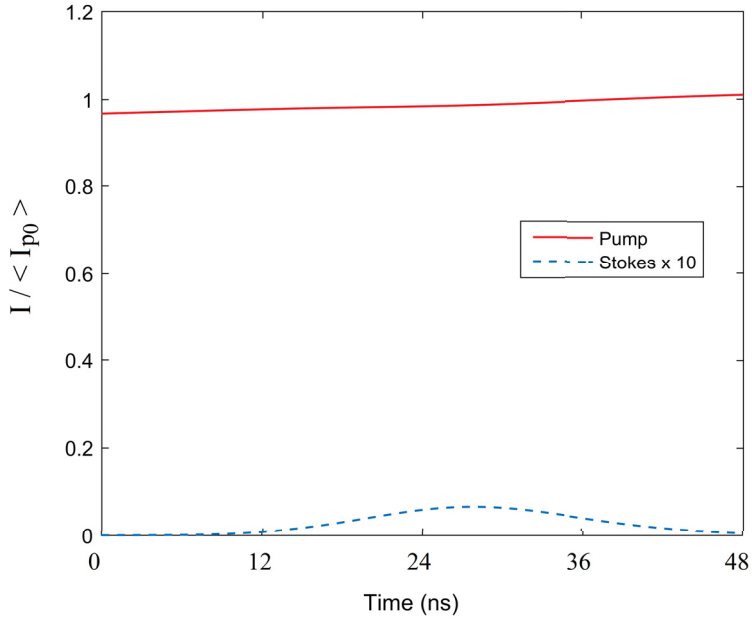

Figure 5.2: Intensity profiles of the pump and Stokes modes at $Z = 0.3$. Numerical values of the parameters are: $T_p = 10^2 T_s$, $P_s = 10^{-3} P_p$ and $\Gamma = 0.24$.

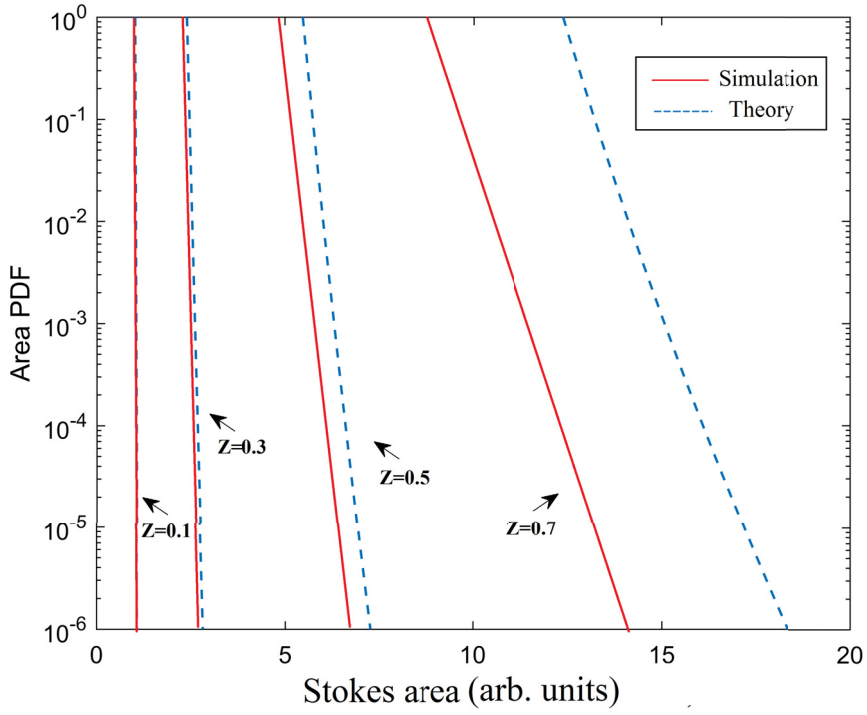

Figure 5.3: Analytical versus numerical Stokes area PDF profiles at several propagation distances inside the fiber. Numerical values of the parameters are: $T_p = 10^2 T_s$, $P_s = 10^{-3} P_p$ and $\Gamma = 0.24$.

parameter regime. The ORW formation can occur at distances of the order $Z \sim 0.1$, though, provided coherent memory, Γ^{-1}, is boosted by two orders of magnitude for the same pump noise level. This can be achieved by increasing the pump intensity, for instance, which would incidentally extend the UPA applicability range. However, the true significance of our UPA theory lies in its ability to qualitatively predict the physical nature of the PDF transformation in SRS with noisy pump. We will use the gained insights to explain the emergence of non-Gaussian statistics beyond the UPA in the following section.

5.6 Non-Gaussian statistics beyond the undepleted pump approximation

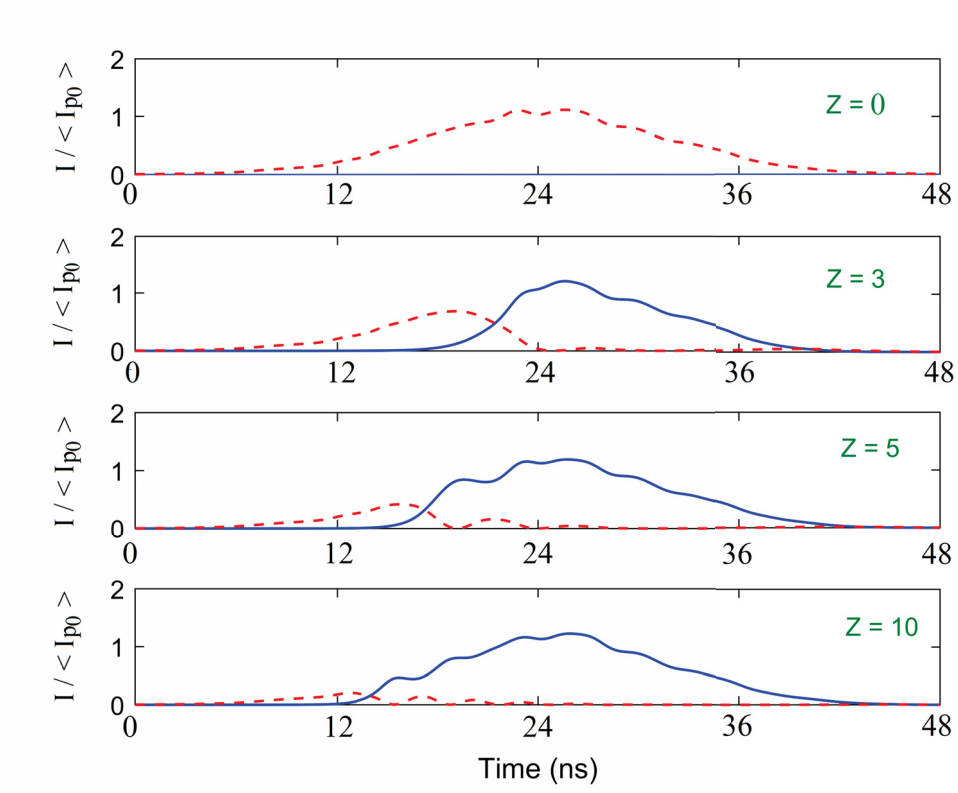

Figure 5.4: Average intensity profiles of the pump (dashed line) and Stokes (solid line) pulses at several propagation distances. The coherent memory parameter is taken to be $\Gamma = 0.24$.

We now numerically simulate SRS with fluctuating pump pulses beyond the UPA.

As a generic realization of the system, we consider a hydrogen-filled HC PCF with typical parameters representative of the HC PCFs previously designed for SRS experiments [124]. The HC PCF has a low-loss transmission window between 1030 and 1150 nm. As a result, only the pump at $\lambda_p = 1064$ nm and first Stokes at $\lambda_s = 1134$ nm modes, interacting with the J=1 to J=3 rotational transition, can co-propagate in the HC PCF. The coherent component of the pump is supplied by a $W_p = 100$ μJ laser operating at 1064 nm. The characteristic Raman interaction length and SRS interaction time are $L_{\mathrm{SRS}} = 1$ mm and $T_{\mathrm{SRS}} = 1.2$ ns, respectively. We assume the relaxation time of hydrogen in the HC PCF to be $\gamma^{-1} = 5$ ns [158]. The coherent memory parameter Γ is then $\Gamma = 0.24$; it can be controlled by adjusting the pump energy W_p. The input pump (coherent component) and Stokes pulses are assumed to be Gaussian of the same duration $t_p = t_s = t_* = 10$ ns, but the Stokes input is much weaker such that the Stokes input energy is just 1% of the pump one. The pump and Stokes pulses centered at $t_0 = 24$ ns. We treat the pump source noise level, quantified by $\Delta P_p/P_p$, as a variable in our simulations.

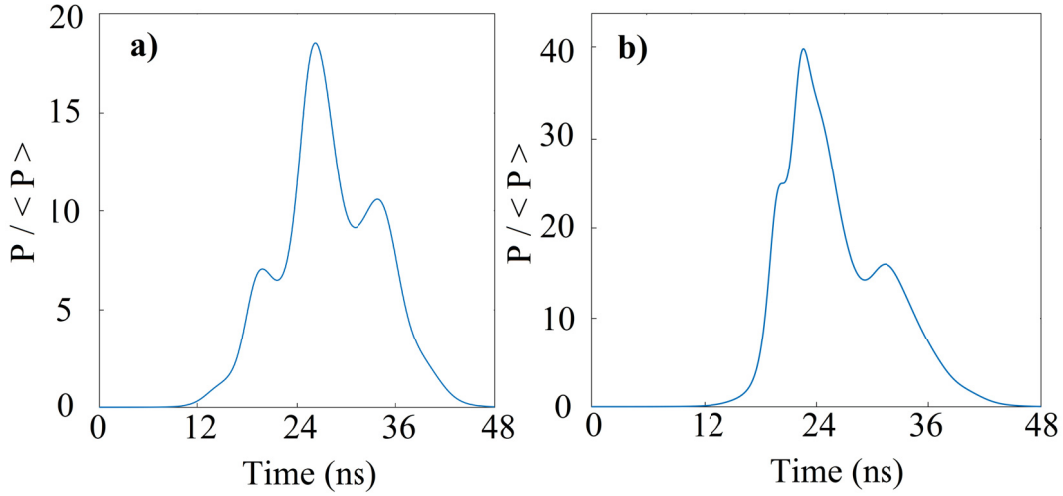

Figure 5.5: Stokes pulse ensemble realization at the fiber exit for (a) $\Delta P_p/P_p = 0.3$ and (b) $\Delta P_p/P_p = 0.5$. The pulse power is scaled to the average power $\langle P \rangle$ at the fiber exit. In both cases, $\Gamma = 0.24$.

In Fig. 5.4 we display the average intensities of the pump and Stokes pulses at several propagation distances. As is expected, the Stokes pulse intensity grows at the pump expense. Notice characteristic oscillations experienced by both average intensity profiles which are unambiguous signatures a transient SRS regime. We then

exhibit a time series of the peak Stokes power in Fig. 5.5 for $\Delta P_p/P_p = 0.3$ (left) and $\Delta P_p/P_p = 0.5$ (right) at the fiber exit. It can be inferred from the figure that although extreme events do take place in both cases–the peak power reaches magnitudes around 20 to 40 times its average value at the fiber exit–the maximum attainable power level strongly depends on the pump noise level. In particular, the curve in Fig. 5.5.b can be interpreted to represent a bona fide ORW with a peak pulse amplitude exceeding 6 times its average value at the fiber output.

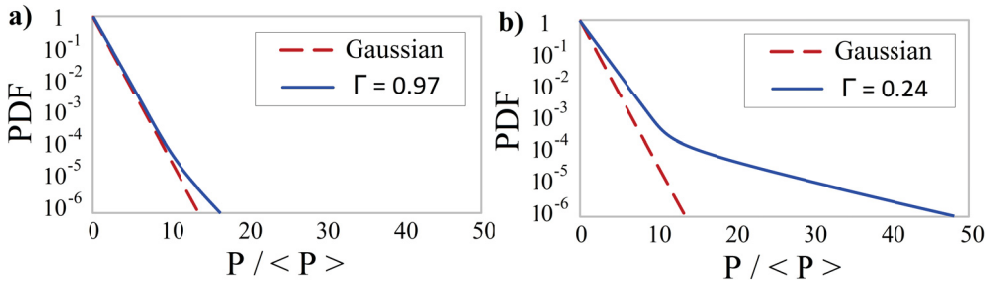

Figure 5.6: Peak power PDF of a Stokes pulse ensemble at the fiber output for (a) relatively short, $\Gamma = 0.97$, and (b) rather long, $\Gamma = 0.24$, coherent memory times. The pulse power is scaled to the average power $\langle P \rangle$ at the fiber exit. The source noise level is $\Delta P_p/P_p = 0.5$.

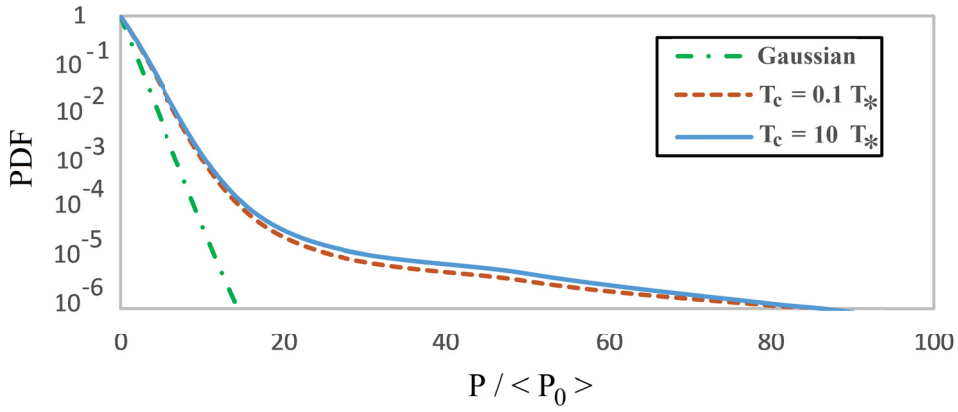

Figure 5.7: Peak power PDF of a Stokes pulse ensemble at the fiber output for relatively coherent (solid line), and nearly incoherent (dashed line) sources. The pulse power is scaled to the average pump power $\langle P_0 \rangle$ at the source. The source noise level is $\Delta P_p/P_p = 0.01$ and $\Gamma = 0.24$.

Next, we examine the Stokes power statistics in the present SRS regime. In Fig. 5.6, we exhibit the peak Stokes power PDF in a logarithmic scale for the two cases: (a) relatively short system memory with $\Gamma = 0.97$ and (b) rather long system memory

with $\Gamma = 0.24$. The peak Stokes power is evaluated at the fiber output and scaled to its average value there. The non-Gaussian behaviour of the PDF is manifest in both cases on comparing it with a straight line Gaussian PDF of the peak pump power. Further, we can infer from Fig. 5.6 that the peak Stokes power PDF acquires a long tail and the tail extent markedly increases as the system coherent memory is enhanced. This is because the enhanced coherent memory implies the SRS interaction is robust against medium dipole damping, thereby accommodating efficient noise transfer from the pump to the Stokes pulses. This point illustrates the crucial role the coherent memory effects play in ensuring that extreme events take place in the system. Finally, we exhibit the peak Stokes power PDF for rather coherent and nearly incoherent pump sources in Fig. 5.7. It is evident from the figure that in sharp contrast to the noisy Stokes SRS case, the PDF in the present regime is virtually independent of the source pump coherence time. This circumstance can be explained by noting again the different physical origin of PDF tails–and hence ORW emergence–in the two SRS regimes that we have already discussed. Specifically, the PDF structure in the present situation depends solely on the amount of pump noise, but not on the noise particulars, including its spectrum and, by extension, its coherence time.

5.7 Summary

We explored the emergence of non-Gaussian statistics and optical rogue waves in stimulated Raman scattering in gases, focusing on a gas filled, hollow core photonic crystal fiber as a particular system realization. We specifically examined the role of coherent memory and source noise modelling in extreme event excitation in the system. We have demonstrated the crucial role that coherent memory plays in triggering heavy-tailed statistics of the system in the situations when the input Stokes or pump pulses are noisy. However, the non-Gaussian statistics emergence has fundamentally different physical origins in the two cases. On the one hand, we demonstrated earlier [17] that heavy-tailed statistics and ORWs result from the competition for the pump energy among coherent modes constituting a statistical Stokes input. On the other hand, we have shown here that the non-Gaussian statistics and ORW excitation

in SRS with noisy pump can be attributed to noise transfer from the pump to initially coherent Stokes pulses. We have developed the analytical theory of such noise transfer in the system in the initial stage of SRS, well described within the undepleted pump approximation. We also discussed the parameter regime in which the emergent extreme events can be quantitatively described under the UPA. The gained insights enabled us to interpret our numerical findings beyond the undepleted pump approximation which qualitatively follow the same scenario as was discovered under the UPA.

Bibliography

[1] A.I. Dyachenko and V. E., Zaklharov, Modulation instability of Stokes waves $\Longrightarrow$ freak wave, JETP Lett., **81**, 255 (2005).

[2] V. E. Zakharov, A. I. Dyachenko and A. O. Prokofiev, Freak waves as nonlinear stage of Stokes wave modulation instability, Eur. J. Mech. B, **25**, 677 (2006).

[3] C. Kharif, E. Pelinovsky, and A. Slunyaev, *Rogue waves in ocean* (Springer, 2009).

[4] M. Onorato, S. Residori, U. Bertolozzo, A. Montina and F. T. Arecchi, Rogue waves and their generating mechanisms in different physical contexts, Phys. Rep. **528**, 47 (2013).

[5] J. M.Dudley, F. Dias, M. Erkintalo and G. Genty, Instabilities, breathers, and rogue waves in optics, Nature Photon., **9**, 306 (2015).

[6] N. Akhmediev, B. Kibler, F. Baronio, M. Belic, W-P Zhong, Y. Zhang, W. Chang, J. M. Soto-Crespo, P. Vouzas, P. Grelu, C. Lecaplain, K. Hammani, S. Rica, A. Picozzi, M. Tlidi, K. Panajotov, A. Mussot, A. Bendahmane, P. Szriftgiser, G. Genty, J. Dudley, A. Kudlinski, A. Demircan, U. Morgner, S. Amiranashvili, C. Bree, G. Steinmeyer, C. Masoller, N. G. R. Broderick, A. F. J. Runge, M. Erkintalo, S. Residori, U. Bortolozzo, F. T. Arecchi, S. Wabnitz, C. G. Tiofack, S. Coulibaly and M. Taki, Roadmap on optical rogue waves and extreme events, J. Opt., **18**, 063001 (2016).

[7] D. R. Solli, C. Ropers, P. Koonath and B. Jalali, Optical rogue waves, Nature (London) 450, 1054 (2007).

[8] M. Erkintalo, G. Genty, and J. M. Dudley, Rogue-wave-like characteristics in femtosecond supercontinuum generation, Opt. Lett., **34** 2468 (2009).

[9] B. Kibler, C. Finot and J. M. Dudley, Soliton and rogue wave statistics in supercontinuum generation with two zero dispersion wavelengths, Eur. Phys. J., **173**, 289 (2009).

[10] A. Montina, U. Bertolozzo, S. Residori, and F. T. Arecchi, Non-Gaussian statistics and extreme waves in a nonlinear optical cavity, Phys. Rev. Lett., **103**, 173901 (2009).

[11] S. Residori, U. Bertolozzo, A. Montina, F. Lenzini and F. T. Arecchi, Rogue waves in spatially extended optical systems, Fluctuat. Noise Lett., **11**, 1240014 (2009).

[12] J.M. Soto-Crespo, Ph. Grelu and N. Akhmediev, Dissipative rogue waves: extreme pulses generated by passively mode-locked lasers, Phys. Rev. E, **84**, 016604, (2011).

[13] A. Zavyalov, O. Egorov, R. Iliew and F. Lederer, Rogue waves in mode-locked fiber lasers, Phys. Rev. A, **85**, 013828 (2012).

[14] A. F. J. Runge, N. G. R. Broderick, and M. Erkintalo, Observation of soliton explosions in a passively mode-locked fiber laser, Optica 2, 36 (2015).

[15] J. He, S. Xu and K. Porsezian, New types of rogue wave in an erbium-doped fiber system, J. Phys. Soc. Japan, **81**, 033002 (2012).

[16] K. Hammani, C. Finot, J. M. Dudley and G. Millot, Optical rogue-wave-like extreme value fluctuations in fiber Raman amplifiers, Opt. Express 16, 16467 (2008).

[17] K. Hammani, A. Picozzi, and C. Finot, Extreme statistics in Raman fiber amplifiers: From analytical description to experiments, Opt. Commun., **284**, 2594 (2011).

[18] J. Kasparian, P. Béjot, J..-P. Wolf, and J. M. Dudley, Optical rogue wave statistics in laser filamentation, Opt. Express **17**, 12070 (2009).

[19] D. Majus, V. Jukhna, G. Valiulis, D. Faccaio and A. Dubietis, Spatiotemporal rogue events in femtosecond filamentation, Phys. Rev A, **83** 2, (2011).

[20] P. M. Lushnikov and N. Vladimirova, Non-Gaussian statistics of multiple filamentation, Opt. Lett., **35**, 1965 (2010).

[21] K. Hammani, C. Finot and G. Millot, Emergence of extreme events in fiber-based parametric processes driven by a partially incoherent pump wave, Opt. Lett., **34**, 1138 (2009).

[22] Y. E. Monfared and S. A. Ponomarenko, Non-Gaussian statistics and optical rogue waves in stimulated Raman scattering, Opt. Express, **25**, 5941 (2017).

[23] F. T. Arecchi, U. Bertolozzo, A. Montina and S. Residori, Granularity and inhomogeneity are joint generators of optical rogue waves, Phys. Rev. Lett., **106**, 153901 (2011).

[24] A. Picozzi, J. Garnier, T. Hanson, P. Suret, S. Randoux, G. Millot, and D. N. Christodoulides, Optical wave turbulence: toward a unified thermodynamic formulation of statistical nonlinear optics, Phys. Rep. **542**, 1-132 (2014).

[25] K. Hammani, B. Kibler, C. Finot, and A. Picozzi, Emergence of rogue waves from optical turbulence, Phys. Lett. A, **374**, 3585 (2010).

[26] B. Kibler, K. Hammani, C. Michel, C. Finot, and A. Picozzi, Rogue waves, rational solitons and wave turbulence theory, Phys. Lett. A, **375**, 3149 (2011).

[27] S. Toenger, T. Godin, C. Billet, F. Dias, M. Erkintalo, G. Genty, and J. M. Dudley, Emergent rogue wave structures and statistics in spontaneous modulation instability, Sci. Rep., **5**, 10380 (2015).

[28] D. Agafontsev and V. E. Zakharov, Integrable turbulence and formation of rogue waves, Nonlinearity, **28**, 2791 (2015).

[29] P. Walczak, S. Randoux, and P. Surret, Optical Rogue Waves in Integrable Turbulence, Phys. Rev. Lett., **114**, 143903 (2015).

[30] P. Surret, R. El Koussaifi, A. Tikan, C. Evain, S. Randoux, C. Szwaj, and S. Bielawski, Single-shot observation of optical rogue waves in integrable turbulence using microscopy, Nat. Commun., **7**, 13136 (2016).

[31] N. Akhmediev, J. M. Soto-Crespo, and N. Devine, Rogue waves, probability density functions and spectral features, Phys. Rev. E, **94**, 022212 (2016)

[32] V. E. Zakharov, Turbulence in integrable systems, Stud. Appl. Math., **122**, 219 (2010).

[33] F. Y,. F. Chu and A. C. Scott, Inverse scattering transform for wave-wave scattering, Phys. Rev. A, **12**, 2060 (1975).

[34] D. J. Kaup, Creation of a soluton out of dissipation, Physica D, **19**, 125 (1986).

[35] J. W. Goodman, *Statistical Optics* (Wiley, New York, 1985).

[36] F. Benabid, G. Bouwmans, J. C. Knight, and P. St. J. Russell, Ultrahigh Efficiency Laser Wavelength Conversion in a Gas-Filled Hollow Core Photonic Crystal Fiber by Pure Stimulated Rotational Raman Scattering in Molecular Hydrogen, Phys. Rev. Lett. **93**, 123903 (2004).

[37] F. Flora and L. Giudicotti, Complete calibration of a Thomson scattering spectrometer system by rotational Raman scattering in H_2, Appl. Opt. **26**, 4001 (1987).

[38] F. Benabid and P. J. Roberts, Linear and nonlinear properties of photonic crystal fibers, J. Mod. Opt., **58**, 87 (2011).

[39] M. G. Raymer and J. Mostowski, Stimulated Raman scattering: Unified theory of spontaneous initiation and spatial propagation, Phys. Rev. A, **24**, 1980 (1981).

[40] A. Nazarkin, A. Abdolvand, A.V. Chugreev, and P. St.J. Russell, Direct Observation of Self-Similarity in Evolution of Transient Stimulated Raman Scattering in Gas-Filled Photonic Crystal Fibers, Phys. Rev. Lett. **105**, 173902 (2010).

[41] R. W. Boyd, *Nonlinear Optics,* (Academic Press, 2003), 2nd ed.

[42] M. Qasymeh, M. Cada and S. A. Ponomarenko, Quadratic Electro-Optical Kerr Effect: Application to Photonic Devices, IEEE J. Quant. Electron., **44**, 740 (2008).

[43] A. Ablovind, A. Nazarkin, A.V. Chugreev, C. F. Kaminski, and P. St.J. Russell, Solitary Pulse Generation by Backward Raman Scattering in H_2-Filled Photonic Crystal Fibers, Phys. Rev.Lett., **103**, 183902 (2009).

[44] L. Mandel and E. Wolf, *Optical Coherence and Quantum Optics* (Cambridge University Press, Cambridge, 1995).

[45] M. H. Frosz, Validation of input-noise model for simulations of supercontinuum generation and rogue waves, Opt. Express, **18**, 14778 (2010).

[46] A. Papoulis, *Probability Random Variables, and Stochastic Processes* (McGraw Hill, New York, 1991) 3rd Ed.

[47] L. Mokhtarpour and S. A. Ponomarenko, Fluctuating pulse propagation in resonant nonlinear media: self-induced transparency random phase soliton formation, Opt. Express **23**, 30270 (2015).

Chapter 6

Rogue waves, self-similarity, and integrable turbulence

Yashar E. Monfared and Sergey A. Ponomarenko
Part of this chapter is submitted to Phys. Rev. Lett., March 2018.

6.1 Abstract

We explore extreme event occurrence in the integrable turbulence with self-similar asymptotics. We posit that rogue waves in such systems manifest themselves as giant fluctuations away from average self-similar dynamics of the system. We support our proposition with numerical simulations of rogue wave excitation in the self-similar regime of stimulated Raman scattering. We show that our results hold irrespective of a specific source correlation model, suggesting the universality of the proposed scenario.

6.2 Introduction

Turbulence, defined as chaotic changes of dynamical variables throughout the evolution of the corresponding physical systems, is a subject with a long and venerable history [166]. The subject has recently acquired a new dimension with the introduction of the integrable turbulence concept by Zakharov [2] who pointed out that nonlinear statistical wave systems, described by the integrable equations, differ from conventional turbulent systems in several important aspects. In this context, the rogue wave (RW), or, in general, extreme event excitation mechanisms in integrable turbulence present a special interest. RWs are extremely rare, giant waves, obeying

non-Gaussian statistics [167]. To date, RWs have been proven ubiquitous in oceanography [4], plasma physics and Bose-Einstein condensates [167] as well as in nonlinear optics [**?**, **?**] among many other branches of physics.

The RW generation in integrable turbulence is commonly studied within the framework of a generic (1+1)D nonlinear Schr odinger equation (NLSE). The latter governs time-evolution of weakly dispersive wave systems with weak instantaneous nonlinearities of the Kerr type [19]. The RW excitation in the NLSE model with random input wave fields has been studied both numerically [178, 179, 115, 19, 105, 24, 181] and experimentally [24, 181]. These studies helped elucidate the respective roles of spontaneous Peregrine-like breather excitation from a noisy environment and of random soliton collisions in triggering the emergence of heavy-tailed probability density distributions (PDF) of field intensities. Such heavy-tailed PDFs herald the RW generation in the system [179, 24, 181, 19, 105].

However, the NLSE model fails to accurately describe the dynamics of nonlinear waves in the vicinity of either wave-wave or wave-matter resonances. The resonant wave-wave or wave-matter interaction regime is characterized by strong nonlinearity, long coherent memory of the system, and strong amplification/absorption near resonance [182]. In optical physics, the resonant RW excitation can be generically modelled through either two-level amplification (TLA) or stimulated Raman scattering (SRS) processes. The energy transfer to an optical wave from either (inverted) medium atoms (TLA) or from another wave via two-photon resonance (SRS) serves as a generic resonant amplification mechanism. In fluid mechanics, a resonant interaction between short surface and long internal waves occurs whenever the phase velocity of a short wave matches the group velocity of a long wave. The short-wave-long-wave interaction equations are known to be integrable [183]. The TLA and SRS are also governed by integrable equations in the transient regime [184, 185, 186]. The key feature of both TLA and SRS is a transient character of solitons and breathers and universal long-term self-similar evolution of the system in the integrable limit [187]. Thus, neither soliton collisions nor breathers can trigger extreme events in the long-term evolution of self-similar integrable turbulence. A fundamental question then arises: What is a physical manifestation of extreme events and, especially, RWs if

any, in the *integrable turbulence with self-similar asymptotics?*

In this work, we explore extreme event excitation in the long-term, self-similar regime of integrable turbulence for the first time to our knowledge. We propose that RWs appear as rare, giant fluctuations away from a self-similar, on average, dynamics of the system. Our extensive numerical simulations of extreme event occurrence in the self-similar regime of SRS reveal the existence of RWs and support the proposed scenario of their emergence. We also confirm that RWs can be excited regardless of the source statistical model. We anticipate the proposed RW excitation scenario to be ubiquitous for self-similar integrable turbulence, characterized by long coherent memory.

6.3 Self-similar regime of SRS

We consider the Raman interaction between a pump and fundamental Stokes modes. This SRS modality can be realized, for instance, in a gas-filled hollow core photonic crystal fiber, designed to suppress higher-order Stokes modes [32]. In the extreme transient regime, the characteristic SRS interaction time T_{SRS} is much shorter than the medium dipole relaxation time T_2 [17]. The slowly-varying pump $\mathcal{E}_p$ and Stokes $\mathcal{E}_s$ pulse amplitude evolution is then governed by simplified Maxwell's equations

$$\partial_Z \mathcal{E}_p = -\kappa\sigma\mathcal{E}_s, \qquad \partial_Z \mathcal{E}_s = \kappa^{-1}\sigma\mathcal{E}_p, \tag{6.1}$$

and the dipole moment matrix element σ obeys the Schr odinger equation, which, in the weak excitation approximation pertaining to realistic experimental conditions, takes the form [17, 18, 185, 186, 187]

$$\partial_T \sigma = \mathcal{E}_p\mathcal{E}_s. \tag{6.2}$$

Here $\kappa = \sqrt{\omega_p n_s/\omega_s n_p} \approx 1$, $\omega_{p,s}$ and $n_{p,s}$ being the carrier frequencies and linear refractive indices of the pump and Stokes modes, respectively. In writing Eqs. (6.1) and (6.2), we assumed chirpless pump and Stokes input pulses, implying that all field variables are real, and used the same dimensionless variables as in Ref. [17, 18].

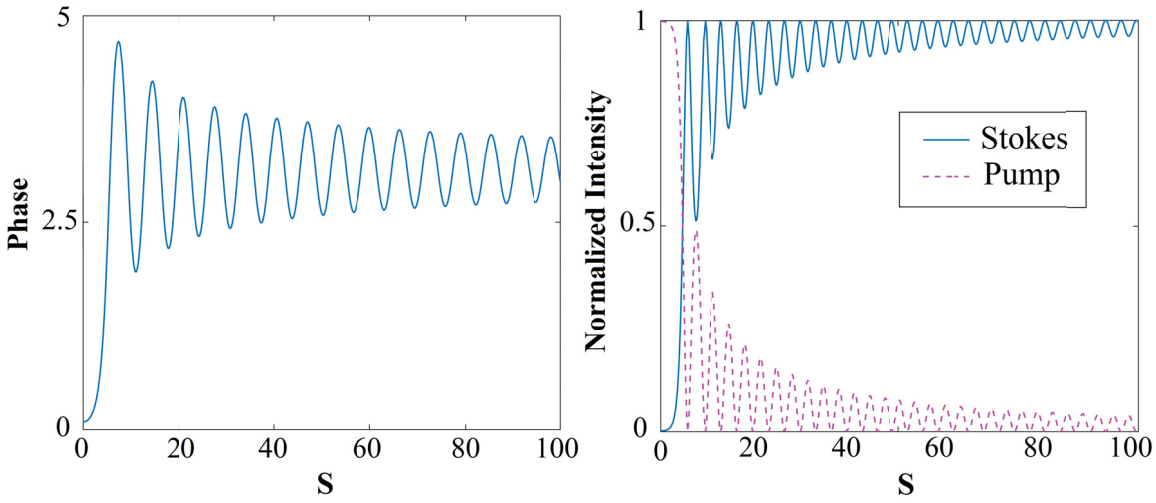

Figure 6.1: (color online). (Left panel:) Self-similar phase θ as a function of the similarity variable s. We take $\kappa = 1$ and assume that the energy initially resides almost entirely with the source pump mode, $P_{0s} = 0.01P_{0p}$. (Right panel:) Normalized intensities of the Stokes (solid blue) and pump (dashed magenta) pulses as functions of s.

The power conservation law implies the following parametrization of the pulse amplitudes

$$\mathcal{E}_p = (\kappa K)^{1/2} \cos(\theta/2), \tag{6.3a}$$

and

$$\mathcal{E}_s = (K/\kappa)^{1/2} \sin(\theta/2). \tag{6.3b}$$

Here θ is a real phase and the integral of motion $K(T)$ is defined as

$$K(T) = \kappa^{-1}\mathcal{E}_p^2(T,0) + \kappa\mathcal{E}_s^2(T,0). \tag{6.4}$$

In SRS in molecular gases, $\kappa \approx 1$ and $K(T)$ is well approximated by the total intensity at the source, $I_{\rm tot}(T,0)$. In the self-similar regime, the phase depends only on the similarity variable s such that [188, 189]

$$\theta = \theta(s), \qquad s = 2\sqrt{Z\int_{-\infty}^{T} dx\, K(x)}. \tag{6.5}$$

The SRS dynamics is then governed by the single ordinary differential equation in

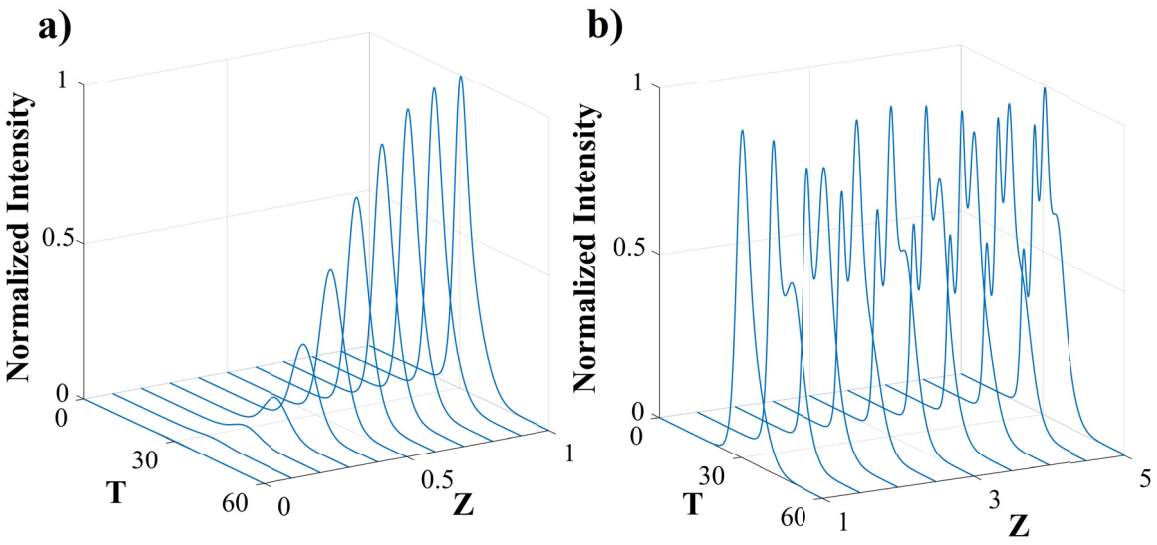

Figure 6.2: (color online). Evolution of the normalized intensity of a Gaussian Stokes pulse with no input noise at the source as a function of dimensionless time T and propagation distance Z for two stages: (a) initial exponential amplification stage and (b) self-similar stage. The other parameters are: $\kappa = 1$, $T_0 = 30$ and the Gaussian pump/Stokes pulse duration is $T_* = 8.3$.

the form

$$\theta''_{ss} + \tfrac{1}{s}\theta'_s = \sin\theta. \tag{6.6}$$

Eq. (6.6) must be solved subject to the boundary conditions, $\theta'(0) = 0$ and $\theta(0) = \tan^{-1}(\kappa\sqrt{n_p P_{0s}/n_s P_{0p}})$, where P_{0s} (P_{0p}) is an input power of the Stokes (pump) pulse. Hereafter, we assume that the energy initially resides almost entirely with the source pump mode, $P_{0s} = 0.01P_{0p}$. In Fig. 6.1, we exhibit a numerical solution to Eq. (6.6) (left panel) and the universal normalized intensity profiles of the pump, $\overline{I}_p = I_p/\kappa K$ (magenta curve, right panel) and Stokes, $\overline{I}_s = \kappa I_s/K$ (blue curve, right panel). We clearly observe gradual pump mode energy depletion, resulting in the Stokes mode amplification in Fig. 6.1. The process is accompanied by coherent oscillations due to long coherent memory of the SRS interaction in this regime. In Fig. 6.2, we display the normalized intensity evolution of a Stokes pulse with no input noise at the source. The input Stokes and pump pulses are assumed to have the same Gaussian profile with the temporal width $T_* = 8.3$, which corresponds to a physical pulse duration of $t_* = 10$ ns and the SRS interaction time $T_{\rm SRS} = 1.2$ ns [18, 32]; the pulses are centred at $T_0 = 30$. The analysis of Fig. 6.2 reveals that an initial, nearly exponential

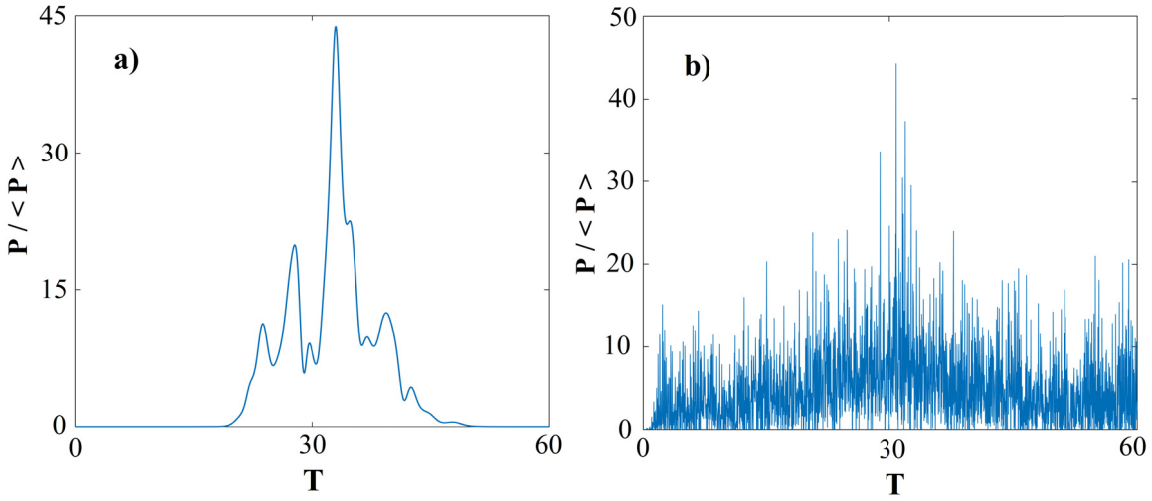

Figure 6.3: (color online). Power fluctuations of a random realization of the Stokes pulse ensemble at $Z = 3$ for (a) GSM and (b) FBWN source pump pulse ensembles. The numerical parameters are: $\Delta P/P_0 = 0.4$, $\kappa = 1$, and $T_c = 0.1T_*$. The Stokes pulse power is normalized to its average value at the same propagation distance, $Z = 3$.

amplification stage (Fig. 6.2a) is followed by a self-similar evolution stage (Fig. 6.2b). The self-similar stage onset is unequivocally marked by the appearance of intensity oscillations. We then infer from the figure that the self-similar regime starts past around $Z_{cr} \simeq 1$ in our units. To ensure that our system is well into the self-similar regime, we examine extreme event excitation in the Stokes output at distances larger than Z_{cr}.

6.4 Extreme events in self-similar integrable turbulence

We study SRS with a small-amplitude coherent Stokes pulse seed, interacting with a strong fluctuating pump pulse. The pump pulse field at the source is assumed to consist of a coherent and random components such that

$$\mathcal{E}_p(T, 0) = \mathcal{E}_{p0}(T, 0) + \Delta\mathcal{E}_p(T, 0), \tag{6.7}$$

where the random component can be expressed in terms of coherent modes $\{\psi_n(T)\}$ of the source as

$$\Delta\mathcal{E}_p(T,0) = 2^{-1/2}\left(\sum_n c_n(T)\psi_n(T) + c.\ c.\right). \tag{6.8}$$

Here $\{c_n\}$ are random complex amplitudes and $c.\ c.$ stands for a complex conjugate.

To explore the generality of our results, we consider two physically very different statistical models of the pump. In the first model, the coherent component has a Gaussian pulse envelope centred at T_0 with the temporal duration T_* (in the dimensionless units). The random component has a Gaussian average intensity profile of the same duration, for simplicity, and a Gaussian fluctuation spectrum of the width inversely proportional to the source coherence time T_c. Thus, the pair correlations among the monochromatic components of such a pump source strongly decay with the frequency separation between the components. This model is known as a Gaussian Schell-model (GSM) which has been extensively employed before in statistical nonlinear optics [17, 18, 120]. The second model allows for an arbitrary temporal envelope of the pump pulse, but assumes, for simplicity, that the random component has the same average intensity profile as the coherent component profile. Further, the model stipulates that the fluctuation spectrum of the random component be flat within a finite bandwidth. In this model, the spectral correlations among pairs of monochromatic components of the source are uniform within the source bandwidth, making this finite-bandwidth white noise (FBWN) model drastically different from GSM. In the Appendix C, we present details of statistical ensemble construction for GSM and FBWN models. In particular, we are able to analytically determine the coherent modes $\{\psi_n(T)\}$ and demonstrate how the statistical properties of $\{c_n\}$'s shall be specified to ensure the source GSM and FBWN ensembles obey Gaussian statistics for any second-order coherence time.

In the self-similar regime of interest, the Stokes and pump field ensemble representations are determined from Eqs. (6.3) with their evolution being governed by Eq. (6.6). We assume that the coherent pump pulse component for both GSM and FBWN ensembles has a Gaussian pulse profile and perform extensive Monte-Carlo simulations

for an ensemble of 10^4 realizations of the pump field. Hereafter, we assume that $\kappa = 1$. We introduce an average peak power ΔP of the random component of the pump pulse at the source and the corresponding peak power of the coherent component P_0 [**?**]; their ratio is taken to be $\Delta P/P_0 = 0.4$ henceforth. In Fig. 6.3, we exhibit the normalized power of a Stokes pulse ensemble realization at a distance $Z = 3$, well within the self-similar evolution domain for both GSM (Fig. 6.3a) and FBWN (Fig. 6.3b) source ensembles; the Stokes pulse power is normalized to its average magnitude at $Z = 3$. We notice a quantitatively different behaviour of the output Stokes pulse fluctuations in the two cases: the FBWN ensemble fluctuations are more spread in time than are the GSM ensemble ones. This is because the Gaussian GSM source time correlations are more localized than are the FBWN ones, the latter being governed by a sinc function, (see the Appendix C for details.) Further, we can infer from the figure that the output Stokes pulse realization for either ensemble attains a peak power nearly 45 times its average power at this propagation distance, thereby unambiguously qualifying the output as an RW. Thus, RWs can be generated in the self-similar regime of SRS which is in qualitative agreement with our previous results for SRS approaching the integrability limit [17]. Most important, we confirm that the RW appearance is independent of a particular source correlation model, thereby representing a universal signature of the self-similar regime of integrable turbulence.

To explore generic features–independent of a particular pump pulse profile at the source–of extreme event generation in the self-similar regime of integrable turbulence, we scale away the source intensity profile by introducing the Stokes and pump pulse intensities scaled to the average total intensity at the source, $\langle I_{\rm tot}\rangle$. In Fig. 6.4a, we display the average dynamics of the scaled Stokes (solid blue curve) and pump (solid red curve) intensities for the GSM source ensemble, together with the corresponding deterministic SRS quantities for which no pump noise is present at the source. The deterministic dynamics of the scaled intensities of the Stokes and pump pulses are displayed with dashed magenta and dash-dotted green curves, respectively. We clearly observe that the average pulse dynamics follows closely the deterministic self-similar evolution scenario. Next, we juxtapose in Fig. 6.4b the self-similar average Stokes pulse intensity evolution in the scaled variables (dashed magenta curve) with a Stokes pulse ensemble realization dynamics in the scaled variables (solid blue curve). Note

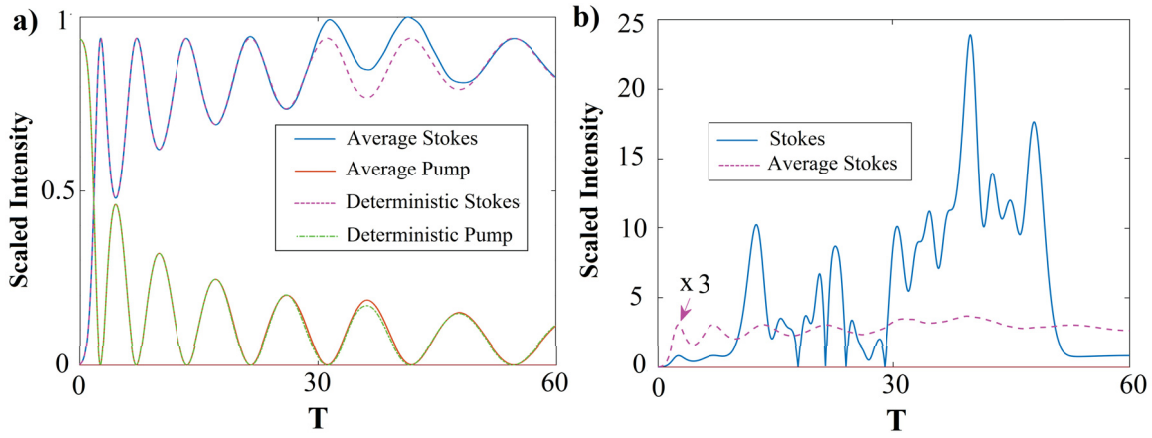

Figure 6.4: (color online). (a) Scaled average intensities of the GSM Stokes (solid blue) and pump (solid red) pulse ensembles at $Z = 3$. The scaled intensities of deterministic Stokes (dashed magenta) and pump (dash-dotted green) pulses in the absence of source noise are shown for comparison as well. (b) Scaled intensity of a random realization of the GSM Stokes pulse ensemble (solid blue) and the average Stokes pulse ensemble intensity (dashed magenta) at $Z = 3$. The average intensity is enhanced by a factor of three to facilitate visualization. All intensities are scaled to the total average intensity at the source. The numerical parameters are: $\kappa = 1$, $\Delta P/P_0 = 0.4$, and $T_c = 0.1T_*$.

that the scaled average intensity is enhanced by a factor of 3 to facilitate visualization. It is evident from the figure that extreme events appear as giant fluctuations away from the average self-similar evolution of the system. Further, we repeat the calculations for the FBWN ensemble and exhibit the corresponding results for a white noise pump source in Fig. 6.5 using the same colour scheme. Despite quantitative differences of Fig. 6.5 from Fig. 6.4, our main conclusion regarding the RW manifestations as enormous fluctuations away from the long-term self-similar evolution of integrable turbulence holds for the FBWN source ensemble as well, supporting the universality of the proposed scenario.

Finally, we examine extreme event statistics by calculating the probability density function (PDF) of the normalized peak power of the Stokes pulse at an output distance. The peak power is normalized to its average value at the output distance. The results are shown in Fig. 6.6 where we display the peak power PDFs of the Stokes pulse output at $Z = 3$ for a nearly incoherent GSM ensemble of pump pulses at the source, with the coherence time being the fraction of the input pulse width,

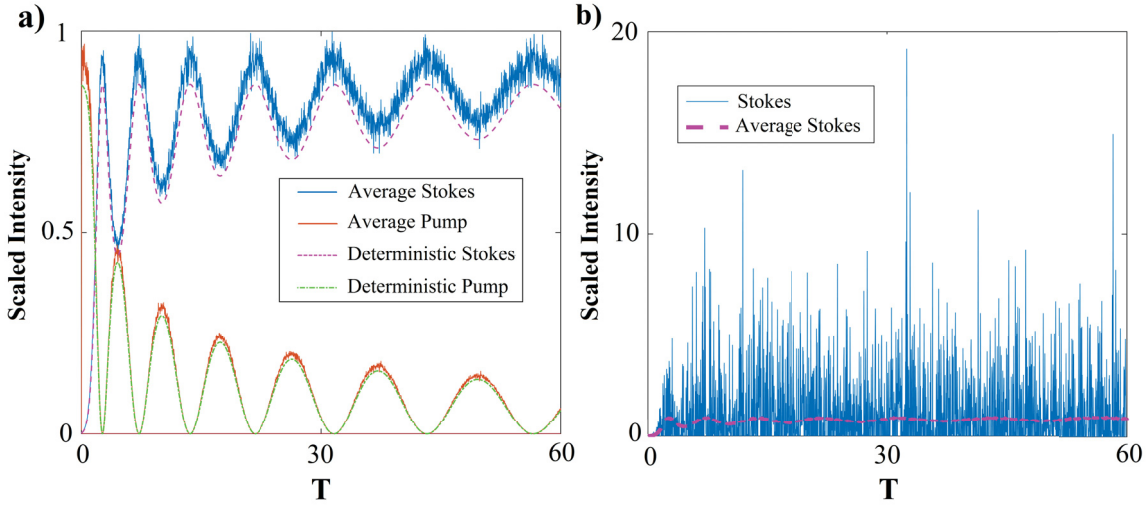

Figure 6.5: (color online). Same as in Fig. 6.4 for FBWN pulse ensembles.

$T_c = 0.1T_*$ (solid magenta curve), and that for a highly coherent GSM ensemble of such pulses with $T_c = 10T_*$ (dashed blue curve). The solid red straight line corresponds to a Gaussian PDF with the same average peak power as the average peak power of the Stokes ensemble at $Z = 3$. We immediately notice that both output PDF curves strongly deviate from the Gaussian by acquiring long tails for the peak powers substantially exceeding their average values. This circumstance points to a greatly enhanced likelihood of extreme event generation in the system, compared against predictions based on Gaussian statistics. We also observe that the solid magenta and dashed blue curves are very close to each other–taking into account inevitable data spread in a Monte-Carlo simulation–reinforcing our message that extreme event excitation in integrable SRS is barely affected by the source coherence time. This conclusion is in qualitative agreement with our previous findings for extreme event excitation in non-integrable regime of SRS with noisy input pump [17]. The solid magenta and dashed blue curves were determined using the self-similar evolution description of SRS with the aid of Eqs. (6.3) through (6.6). To confirm that the system is indeed in the self-similar regime, we repeated the PDF calculations using the full set of SRS equations, Eqs. (6.1) and (6.2). The resulting PDF is represented by a dash-dotted green curve for a highly coherent GSM ensemble with $T_c = 10T_*$. We can clearly see in the figure that the dash-dotted green curve nearly coincides with the dashed blue curve, as expected, and is very close to the solid magenta one. It follows

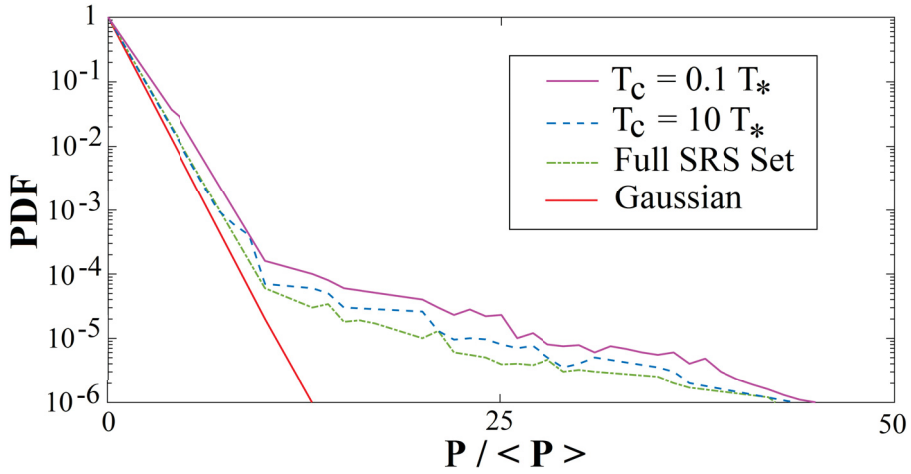

Figure 6.6: (color online). Normalized peak power PDF of a GSM Stokes pulse ensemble at $Z = 3$ for a nearly incoherent $T_c = 0.1T_*$ (solid magenta), and fairly coherent, $T_c = 10T_*$ (dashed blue) ensembles; the solid magenta and dashed blue curves are obtained using the self-similar evolution equations, Eqs. (6.3) through (6.6). The dash-dotted green curve displays the peak power PDF for a fairly coherent ensemble, $T_c = 10T_*$, evaluated using the full set of SRS equations, Eqs. (6.1) and (6.2). The peak power is normalized to its average value at $Z = 3$. The solid red line represents a Gaussian PDF with the same average peak power. The other numerical parameters are: $\kappa = 1$ and $\Delta P/P_0 = 0.4$.

that the self-similar evolution description accurately captures the system statistics behaviour.

6.5 Conclusion

We have demonstrated that RWs can be excited in a self-similar asymptotic regime of integrable turbulence and they appear as giant fluctuations away from the average (self-similar) evolution of the system. Although our results are based on numerical simulations of SRS in the transient regime, the conclusions are model independent; we can expect qualitatively similar findings in the TLA case. Indeed, the TLA and SRS in the integrable regime can be shown to be governed by the same set of evolution equations with an appropriate choice of variables [185]. However, there is an important difference: While one can neglect the amplified spontaneous emission noise contribution to SRS in gases in the weak excitation approximation–because there is

a negligible population of the excited virtual states of the two-photon transition–strongly amplified spontaneous emission noise cannot be neglected in TLA. We anticipate that the additional amplified noise in the TLA case will only increase the likelihood of extreme event occurrence in the system.

Bibliography

[1] G.K.Batchelor, *The Theory of Homogeneous Turbulence,* (Cambridge University Press, Cambridge, 1986).

[2] V. E. Zakharov, Turbulence in integrable systems, Stud. Appl. Math., **122**, 219 (2010).

[3] M. Onorato, S. Residori, U. Bertolozzo, A. Montina and F. T. Arecchi, Rogue waves and their generating mechanisms in different physical contexts, Phys. Rep. **528**, 47 (2013).

[4] V. E. Zakharov, A. I. Dyachenko and A. O. Prokofiev, Freak waves as nonlinear stage of Stokes wave modulation instability, Eur. J. Mech. B, **25**, 677 (2006).

[5] M. Shats and X. H. Punzmann, Capillary rogue waves, Phys. Rev. Lett., **104**, 104503 (2010).

[6] R. H ohmann U. Kuhl, H.-J.St ockmann, I. Kaplan and E. J. Heller, Freak waves in a linear regime: a microwave study, Phys. Rev. Lett., **104**, 093901 (2010).

[7] F. T. Arecchi, U. Bertolozzo, A. Montina and S. Residori, Granularity and inhomogeneity are joint generators of rogue waves, Phys. Rev. Lett., **106**, 153901 (2011).

[8] W.M. Moslem R. Sabry, S. K. El-Labany, and P. K. Shukla, Dust-acoustic rogue waves in nonextensive plasma, Phys. Rev. E, **84**, 066402 (2011).

[9] Y. Bludov, V. Konotop and N. Akhmediev, Matter rogue waves, Phys. Rev. A, **80**, 33610 (2009).

[10] D.R. Solli, C. Ropers, P. Koonath and B. Jalali, Optical rogue waves, Nature (London) **450**, 1054 (2007).

[11] M. Erkintalo, G. Genty and J. M. Dudley, Rogue-wave-like characteristics in supercontinuum generation, Opt. Lett., **34**, 2468 (2009).

[12] A. Montina U. Bertolozzo, S. Residori, and F. T. Arecchi, Non-Gaussian statistics and extreme waves in a nonlinear optical cavity, Phys. Rev. Lett., **103**, 173901 (2009).

[13] J.M. Soto-Crespo, Ph. Grelu, and N. Akhmediev, Dissipative rogue waves: extreme pulses generated by passively mode-locked lasers, Phys. Rev. E, **84**, 016604 (2011).

[14] A. F. J. Runge, N. G. R. Broederick, and M. Erkintalo, Observations of soliton explosions in a passively mode-locked fiber laser, Optica, **2**, 36 (2015).

[15] K. Hammani, C. Finot, J. M. Dudley and G. Millot, Optical rogue-wave-like extreme value fluctuations in fiber Raman amplifiers, Opt. Express, **16**, 16467 (2008).

[16] J. Kasparian, P. Béjot, J..-P. Wolf, and J. M. Dudley, Optical rogue wave statistics in laser filamentation, Opt. Express, **17**, 12070 (2009).

[17] Y. E. Monfared and S. A. Ponomarenko, Non-Gaussian statistics and optical rogue waves in stimulated Raman scattering, Opt. Express, **25**, 5941 (2017).

[18] Y. E. Monfared and S. A. Ponomarenko, Non-Gaussian statistics of extreme events in stimulated Raman scattering: The role of coherent memory and source noise, Phys. Rev. A, **96**, 043817 (2017).

[19] G.P. Agrawal, *Nonlinear Fiber Optics,* (Academic Press, Amsterdam, 2007) 4th ed.

[20] A.Sauter, S.Pitsois, G. Millot, and A.Picozzi, Incoherent modulation instability in instantaneous nonlinear Kerr media, Opt. Lett., **30**, 2143 (2005).

[21] S.Toenger, T.Godin, C.Billet, F. Dias, M.Erkintalo, G.Genty, J.M. Dudley, Emergent rogue wave structures and statistics in spontaneous modulation instability, Sci. Rep., **5**, 10380 (2015).

[22] D.S. Agafontsev and V.E. Zakharov, Integrable turbulence and formation of rogue waves, Nonlinearity, **28**, 2791 (2015).

[23] J.M. Soto-Crespo, N. Devine, and N. Akhmediev, Integrable Turbulence and Rogue Waves: Breathers or Solitons? Phys. Rev. Lett., **116**, 103901 (2016).

[24] P. Walczak, S. Randoux, and P. Surret, Optical Rogue Waves in Integrable Turbulence, Phys. Rev. Lett., **114**, 143903 (2015).

[25] P. Surret, R. El Koussaifi, A. Tikan, C. Evain, S. Randoux, C. Szwaj, and S. Bielawski, Single-shot observation of optical rogue waves in integrable turbulence using microscopy, Nat. Commun., **7**, 13136 (2016).

[26] L. Allen and J. H. Eberly, *Optical resonance and two-level atoms,* (Dover Publications Inc., New York, 1975).

[27] K. Sakai and A. Noguchi, Dark Soliton in Long and Short Wave Resonant Interaction, J. Phys. Soc. Jpn, **49**, 2009 (1980).

[28] G L.Lamb, Jr., *Elements of soliton theory* (Wiley, New York, 1976).

[29] F. Y,. F. Chu and A. C. Scott, Inverse scattering transform for wave-wave scattering, Phys. Rev. A, **12**, 2060 (1975).

[30] D. J. Kaup, Creation of a soluton out of dissipation, Physica D, **19**, 125 (1986).

[31] C. R. Menyuk, Transient solitons in stimulated Raman scattering, Phys. Rev. Lett., **62**, 2937–2940 (1989).

[32] A. Nazarkin, A. Abdolvand, A.V. Chugreev, and P. St.J. Russell, Direct Observation of Self-Similarity in Evolution of Transient Stimulated Raman Scattering in Gas-Filled Photonic Crystal Fibers, Phys. Rev. Lett. **105**, 173902 (2010).

[33] J.N.Elgin and T.B.O'Hare, Saturation effects in transient stimulated Raman scattering, J. Phys. B, **12**, 159 (1979).

[34] C.R. Menyuk, D. Levi and P. Winternitz, Self-similarity in Transient Stimulated Raman Scattering, Phys. Rev. Lett., **69**, 3048 (1992).

[35] L. Mokhtarpour and S. A. Ponomarenko, Fluctuating pulse propagation in resonant nonlinear media: self-induced transparency random phase soliton formation, Opt. Express **23**, 30270- 30282 (2015).

Chapter 7

Slow light generation via stimulated Brillouin scattering in liquid-filled photonic crystal fibers

Yashar E. Monfared and Sergey A. Ponomarenko
Published in: Optik - International Journal for Light and Electron Optics, August 2016, Vol. 127, No. 15, pp. 5800-5805
URL: https://www.sciencedirect.com/science/article/pii/S0030402616302893

7.1 Abstract

We theoretically investigate slow light generation using stimulated Brillouin scattering (SBS) in a short highly nonlinear liquid-filled photonic crystal fiber (PCF). We study optical properties of hollow-core PCFs, filled with liquids exhibiting strong optical nonlinearities. We propose a design of carbon-disulfide-filled fiber with an effective area of $1.8\mu m^2$, nonlinear coefficient larger than 7300 $W^{-1}.Km^{-1}$, confinement loss of 0.007 dB/km and total loss lower than 0.3 dB/m over the C-band. Relative to standard single mode fibers, the proposed fiber reduces power$\times$ fiber length requirement for a given gain (delay) by nearly three orders of magnitude (830 times). Furthermore, using just a one-meter long fiber, we demonstrate that pulses can be slowed down to c/50 with a required power level of only 25mW. We show that our PCF is about 7 times more efficient than the previously reported fiber designs.

7.2 Introduction

The group velocity of light control has attracted much attention in both academia and industry because it provides optically controllable pulse delays for applications such as data synchronization, optical memory, optical buffering, and optical signal processing [1]. The prevalent protocols for slowing down optical pulses in bulk media and semiconductor devices include the electromagnetically induced transparency and coherent population oscillations [1]. However, slow light generation inside optical fibers can be realized at room temperature with a good deal of flexibility and rather simple configurations via stimulated Brillouin scattering (SBS) [2, 3]. The SBS slow light generation makes use of an optically controlled narrowband gain in a fiber, thus the group velocity of optical pulses can be tuned continuously by simply controlling the pump power level. There are two main research trends around the world in this area. First, optimizing SBS pump profiles for increasing the bandwidth, reducing pulse distortions, and overcoming inherent SBS line width limitations [4, 5]. The second amounts to SBS slow light realization in highly nonlinear fibers. The SBS gain coefficient in silica fibers is just about 5×10^{-11} m/W. Thus, we cannot attain a considerable change of group velocity using SBS in short span standard fibers or with low pump powers [6]. Okawachi et al. [6], have achieved a 25 ns long slow light delay of signal pulses along a 500 meter long SMF-28e fiber. Using shorter fiber lengths has a benefit for overall performance of the system in terms of minimizing the inherent latency of the device [7]. In recent years, SBS slow light generation has been caried out in chalcogenide glass, bismuth oxide glass, tellurite glass fibers and PCFs [5, 7, 8]. Nonstandard fibers, made of nonlinear glass materials, could support the SBS interaction that is $2-3$ orders of magnitude stronger than that obtained in standard silica fibers. For example, J. Misas et al. [7] substantially slowed down pulses over a distance of just 2 meters using a pump power level of 400mW in a BiO_2 nonlinear fiber. However, the loss in this type of glasses is really high within the optical communication window. Thanks to small effective mode areas in photonic crystal fibers (PCFs), we could also achieve an enhanced SBS interaction there. The highly nonlinear PCFs (HNPCFs) made with silica have nonlinear coefficients less

than 60.5 W^{-1} km^{-1}, while nonlinear coefficients of the conventional SMFs are only around 1.3W^{-1} km^{-1} [9]. For example, using a 50m long PCF, Yang et al. [10] demonstrated a delay of a half a pulse length. One way to enhance both nonlinear and Brillouin gain coefficients of a fiber is to infiltrate PCFs with highly nonlinear liquids. The technique to fill in the hole of a hollow-core PCF with a liquid has already been developed and utilized experimentally [11-13]. In recent years, researchers have worked on designing liquid-filled optical fibers filled by highly nonlinear liquids such as carbon disulfide (CS_2) and nitrobenzene. Previous studies on liquid filled PCFs have shown that extremely high values of nonlinear coefficients of the order of $2000-4000$ $W^{-1}.km^{-1}$ can be achieved [12-14]. Poletti et al. [15] proposed theoretically a highly nolinear CS_2-filled PCF with the nonlinear coefficint of 6548 $W^{-1}.km^{-1}$ at 1550nm. However, their proposed PCF structure has a relatively large filling fraction, which makes the PCF fabrication process rather difficult. Combining small effective areas in PCFs and large Brillouin gain coefficients of nonlinear liquids can result in minimizing power and length requirements for a given delay and, at the same time, increase the delay time. In this work, we will present a comprehensive study of liquid-filled PCFs with different materials and different structural parameters. We then demonstrate how the novel fiber design becomes highly advantageous for slow light generation using SBS.

7.3 PCF design

We will now present our liquid-filled hollow-core PCF design and optimize its parameters for slow light generation. The liquids that we use in our simulations are CS_2, nitrobenzene, toluene, benzene, chloroform and methanol, and the corresponding linear refractive indices at 1550 nm are 1.59, 1.524, 1.477, 1.476, 1.433,1.317 respectively. PCFs are a class of optical fibers, usually designed and fabricated with a solid pure silica core, surrounded by periodic air holes which serve as a cladding [16]. The air holes makeup in the cladding region of the PCF leads to tailored optical properties such as nearly zero flattened dispersion and low confinement loss; further, one can adjust the PCF core area to control the fiber nonlinearity [16, 17]. For example, by increasing the number of air holes in the cladding region, we can decrease the

confinement loss of the fiber dramatically. Although we use only six liquids for our investigations, our studies can be extended to other liquids as well. The cladding material of our proposed PCF is silica with the linear refractive index of n=1.446 at 1550nm. Our proposed PCF has a hexagonal lattice with five rings of air holes surrounding a liquid-filled core in the center of the fiber. Thus, the design parameters of the liquid-filled PCF are the hole diameter d, hole pitch Λ, and core diameter D. The cross section of the proposed liquid-filled PCF is shown in Fig. 7.1. Our analysis

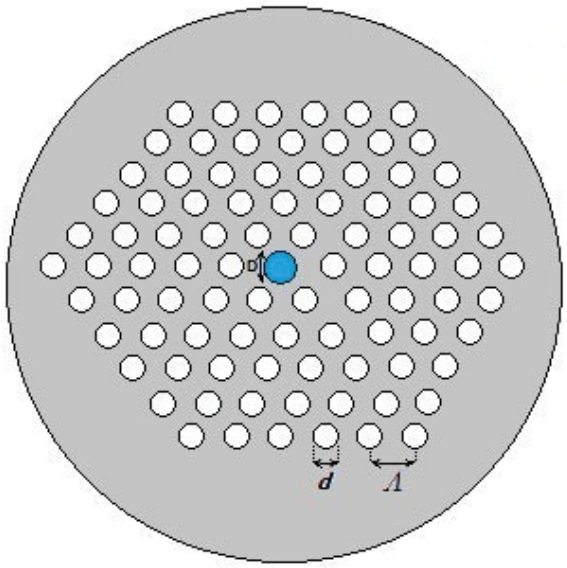

Figure 7.1: Cross section of the liquid-filled PCF with hole dimension (d), hole pitch (Λ) and core diameter (D).

is restricted to mode confinement through multiple total internal reflections. We do not consider the bandgap guiding mechanism in hollow-core PCFs because it would greatly restrict benefits of the high nonlinear index of the liquid. Using a finite difference time domain analysis [17-18] applied with OptiFDTD commercial software [19], we theoretically study the effective mode area, nonlinear coefficient and confinement loss properties of the liquid-filled PCFs. One of the most important characteristics of a highly nonlinear fiber is its nonlinear coefficient which contains information about both mode confinement (effective mode area) and the nonlinear refractive index of the medium. The nonlinear coefficient γ is defined as [17, 20]

$$\gamma = \frac{2\pi n_2}{\lambda A_{eff}}, \tag{7.1}$$

where n_2 is a nonlinear refractive index and A_{eff} is an effective area of the fundamental fiber mode, defined as [17, 20]

$$A_{eff} = \frac{\int\int(|E|^2 dA)^2}{\int\int(|E|^4 dA)}. \tag{7.2}$$

Due to the high refractive index contrast between silica and air, the PCFs offer a much tighter mode confinement over a wide range of wavelengths and thereby a lower effective mode area than do conventional optical fibers. In our case, this index contrast is very high, especially in the case of CS_2 and nitrobenzene, due to a large liquid core refractive index. First, the dependences of the nonlinear coefficient on the core filling liquids are simulated and shown in Fig. 7.2, with the fixed hole pitch Λ=1.5μm, d/Λ=0.66 and D/Λ=0.53 while changing the operation wavelength from 1μm to 1.8μm in steps of 0.2μm. As we can see in Fig. 7.2, the CS_2 has the highest γ due to its huge nonlinear refractive index (n_2=320$\times 10^{-20}$ m^2/W at 1550nm) and a rather tight mode confinement which results in the ultra small effective mode area (A_{eff}=1.8μm^2 at 1550nm). These exceptional values lead to the magnitude of γ between 7300 and 8000 over the S-, C- and L-bands (1460nm to 1625nm). We note that n_2 decreases and A_{eff} increases with the wavelength for nonlinear liquids. Therefore, we expect γ to decrease with the wavelength according to Eq. (1). As we can see in Fig. 7.2, γ decreases gradually with the wavelength and agrees well with the theoretical prediction. We also notice that the rate of decrease of γ with the wavelength is faster for CS_2 and nitrobenzene than for the other liquids we examine. The second critical parameter of a highly nonlinear fiber is its energy loss. We examine different kinds of filling liquids in the PCF and compare the amount of confinement loss for fixed structural parameters. Confinement loss of a liquid-filled PCF with fixed hole pitch Λ=1.5μm, d/Λ = 0.66 and D/Λ=0.53 at the operation wavelength of 1550nm for different core filling liquids is simulated and displayed in Fig. 7.3. As we can see in the figure, confinement loss strongly depends on the filling liquid type. The amount of confinement loss in the proposed fiber design for CS_2 and nitrobenzene is really low (in order of 10^{-3} dB/km), and for liquids like toluene and benzene is low (in order of 10^{-2} dB/km). Losses will increase dramatically (larger than

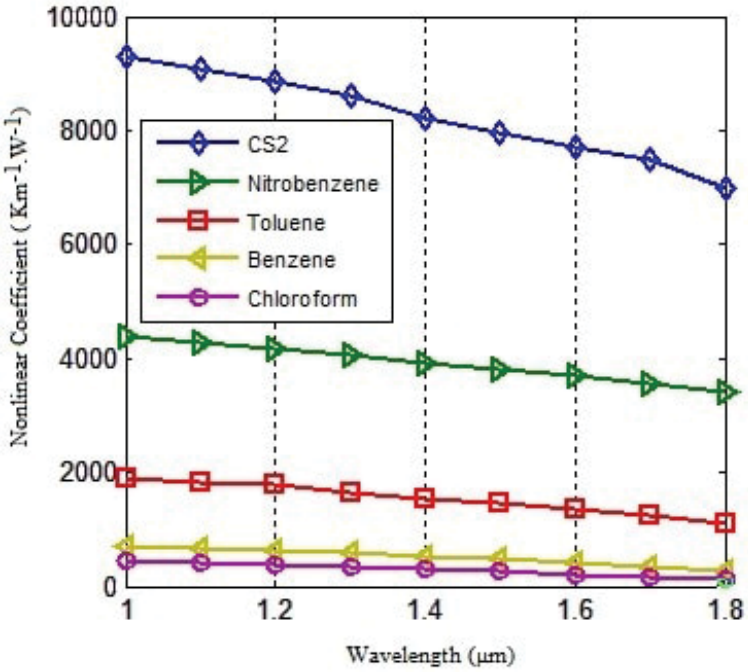

Figure 7.2: Nonlinear coefficient of the liquid-filled PCF with Λ=1.5μm, d/Λ=0.66 and D/Λ=0.53 and different core filling liquids as a function of wavelength.

5 dB/km) for low index liquids such as methanol, ethanol and water. Due to nearly-zero confinement loss of CS_2-filled PCF, however, the total fiber loss will be likely dominated by absorption and scattering losses in the liquid. Fortunately, the CS_2 transmission spectrum is almost absorption peak free in the spectral range extending from the visible to the midinfrared [15]. Therefore, we can expect an overall loss lower than 0.3dB/m for our CS_2-filled fiber [15]. The proposed fiber with ultra-high nonlinearity and relatively low loss, can have other applications in nonlinear devices. We can use the proposed fiber as a nonlinear medium for wavelength conversion based on four-wave mixing, frequency comb generation, supercontinuum generation and other nonlinear processes.

7.4 Slow light generation

The SBS process can be described as an interaction of a strong pump and counter-propagating weak probe waves. An acoustic wave will be generated if the frequency-matching condition is satisfied, $\Omega_B = \Omega_p$ - Ω_s, where Ω_B is the Brillouin frequency,

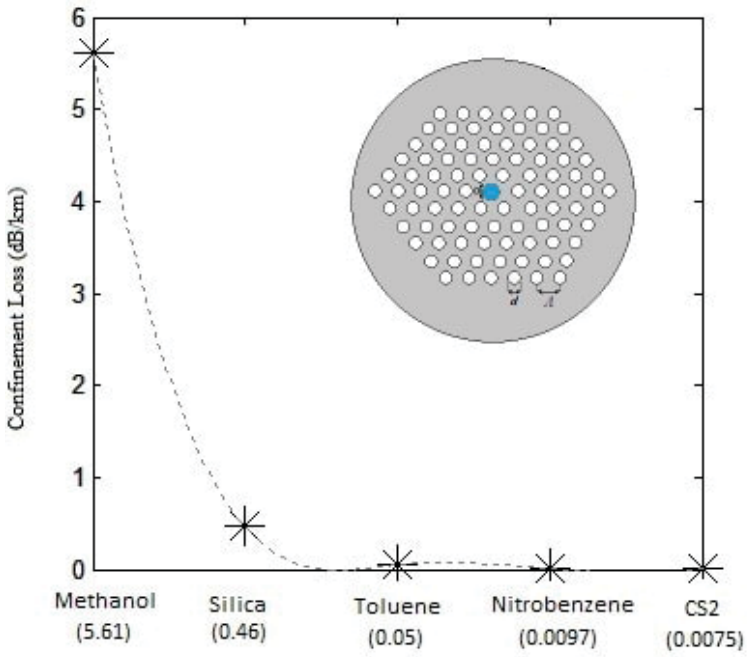

Figure 7.3: Confinement loss of the liquid-filled PCF with Λ=1.5μm, d/Λ = 0.66 and D/Λ=0.53 as a function of core filling liquid.

Ω_p is a pump frequency and Ω_s is a probe frequency. The Brillouin gain bandwidth is usually very small in optical fibers; for example, it is about 30 MHz in conventional optical fibers. Thus, we can view SBS as a narrowband amplification process. In this process, a strong pump wave produces a narrowband gain in a spectral region around $\Omega_p - \Omega_B$ and a loss around $\Omega_p + \Omega_B$ [5, 8]. The group index of a pulse is defined as $n_g = n + \omega\frac{dn}{d\omega}$. The group index change can serve as a control parameter to realize an optical time delay [5]. These changes in the group index can be used as a controllable optical time delay. The linear Brillouin gain along a fiber can be expressed as [6]

$$G = \frac{g_0 L_{eff} P_{pump}}{A_{eff}}, \tag{7.3}$$

where L_{eff} is an effective fiber length, $L_{eff} = 1 - e^{\alpha L}/\alpha$, where L is the physical length of the fiber,α is the loss coefficient of the fiber and P_{pump} is the pump power. The center-line gain coefficient g_0 depends only on the fiber core material [21]. In our calculations, we take g_0=1.5m/GW, an estimate for CS_2 known from the literature [21]. Using realistic physical dimensions and an optimized design for the proposed CS_2-filled PCF with d/Λ=0.75, D/Λ=0.58 and Λ=1.2μm, we exhibit the Brillouin

gain of the proposed fiber for different pump powers and fiber lengths in Fig. 7.4. As we can see in the figure, G strongly depends on the fiber length and pump power.

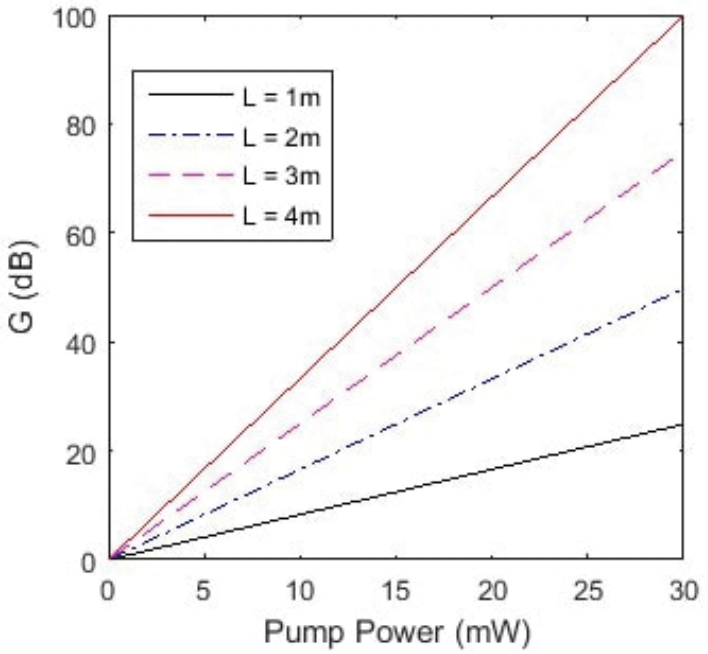

Figure 7.4: Amount of Brillouin gain as a function of the pump power in the CS_2-filled PCF for different fiber lengths.

Thanks to the small effective area and high g_0 of CS_2, we can achieve a relatively high exponential gain (around G=20) at a very low power level in a quite short fiber. We note that the gain parameter G is limited by the exponential gain threshold of the fiber G_{th} due to spontaneous Brillouin scattering. For $G = G_{th}$, photons spontaneously scattered from thermal phonons are exponentially amplified which leads to the Stokes field generation at the output that saturates the pump field [22]. For bulk media it has been shown that G_{th} is approximately constant [23]. For CS_2 bulk material, G_{th} is measured to be 22.8 at 1060nm [23]. In optical fibers, G_{th} depends on the experimental parameters such as input pulse, material, length and numerical aperture (NA) of the fiber [6, 23]. However, it can be shown that in a very short fiber with a moderate numerical aperture, G_{th} tends to its value in the bulk material[23]. In our case, we utilize a very short fiber (only 1 meter long) with NA=0.5, thus we can expect G_{th} to be around 20-28, depending on the experimental parameters. Moreover, G_{th} is generally taken to be equal to 21 in optical fibers [23, 24]. Therefore, we may

Table 7.1: Simulation parameters and optical properties of the proposed PCF at $\lambda = 1.55\mu$m.

A_{eff} (μm^2)	γ (W^{-1}km^{-1})	α(dB/m)	g$_0$(m/W)	L(m)	P$_{pump}$ (mW)
1.8	7300	0.3	1.5×10^{-9}	1	25

estimate the pump power threshold as [24]

$$P_{th} = \frac{G_{th} K_B A_{eff}}{g_B L_{eff}}, \tag{7.4}$$

where K_B is a constant depending on the polarization property of the fiber which is equal to 1 if the fiber is polarization maintaining and 1.5 otherwise [24]. Considering G_{th}=21 and $L = 1m$, we obtain P_{th}=25.2 mW for the proposed fiber. Table 1 shows all of the simulation parameters and optical characteristics of the proposed PCF for slow light generation via SBS.

In order to compare optical fibers as SBS slow light media, it is necessary to define a proper figure of merit for evaluation. According to the previous experimental and theoretical analyses of the SBS process, the slope of the time delay versus Brillouin gain only depends on the inverse of the gain bandwidth [5]. However, this bandwidth can be arbitrarily extended in the broadband scheme by pump dithering [5]. Thus, the gain coefficient and effective area are the only parameters that will scale the efficiency in the time delay generation. Response speed and the stability are other significant parameters [5]. These parameters are inversely proportional to the refractive index of the fiber. Therefore, we can define the Brillouin figure of merit (FOM), following the FOM in the [5] as

$$FOM = \frac{G}{P_{pump} L_{eff} n} = \frac{g_0}{n A_{eff}}. \tag{7.5}$$

As our analysis is restricted to very short fibers, we can neglect fiber birefringence and the effect of random polarization change along the fiber. Using realistic physical parameters and optimized design for the proposed CS_2-filled PCF with d/Λ=0.75, D/Λ=0.58 and Λ=1.2μm, and considering $L = 1m$, we can obtain total loss lower than 0.3dB/m, A_{eff}=1.8 μm^2, P$_{th}$=25.2mW and B-FOM=0.528dB/mW/m. For a sufficiently weak Stokes field which is the case for most of the SBS slow light

Table 7.2: Optical properties of different fibers near $\lambda = 1.55\mu$m for SBS slow-light generation.

Property	SMF-28 Silica fiber	Tellurite fiber [8]	As_2S_3 fiber [5]	CS_2-filled PCF
g_0(m/W)	5×10^{-11}	2.16×10^{-10}	6.08×10^{-9}	1.5×10^{-9}
α(dB/m)	0.2×10^{-3}	0.51	0.84	$\sim$0.3
n	1.44	2.3	2.8	1.59
A_{eff} (μm^2)	50	9.2	$\sim$30	1.8
FOM	0.0007	0.011	0.079	0.528

experiments, a continuous-wave (cw) pump is undepleted. Using the undepleted CW pump approximation and following the procedure of [22], we can obtain the expression for the group index of a probe pulse as

$$n_g(\omega) = n_{fg} + \left(\frac{cg_0P_{pump}}{\Gamma_B A_{eff}}\right)\frac{1 - 4\delta\omega^2/\Gamma_B^2}{\left(1 + 4\delta\omega^2/\Gamma_B^2\right)^2}, \tag{7.6}$$

where $\Gamma_B/2\pi$ is a FWHM bandwidth of Brillouin gain, n_{fg} is the group index of the fiber mode and $\delta\omega$ is the frequency detuning between the Stokes pulse (Ω_s) and the line center of the SBS gain bandwidth ($\Omega_p - \Omega_B$). The SBS-induced group index change ($n_g - n_{fg}$) depends on the fiber type and the pump power. Assuming 1 mW pump power, the group-index change in the proposed CS_2-filled fiber is 1.9 while it is equal to 3.4×10^{-4} in the standard SMF-28-e fiber. In order to achieve the maximum delay, the frequency difference between the pump and Stokes waves is set to the Brillouin shift of the fiber ($\delta\omega = 0$). For CS_2, $\Gamma_B/2\pi = 52.3MHz$ at 694nm and it is proportional to ω^2 [21]. Thus, we can estimate $\Gamma_B/2\pi = 21MHz$ at 1550nm. Assuming P_{pump}=25mW, we obtain a group index of 49.3 which approximately corresponds to the group velocity of $c/50$. Comparing this with the group velocity of $c/10$ in BiO_2 fiber, which is reported in [8], we can achieve 5 times greater delay in the proposed PCF at a lower pump power and shorter length of the fiber. As we can see from Table 2, FOM in the proposed fiber has improved significantly as compared with the standard silica fibers or non-standard nonlinear glasses. The FOM of the proposed fiber is about 750 times greater than that of the conventional silica fibers and about 7 times larger than

that in the As_2S_3 fiber considered in [5]. The main reasons for these improvements are high SBS gain coefficient of CS_2, low effective area and relatively low loss of our proposed fiber. Our results also suggest that the proposed fiber reduces the power to fiber length ($P_{pump} \times L$) requirement for a given gain (delay) by nearly three orders of magnitude (830 times) relative to standard single mode fibers. Note that in our case, the pump power is only 25 mW and length of the fiber is only 1 m.

7.5 Conclusion

In this paper, slow light generation using stimulated Brillouin scattering (SBS) in a short highly nonlinear liquid-filled photonic crystal fiber (PCF) has been investigated. We studied optical properties of hollow-core PCFs, filled with highly nonlinear liquids such as nitrobenzene and carbon-disulfide. We proposed a design of carbon-disulfide-filled fiber with an effective area of $1.8\mu m^2$, nonlinear coefficient larger than 7300 $W^{-1}.Km^{-1}$, confinement loss of 0.007 dB/km and total loss lower than 0.3 dB/m over the C-band. Relative to standard single mode fibers, the proposed fiber reduces power$\times$ fiber length requirement for a given gain (delay) by nearly three orders of magnitude (830 times). Furthermore, using just a one-meter long fiber, we demonstrate that pulses can be slowed down to c/50 with a required power level of only 25mW. We show that our PCF is about 7 times more efficient than the previously reported fiber designs.

Bibliography

[1] T. Baba,Slow light in photonic crystals, Nature Photonics 2, 465-473, (2008).

[2] R. Pant, M. D. Stenner, M. A. Neifeld, and D. J. Gauthier, Optimal pump profile designs for broadband SBS slow-light systems, Opt. Express 16, 2764-2777, (2008).

[3] D. Dahan and G. Eisenstein, Tunable all optical delay via slow and fast light propagation in a Raman assisted fiber optical parametric amplifier: a route to all optical buffering, Opt. Express 13, 6234-6249, (2005).

[4] A. Zadok, A. Eyal, and M. Tur, Stimulated Brillouin scattering slow light in optical fibers [Invited], Appl. Opt. 50, E38-E49, (2011).

[5] K. Y. Song, K.S. Abedin, K. Hotate, M. Gonz?lez Herr?ez, and L. Thaivenaz, Highly efficient Brillouin slow and fast light using As2Se3 chalcogenide fiber, Opt. Express 14, 5860-5865, (2006).

[6] Y. Okawachi, M. S. Bigelow, J. E. Sharping, Z. Zhu, A. Schweinsberg, D. J. Gauthier, R. W. Boyd, and A. L. Gaeta, Tunable all-optical delays via Brillouin slow light in an optical fiber, Phys. Rev. Lett. 94, 153902, (2005).

[7] C. Jauregui Misas, P. Petropoulos, and D. J. Richardson, Slowing of pulses to c=10 with subwatt power levels and low latency using Brillouin amplification in a bismuth-oxide optical fiber, J. Lightwave Technol. 25, 216-V221, (2007).

[8] K. Y. Song, K. S. Abedin, and K. Hotate, Gain-assisted superluminal propagation in tellurite glass fiber based on stimulated Brillouin scattering, Opt. Express 16, 225-230, (2008).

[9] S. G. Yang, H. W. Chen, C. Y. Qiu, M. Chen, M. Chen, S. Xie, J. Li, and W. Chen, Slow-light delay enhancement in small-core pure silica photonic crystal fiber based on Brillouin scatter- ing, Opt. Lett. 33, 95-V97, (2008).

[10] Y. E. Monfared, A. Mojtahedinia, A. R. Maleki Javan and A. R. Monajati Kashani, Highly Nonlinear EnhancedcorePhotonic Crystal Fiber with Low Dispersion for Wavelength Conversion Based on Four-Wave Mixing, Front.Optoelectron. 6, 3, 297-302, (2013).

[11] S. Yiou, P. Delaye, A. Rouvie, J. Chinaud, R. Frey, G. Roosen, P. Viale, S. Faivrier, P. Roy, J. Auguste, and J. Blondy, Stimulated Raman scattering in an ethanol core microstructured optical fiber, Opt. Express 13, 4786-4791, (2005).

[12] F. M. Cox, A. Argyros, and M. C. J. Large, Liquid-filled hollow core microstructured polymer optical fiber, Opt. Express 14, 4135-4140, (2006).

[13] D. Churin, T.N. Nguyen, K. Kieu, R. A. Norwood, and N. Peyghambarian, Mid-IR supercontinuum generation in an integrated liquid-core optical fiber filled with CS2, Opt. Mater. Express 3, 1358-1364, (2013).

[14] O. D. Herrera, L. Schneebeli, K. Kieu, R. A. Norwood, and N. Peyghambarian, Slow light based on stimulated Raman scattering in an integrated liquid-core optical fiber filled with CS2, Opt. Express 21, 8821-8830, (2013).

[15] F. Poletti, A. Camerlingo, P. Petropoulos, D. J. Richardson, Dispersion Management in Highly Nonlinear, Carbon Disulfide Filled Holey Fibers, IEEE Photonics Technology Letters 20, 17, 1449-1451, (2008).

[16] P. Russell, Photonic-crystal fibers, J. Lightwave Technol. 24, 4729-V4749, (2006).

[17] K. Saitoh and M. Koshiba, Numerical Modeling of Photonic Crystal Fibers, J. Lightwave Technol. 23, 3580, (2005).

[18] H. Taniyama, H. Sumikura, and M. Notomi, Finite-Difference Time-Domain Analysis of Photonic Crystal Slab Cavities with Two-Level Systems, Opt. Express 19, 23067-23077, (2011).

[19] Optiwave Systems Inc., http://www.optiwave.com.

[20] T. Yang, E. Wang, H. Jiang, Z. Hu, and K. Xie, High birefringence photonic crystal fiber with high nonlinearity and low confinement loss, Opt. Express 23, 8329-8337, (2015).

[21] R. D. Boyd, Nonlinear Optics, Academic Press, (2003).

[22] Z. Zhu, D. J. Gauthier, Y. Okawachi, J. E. Sharping, A. L. Gaeta, R. W. Boyd, and Al. E. Willner, Numerical study of all-optical slow-light delays via stimulated Brillouin scattering in an optical fiber, J. Opt. Soc. Am. B 22, 2378-2384, (2005).

[23] V. I. Kovalev and R. G. Harrison, Threshold for stimulated Brillouin scattering in optical fiber, Opt. Express 15, 17625-17630, (2007).

[24] M. F. S. Ferreira, Nonlinear Effects in Optical Fibers, Wiley, (2011).

Chapter 8

Design of a dispersion-flattened highly nonlinear carbon-disulfide-filled photonic crystal fiber for broadband wavelength conversion based on four-wave mixing

Yashar E. Monfared and Sergey A. Ponomarenko

Part of this chapter is submitted to Optik - International Journal for Light and Electron Optics

8.1 Abstract

We present a theoretical study of widely tunable wavelength conversion based on four-wave mixing using a carbon-disulfide-filled photonic crystal fiber (CS_2-PCF). Considering the fabrication challenges and using realistic hole dimensions, we design a CS_2-PCF with nonlinear coefficient of 7740 $W^{-1}km^{-1}$, total loss lower than 0.3 dB/m, SBS threshold of more than 28 mW, nearly-zero dispersion of 0.00007 ps/(nm km) and a dispersion slope of 0.0000018 near 1550 nm. We further investigate the tolerance of the design to fabrication imperfections. A two-meter long CS_2-PCF is used as a nonlinear medium for an all-optical wavelength conversion. A 3-dB tunable wavelength conversion bandwidth is 108 nm and the conversion efficiency is about -10.6 dB when the pump power is only 14 dBm.

8.2 Introduction

Wavelength conversion is a promising candidate for providing wavelength flexibility in the high-capacity optical telecommunication systems [1]. Wavelength converters

perform functions such as wavelength routing and switching in the wavelength division multiplexing (WDM) systems [2]. Among all of the methods for all-optical wavelength conversion, four-wave mixing (FWM) is one of the most reliable techniques due to the ultra fast nonlinear medium response and high transparency to bit rate and modulation format [3]. In conventional setups, a strong pump wave is combined with an incoming signal wave and the combined wave is launched into a several kilometer long fiber, such that a desirable converted wave is generated by the FWM process [2-4].

In order to have tunability over a broad wavelength range, maintaining phase matching between the signal and pump is the main concern [5]. Due to group velocity dispersion (GVD), it is difficult to maintain phase matching in a long fiber, especially in a fiber with large GVD [2-5]. It should be mentioned that not only the amount of GVD, but also the slope of GVD curve is important for phase matching over a range of wavelengths [6]. For example, Inoue et al. reported a wavelength converter with only 7.6 nm bandwidth and conversion efficiency of -24 dB using a 10km-long conventional dispersion-shifted optical fiber with the dispersion slope of 0.07 ps/(nm^{2}km) [6]. The phase mismatch problem can even exists in a one-meter-long fiber with moderate dispersion [3]. One solution is to use highly nonlinear fibers as the nonlinear medium with nearly-zero flattened dispersion characteristics. In photonic crystal fibers (PCFs) [7], FWM can occur for low pump powers and over short propagation distances due to tight mode confinement and, as a consequence, high nonlinear coefficient of PCFs. Moreover, using a small dispersion slope in PCFs, wavelength conversion can be attained in a wide frequency range. Recently, PCFs with low effective area (in the order of $2\mu m^2$), high nonlinear coefficient (60.5-72 W^{-1}km^{-1}) and low dispersion (in the order of 0.3-0.7 ps/(nm km)) have been reported [5, 8].

Although these PCFs show promise for FWM applications, the amount of dispersion slope (0.002 ps/[nm^{2}km]) can still lead to phase mismatch. Using dispersion engineering techniques, we can further decrease dispersion slope and achieve an ultra-flattened dispersion in PCFs [9-16]. There is further room for increasing the nonlinear coefficient using non-silica fibers. Using bismuth-oxide PCF (Bi-PCF), Chow et al. [3]

obtained the nonlinear coefficient of 580 $W^{-1}km^{-1}$ at 1550 nm wavelength. The magnitude of nonlinear coefficient is about 100 times greater than that in silica fibers and 10 times greater than that in highly nonlinear silica-based PCFs. Chow et al. [3] obtained a 3-dB conversion bandwidth of 35nm with the conversion efficiency near -20dB using only a 1.09m dispersion-shifted Bi-PCF. By filling a core of a hollow core PCF with a highly nonlinear liquid, we can increase nonlinear coefficients and still benefit from tight mode confinement of PCFs. The technique to fill the hole of a hollow-core PCF with a liquid has already been taken into practice [17, 18]. Previous studies on liquid filled PCFs have shown that extremely high nonlinear coefficient magnitudes of the order of $2000-4000$ $W^{-1}km^{-1}$ can be achieved [17-19]. Poletti et al. [19] attempted to flatten the liquid-filled PCFs dispersive properties. They obtained an optimized carbon-disulfide-filled PCF (CS_2-PCF) with γ=6548 $W^{-1}km^{-1}$ and dispersion of 0.6 ps/(nm km) at 1550nm wavelength. However, the PCF structure proposed in [19] has a relatively large filling fraction which makes the fabrication process of the PCF difficult.

In our previous work on liquid-filled hollow-core PCFs [20], we demonstrated the possibility of design of a liquid-filled PCF with huge nonlinearity, moderate loss and high stimulated Brillouin scatterig (SBS) threshold. In this paper, we first design a highly nonlinear CS_2-PCF and show how the desired flat dispersion characteristics can be engineered. We then use the optimized PCF structure to design a wavelength converter based on FWM and obtain conversion efficiency and bandwidth.

8.3 Fiber design

PCFs are usually designed and fabricated with a solid pure silica core, surrounded by periodic air holes that serve as a cladding [7, 21]. The air holes make-up in the cladding region of the PCF leads to tailored optical properties, such as flattened dispersion and low confinement loss. Furthermore, one can adjust the PCF core area to control the fiber nonlinearity [21]. First, we use silica with the linear refractive index of n=1.446 at 1550nm as the cladding material for our proposed CS_2-PCF. Our proposed PCF has a hexagonal lattice with five rings of air holes, surrounding

a CS_2-filled-core in the center of the fiber. Therefore, the design parameters of the CS_2-PCF are the hole diameter d, hole pitch Λ, and core diameter D. The cross section of the proposed CS_2-PCF is shown in Fig. 8.1.

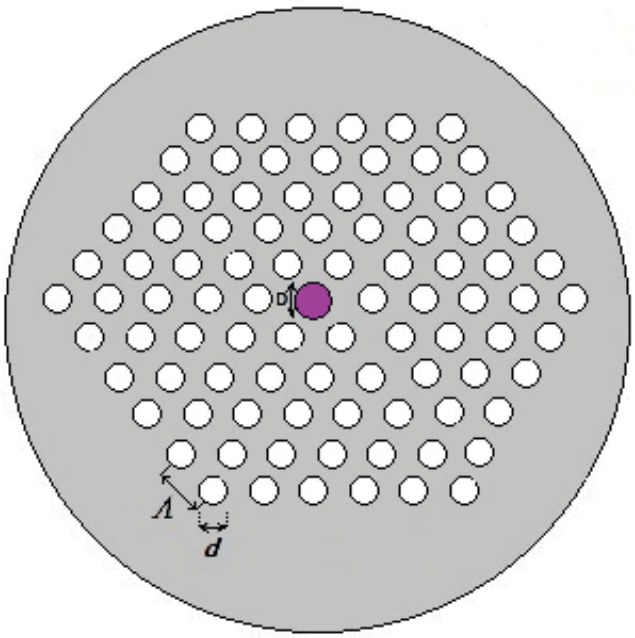

Figure 8.1: Cross section of the CS_2-PCF with holes dimension (d), holes pitch (Λ) and core diameter (D).

Our analysis is restricted to mode confinement through multiple total internal reflections (MTIR). Using a finite difference time domain (FDTD) analysis [21-23], we theoretically study the effective mode area, nonlinear coefficient and dispersion properties of the CS_2-PCFs. One of the most important characteristics of a highly nonlinear fiber is its nonlinear coefficient. The nonlinear coefficient γ is defined as [21-23]

$$\gamma = \frac{2\pi n_2}{\lambda A_{eff}}, \tag{8.1}$$

where n_2 is a nonlinear refractive index and A_{eff} is an effective area of the fundamental fiber mode, defined as [21-23]

$$A_{eff} = \frac{\int\int(|E|^2 dA)^2}{\int\int(|E|^4 dA)}. \tag{8.2}$$

Like any other broadening processes, FWM relies on the optical nonlinearities which

act on the femtosecond and picosecond scales. The fastest of such nonlinearities is a regular electronic Kerr-type nonlinearity. For certain materials, especially highly nonlinear liquids, reorientational nonlinearity comes into play [24-26]. The mechanism for this type of nonlinearity is a reorientation of the liquid molecules each of which having a significant dipole moment caused by an applied external electric field [24, 25]. Therefore this nonlinearity can be described as slow, since the modification of the refractive index depends not only on the intensity at the given moment but also on its past history [24, 25].

CS_2 exhibits a strong non-instantaneous third-order response, arising from motions of the molecules. In fact, the nonlinear optical response of CS_2 varies by more than 1 order of magnitude in pulsed experiments. Previous studies show that n_2 of CS_2 will dramatically increases as the pulse duration increases from 110 fs to 75 ns dramatically (from 3 $\times 10^{-15} cm^2/W$ to $4 \times 10^{-14} cm^2/W$) [24]. However, the effect of the reorientational nonlinearity remains small for short pulses (below 50 fs) since the response does not have sufficient time to accumulate [24, 25]. On the other hand, due to a high refractive index contrast between silica and air, the PCFs offer a much tighter mode confinement and thereby a lower effective mode area than do conventional optical fibers.

In our case, this index contrast is even higher due to a large refractive index of CS_2 (n_{CS_2}=1.59). The dependence of the nonlinear coefficient on the core diameter D is shown on in Fig. 8.2 for d/Λ=0.7 and Λ=1.2μm, as the core filling fraction D/Λ varies from 0.4 to 0.8 in steps of 0.2. It is obvious that by decreasing the core diameter, the nonlinear coefficient increases dramatically due to tight mode confinement in a reduced size core. Also, the value of nonlinear coefficient decreases gradually with the wavelength. The amount of confinement loss in the proposed fiber design for CS_2 is really low (in order of 10^{-3} dB/km). However, the total fiber loss will be likely dominated by absorption and scattering losses in the liquid. Fortunately, CS_2 boasts a nearly absorption free transmission spectrum in the spectral range extending from the visible to the midinfrared [19]. Therefore, we can expect overall loss lower than

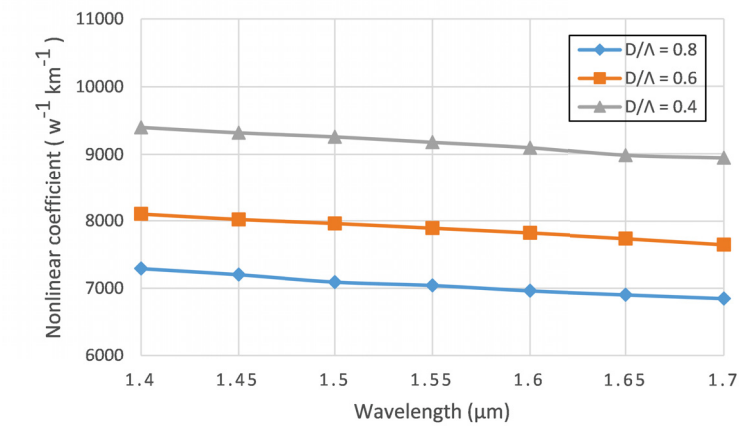

Figure 8.2: Nonlinear coefficient of the CS_2-PCF with d/Λ=0.7 and Λ=1.2μm and different core diameters as a function of wavelength.

0.3 dB/m for our CS_2-filled fiber [19, 20].

Fiber dispersion is another important parameter. The total dispersion is calculated as the sum of waveguide and material dispersion. In our calculations, the material dispersion, quantitatively described by Sellmeyer's formula, has been taken into account. Due to large material dispersion of CS_2, we should compensate material dispersion using waveguide dispersion of the PCF. The waveguide dispersion in PCFs can be easily controlled by varying the air hole diameter, shape, number and pitch. In our CS_2-PCF, we can control dispersion not only by adjusting the hole dimensions in the cladding, but also by adjusting core dimensions or changing the background material. In order to achieve large waveguide dispersion –with the opposite sign to material dispersion– we need to increase either the core size or air hole dimensions. There is a threshold for a filling fraction in the PCF design. Specifically, the fabrication of large filling fraction PCFs (d/Λ larger than 0.8) is known to be quite challenging because of potential fiber core or air hole deformations. If the d/Λ value is larger than 0.9 (filling fraction being larger than 90%), the fabrication of the PCF is almost impossible with the current fabrication technology. Thus, we should keep our d/Λ and D/Λ sufficiently small (no larger than 0.8). The GVD parameter of a fiber is usually calculated in terms of the dispersion parameter Di, defined as [5, 13]

$$Di = -\frac{\lambda}{c}\frac{d^2 n_{eff}}{d\lambda^2}. \tag{8.3}$$

The dispersion parameter Di and GVD parameter β_2 are related to each other as [13]

$$Di = -\frac{2\pi c}{\lambda^2}\beta_2. \tag{8.4}$$

In Fig. 8.3, we show dispersion as a function of the hole diameter d for different operation wavelengths, ranging from 1.4μm to 1.6μm in steps of 0.05μm. It can be

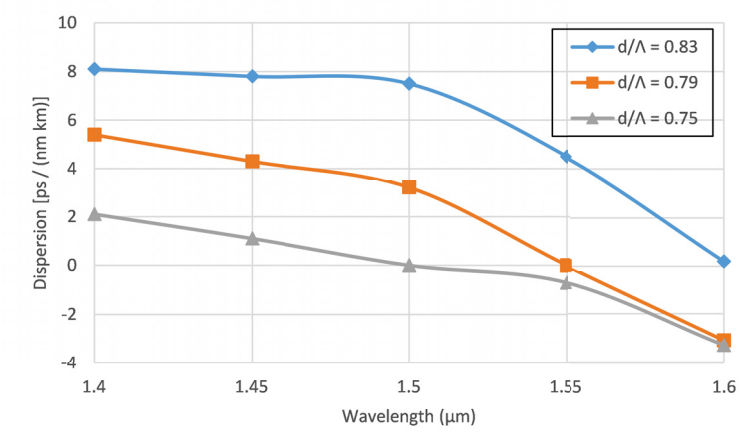

Figure 8.3: Dispersion of the liquid-filled PCF with fixed hole pitch Λ=1.2μm and D/Λ=0.8 as a function of the wavelength.

seen from Fig. 8.3 that the proposed PCF has a negative dispersion slope in the wavelength range around 1.55μm. Upon increasing the filling fraction from 0.75 to 0.83, the amount of dispersion increases and a zero dispersion wavelength (ZDW) of the fiber will shift slightly to the right. Next, fixing d/Λ=0.7 and Λ=1.2μm, while varying the core filling fraction D/Λ, we further analyze the dependence of dispersion on the wavelength. It is manifest in Fig. 8.4 that three dispersion curves have nearly the same shape in a spectral region around 1.55μm. In this neighbourhood, dispersion increases with D, as we vary D/Λ from 0.76 to 0.81. Moreover, dispersion decreases gradually with the wavelength over the telecommunication band. Thus, the core diameter adjustment can affect dispersion (mostly its magnitude) while the hole diameter controls both the dispersion magnitude and dispersion curve shape. We infer that liquid-filled PCF dispersion strongly depends on the core as well as hole diameters. We can find an optimized value for the near zero flattened dispersion curve but the problem is the magnitudes of d/Λ and D/Λ are relatively large (filling fraction is near 80%) which makes the fabrication process rather formidable. The proposed

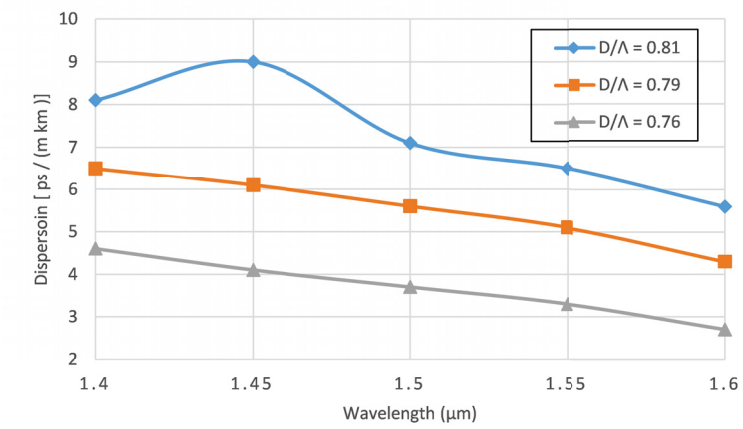

Figure 8.4: Dispersion of the liquid-filled PCF with d/Λ=0.7 and Λ=1.2μm as a function of wavelength.

CS_2-filled PCF of Poletti et al. [19] has a relatively large filling fraction as well (d/Λ=0.75 in one case and D/Λ=0.9 in the other case). To overcome the fabrication challenge, we propose to replace the background material with an optical soft glass. We inspected a range of commercial borosilicate glasses from Schott Company for this purpose [27]. We use BK10, BK7 and BAK2 which have the following linear refractive indices at 1550 nm: 1.482, 1.500 and 1.523 respectively [27]. We display the CS_2-filled soft-glass PCF dispersion analysis in the Fig. 8.5. Using BK10 soft glass we can achieve a nearly-zero ultra-flattened dispersion (ultra small dispersion slope or S_0) near 1550 nm wavelength. By optimized design of PCF with d/Λ=0.7, D/Λ=0.58 and Λ=1.2μm, we obtain ultra-flattened dispersion with a variation between ± 0.005 ps/(nm.km) over a 60 nm wavelengths range (1530-1590 nm). This dispersion is also easily adjustable by adjusting hole dimensions. We obtain γ=7740 , Di=7×10^{-5} ps/(nm km) and $S_0 = \partial Di/\partial\lambda$=1.8×$10^{-6}$ ps/(nm^{2}km) at 1550 nm. The proposed PCF with a high nonlinearity and low dispersion at 1550 nm will result in a wideband wavelength conversion. The conversion efficiency of FWM depends on the nonlinear coefficient, dispersion slope, loss and a fiber length. Table 1 summarizes the optical parameters of the proposed CS_2-PCF, Bi-PCF in [3] and common highly nonlinear silica fibers. We further study the tolerance of the design to variations in geometry due to fabrication imperfections. To this end, we investigate the change in dispersion curve as a function of wavelength when fiber filling fraction (d/Λ) is varied from 0.68 to 0.74 (which is a possible range of variation due to fabrication imperfections in

Table 8.1: Optical properties of different fibers near $\lambda = 1.55\mu$m for Wavelength conversion based on FWM.

Property	common HNLF	Bi-PCF[3]	CS_2-PCF
Di[ps/(nm km)]	1.7	-9.9	0.00007
α(dB/m)	0.2×10^{-3}	1.9	~0.3
n	1.44	2.02	1.59
A_{eff} (μm^2)	11	3.71	1.8
γ (W^{-1}km^{-1})	15.5	580	7740

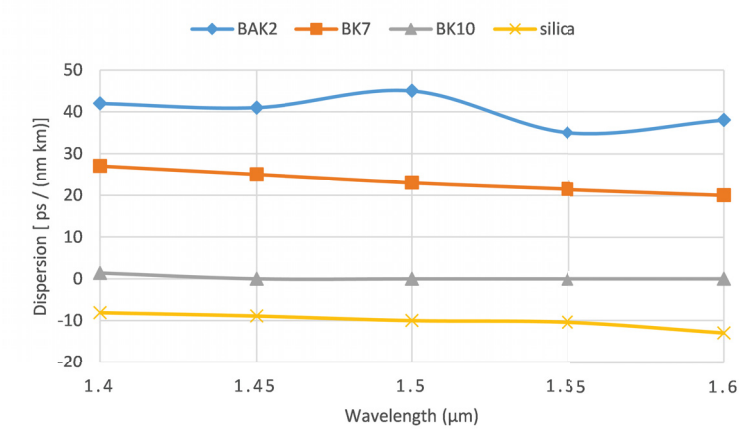

Figure 8.5: Dispersion of the liquid-filled hollow-core PCF with d/Λ=0.7, D/Λ=0.6 and Λ=1.2μm and different background materials as a function of wavelength.

fabrication process of PCFs). It can be seen from Fig. 8.6 that the small changes due to fabrication imperfections does not have a significant effect on the dispersion characteristics of the proposed PCF near 1.55 μm. It can be inferred from Fig. 8.6 that the proposed PCF has a good tolerance to variation in geometry due to fabrication imperfections. The reduction of stimulated Brillouin scattering (SBS) effects is one of the main concerns in wavelength conversion systems. To this end, we propose to increase the SBS pump power threshold in our fiber to suppress SBS-induced pump power loss. To do this, we first need to estimate the exponential gain threshold (G_{th}) of the fiber. For bulk media it has been shown that G_{th} is approximately constant [28]. For CS_2 bulk material, G_{th} is measured to be 22.8 at 1060nm [28]. In optical fibers, G_{th} depends on the experimental parameters such

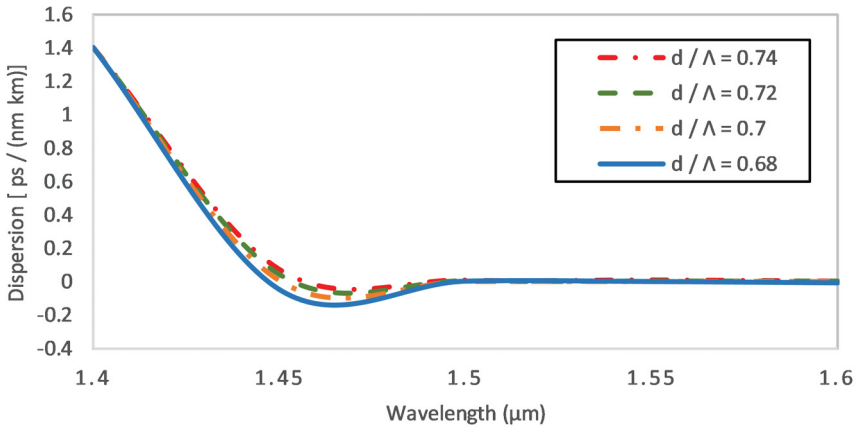

Figure 8.6: Dispersion of the liquid-filled hollow-core PCF with D/Λ=0.6 and Λ=1.2μm and different d/Λ, as a function of wavelength.

as input pulse, material, length and numerical aperture (NA) of the fiber [28, 29]. However, it can be shown that in a very short fiber with a moderate numerical aperture, G_{th} tends to its value in the bulk material [28]. In our case, we utilize a very short fiber with NA=0.5, thus we can expect G_{th} to be around 20-28, depending on the experimental parameters. Moreover, G_{th} is generally taken to be equal to 21 in optical fibers [28, 29]. Therefore, we may estimate the pump power threshold as [29]

$$P_{th} = \frac{G_{th} K_B A_{eff}}{g_B L_{eff}}, \tag{8.5}$$

where K_B is a constant depending on the polarization property of the fiber which is equal to 1 if the fiber is polarization maintaining and 1.5 otherwise [29] and L_{eff} is an effective fiber length, $L_{eff} = 1 - e^{\alpha L}/\alpha$. Considering G_{th}=21 and g_B=1.5 m/GW, we obtain P_{th}=27 mW for the proposed fiber.

8.4 Wavelength conversion

An ideal wavelength converter should be tunable over a broad wavelength range, have a high conversion efficientcy and the linewidth of the converted wave should be narrow [2, 3]. The conversion tunability of a wavelength converter is limited by the finite

phase mismatch $\Delta k = \beta_2 \Omega^2$ caused by the fiber GVD, where β_2 is the GVD parameter at the pump wavelength and Ω is the optical frequency shift between signal and pump waves [3]. The conversion range is limited by the Ω and dispersion slope of fiber S_0 [2]. Therefore, a smaller S_0 will result in a wider frequency range at which we can obtain efficient wavelength conversion [2]. The dispersion slope of the proposed CS_2-PCF is about 0.0000018 ps/(nm^{2}km). This dispersion slope is much smaller than that of the conventional dispersion shifted fiber, which is about 0.07 ps/(nm^{2}km). When β_2 is small, we must take into account the fourth-order term in the expansion of Δk since the odd terms (such as β_3) exactly cancel out due to opposite detuning [29]. Thus the finite phase mismatch parameter becomes $\Delta k = \beta_2 \Omega^2 + (\beta_4/12)\Omega^4$, where β_4 is the fourth order dispersion defined as $\beta_4 = d^4\beta/d\omega^4$ [29]. The conversion efficiency can be expressed as [3]:

$$\eta\left(L\right) = \left[\gamma P_{av} L \frac{sin(\Delta k L/2)}{\Delta k L/2}\right]^2, \tag{8.6}$$

where P_{av} is the path average pump power

$$P_{av} = \frac{P\left[1 - exp(-\alpha L)\right]}{\alpha L}. \tag{8.7}$$

Here α is the linear fiber loss rate and P is the input pump power. When the signal and pump wavelengths are close enough (near zero-dispersion wavelength) we can neglect the effect of phase mismatch and the peak conversion efficiency follow from Eq. (8.6):

$$\eta\left(L\right) = \left(\gamma P_{av} L\right)^2. \tag{8.8}$$

It follows from Eq. (8.8) that the peak conversion efficiency is calculated as -10.6 dB, which is consistent with our simulation results. The peak conversion efficiency in Ref [3] is -20.9 dB. In Ref [2], a -16 dB peak conversion efficiency is obtained when the pump power is as high as 22.5 dBm and the fiber length there was 20 m. Note that in our case, the pump power is only 14 dBm,the input signal power is 0 dBm and the fiber length is only 2 m. In our simulations, the signal wavelength is varied near the zero-dispersion wavelength in order to obtain a tunable converted wavelength while the pump wavelength is fixed. We can determine the conversion efficiency over a

given spectral range from Eq. (6). The conversion efficiency spectrum obtained from analytical calculations and also from simulation results using Optisystem commercial software [30] are shown in Fig. 8.7. Note that in our simulations we take the higher order dispersions into account. The wavelength of the converted signal can be varied from 1510 to 1618 nm by adjusting the signal wavelength accordingly. The conversion efficiency drops by 3 dB from its maximum value within 108 nm and thus, the 3 dB tunable bandwidth corresponds to about 108 nm. The usual bandwidth of HNLFs is about 8 nm [6]. The 3-dB bandwidth of the Bi-PCF in Ref [3] is 35 nm due to their dispersion engineered fiber design. In Ref [2], the authors used an ultra-flattened dispersion fiber with S_0=0.0004 ps/(nm^{2}km) which is larger than our design with S_0=0.0000018. Therefore, the 3-dB bandwidth of their fiber is about 100 nm [2] which is smaller than ours (108 nm). In the conventional optical fibers, the pump frequency spectrum is required to be broadened to increase the threshold of SBS. This broadening of pump source will result in broadened signals at the output which degrade the overall system performance. In our case, the SBS threshold of the proposed fiber is 27mW. Therefore, no stimulated Brillouin backscattering exists when the pump power is as high as 14 dBm (25mW). Thus, we have no need to use broadened pump sources or any other SBS suppression scheme. Emphasizing

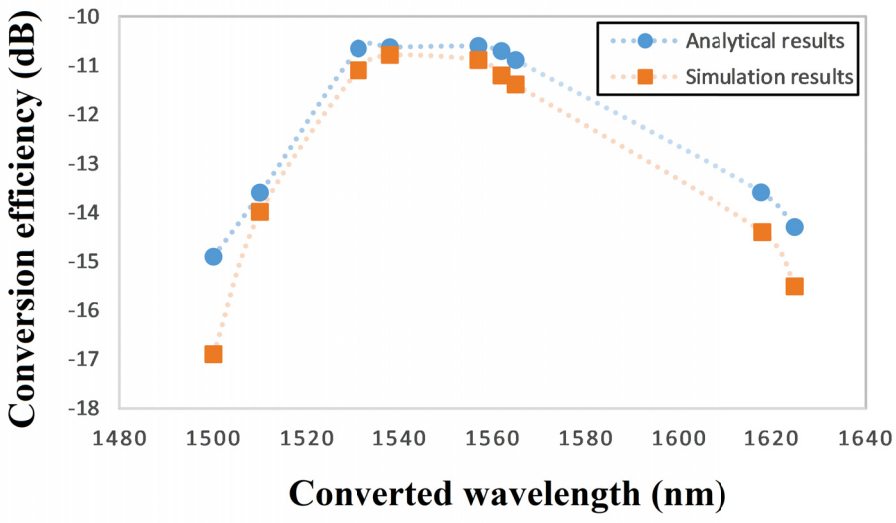

Figure 8.7: Conversion efficiency versus converted signal wavelength.

the potential of the proposed fiber design, it should also be noted that the ability to control the dispersion properties of the fibers makes it possible to design new fibers

with other phase matching properties. The freedom to move the ZDWs can be used to make the zones of high tunability coincide with available pump sources. Due to the fast response time of the fiber Kerr nonlinearity, it should be possible to use this wavelength converter at high speeds (bit rates) using ultra short pulses (below 50 fs)and an appropriate choice of pump power.

8.5 Conclusion

We have theoretically demonstrated widely tunable wavelength conversion based on four-wave mixing using a carbon-disulfide-filled photonic crystal fiber (CS-PCF). We designed a CS_2-PCF with a nonlinear coefficient of 7740 $W^{-1}km^{-1}$, nearly-zero dispersion of 0.00007 ps/(nm km) and a dispersion slope of 0.0000018 near 1550 nm. We show that the proposed PCF has a good tolerance to fabrication imperfections near 1550 nm. A 2-meter-long CS_2-PCF is used as the nonlinear medium for all-optical wavelength conversion with feasibility of high bit rates. A 3-dB tunable wavelength conversion bandwidth is about 108 nm and the conversion efficiency is about -10.6 dB when the pump power is only 14 dBm.

Bibliography

[1] C. Meuer, C. Schmidt-Langhorst, H. Schmeckebier, G. Fiol, D. Arsenijevic, C. Schubert, and D. Bimberg, "40 Gb/s wavelength conversion via four-wave mixing in a quantum-dot semiconductor optical amplifier," Opt. Express vol. 19, no. 4, pp. 3788-3798, 2011.

[2] A. Zhang and M. S. Demokan, "Broadband wavelength converter based on four-wave mixing in a highly nonlinear photonic crystal fiber," Opt. Lett. vol. 30, no. 18, pp. 2375-2377, 2005.

[3] K. K. Chow, K. Kikuchi, T. Nagashima,T. Hasegawa , S. Ohara, N. Sugimoto, "Four-wave mixing based widely tunable wavelength conversion using 1-m dispersion-shifted bismuth-oxide photonic crystal fiber," Opt. Express 15, no. 23, pp. 15418-15423, 2007.

[4] C. H. Kwok, S. H. Lee, K. K. Chow, C. Shu, C. Lin and A. Bjarklev, "Widely tunable wavelength conversion with extinction ratio enhancement using PCF-based NOLM," in IEEE Photonics Technology Letters, vol. 17, no. 12, pp. 2655-2657, 2005.

[5] Y. E. Monfared, A. Mojtahedinia, A. R. Maleki Javan and A. R. Monajati Kashani, "Highly Nonlinear Enhanced core Photonic Crystal Fiber with Low Dispersion for Wavelength Conversion Based on Four-Wave Mixing," Front. Optoelectron., vol. 6, no. 3, pp. 297-302, 2013.

[6] K. Inoue and H. Toba, "Wavelength conversion experiment using fiber four-wave mixing," IEEE Photon. Technol. Lett. vol. 4, no. 1, pp. 69-72, 1992.

[7] P. Russell, "Photonic-crystal fibers," J. Lightwave Technol., vol. 24, no. 12, pp. 4729-4749, 2006.

[8] Q. Xu, R. Miao, Y. Zhang, "Highly nonlinear low-dispersion photonic crystal fiber with high birefringence for four-wave mixing, Opt. Materials, vol. 35, no. 2, pp. 217-221, 2012.

[9] I. Abdelaziz, F. AbdelMalek, S. Haxha, H. Ademgil and H. Bouchriha, "Photonic Crystal Fiber With an Ultrahigh Birefringence and Flattened Dispersion by Using Genetic Algorithms," in Journal of Lightwave Technology, vol. 31, no. 2, pp. 343-348, 2013.

[10] D. Lu, X. Li, G. Zeng and J. Liu, "Dispersion Engineering in Single-Polarization Single-Mode Photonic Crystal Fibers for a Nearly Zero Flattened Profile," in IEEE Photonics Journal, vol. 9, no. 5, pp. 1-8, 2017.

[11] J. Liao, J. Sun, M. Du and Y. Qin, "Highly Nonlinear Dispersion-Flattened Slotted Spiral Photonic Crystal Fibers," in IEEE Photonics Technology Letters, vol. 26, no. 4, pp. 380-383, 2014.

[12] F. Shi, Y. Wu, M. Li, Y. Zhao and L. Zhao, "Highly Birefringent Two-Mode Photonic Crystal Fibers With Near-Zero Flattened Dispersion," in IEEE Photonics Journal, vol. 3, no. 6, pp. 1181-1188, 2011.

[13] J. Wang, C. Jiang, W. Hu, M. Gao, "Modified design of photonic crystal fibers with flattened dispersion," Opt. Laser Technol., vol. 38, no. 3, pp. 169172, 2006.

[14] R. R. Mahmud, M. A. G. Khan and S. M. A. Razzak, "Design and Comparison of SF57 Over SiO2 on Same Structured PCF for Residual Dispersion Compensation," in IEEE Photonics Journal, vol. 8, no. 6, pp. 1-10, 2016.

[15] M. I. Hasan, S. M. A. Razzak, G. K. M. Hasanuzzaman and M. S. Habib, "Ultra-Low Material Loss and Dispersion Flattened Fiber for THz Transmission," in IEEE Photonics Technology Letters, vol. 26, no. 23, pp. 2372-2375, 2014.

[16] M. E. Heidari, F. Dehghan, H. Saghaei, F. K. Kamali and M. M. Farshi, "Dispersion engineering of photonic crystal fibers by means of fluidic infiltration," J. Mod. Opt., 59, pp. 1384-1390, 2012.

[17] D. Churin, T.N. Nguyen, K. Kieu, R. A. Norwood, and N. Peyghambarian, "Mid-IR supercontinuum generation in an integrated liquid-core optical fiber filled with CS2," Opt. Mater. Express, vol. 3, no. 9, pp. 1358-1364, 2013.

[18] O. D. Herrera, L. Schneebeli, K. Kieu, R. A. Norwood, and N. Peyghambarian, "Slow light based on stimulated Raman scattering in an integrated liquid-core optical fiber filled with CS2," Opt. Express, vol. 21, no. 7, pp. 8821-8830, 2013.

[19] F. Poletti, A. Camerlingo, P. Petropoulos, D. J. Richardson, "Dispersion Management in Highly Nonlinear Carbon Disulfide Filled Holey Fibers," IEEE Photonics Technology Letters, vol.20, no.17, pp. 1449-1451, 2008.

[20] Y. E. Monfared and S. A. Ponomarenko, "Slow light generation in liquid-filled photonic crystal fibers via stimulated Brillouin scattering," Optik - Int. J. Light Electron Opt., vol. 127, no. 15, pp. 5800-5805, 2016.

[21] K. Saitoh and M. Koshiba, "Numerical Modeling of Photonic Crystal Fibers," J. Lightwave Technol., vol. 23, no. 11, pp. 3580, 2005.

[22] Z. Zhu and T. G. Brown, "Full-vectorial finite-difference analysis of microstructured optical fibers," Opt. Express, vol. 10, pp. 853-864, 2002.

[23] T. Yang, E. Wang, H. Jiang, Z. Hu, and K. Xie, "High birefringence photonic crystal fiber with high nonlinearity and low confinement loss," Opt. Express, vol. 23, pp. 8329-8337, 2015.

[24] R. A. Ganeev *et. al.*, "Nonlinear refraction in CS2," Appl. Phys. B, vol. 78, no. 3-4, pp. 433-438, 2004.

[25] M. Reichert *et. al.*, "Temporal, spectral, and polarization dependence of the nonlinear optical response of carbon disulfide," Optica, vol. 1, no. 6, pp. 436-445, 2014.

[26] R. V. J. Raja, A.Husakou, J. Hermann, and K. Porsezian, "Supercontinuum generation in liquid-filled photonic crystal fiber with slow nonlinear response," J. Opt. Soc. Am. B, vol. 27, no. 9, pp. 1763-1768, 2010.

[27] Schott company, http://www.schott.com.

[28] V. I. Kovalev, R. G. Harrison, "Threshold for stimulated Brillouin scattering in optical fiber," Opt. Express, vol. 15, no. 26, pp. 1762517630, 2007.

[29] M. F. S. Ferreira, "Nonlinear Effects in Optical Fibers," Wiley, 2011.

[30] Optiwave Systems Inc., http://www.optiwave.com.

Chapter 9

Discussion

9.1 Conclusions

In this thesis, our aim was to focus on the optical rogue wave (ORW) formation and nonlinear effects inside hollow-core photonic crystal fibers (HCPCFs). In the first several chapters, the effects of input pulse parameters such as coherence time, noise model and power on the dynamics of ORW were studied based on optical coherence theory. Moreover, analytical and numerical propagation methods were applied to explore evolutions of stochastic pulses in the vicinity of optical resonance in stimulated Raman scattering (SRS) inside a gas-filled PCF. In the subsequent chapters, we studied different design parameters of liquid-filled PCFs and showed the possibility of designing a highly nonlinear PCF for different nonlinear applications. Our studies on ORW and nonlinear effects are divided into five distinct phases. A general description of each project and its main results are given in the following.

Project 1: ORW formation in SRS in the case of noisy Stokes pulses inside HCPCF.

In this project, we have studied the role of coherence time and source noise in the formation of a long-tailed probability density function (PDF) as a signature of ORW. ORW formation in the noisy Stokes case is mainly affected by two factors: coherence time and pump power. Our main objective of this phase was to show that when the initial Stokes pulse is noisy and the pump pulse is fully coherent, the coherence time of Stokes pulses has a major role in formation of non-Gaussian statistics in the output. To study the impact of statistical properties of the source pulses on output upon propagation, three types of partially coherent pulses with different levels of coherence—fully coherent, partially coherent and nearly incoherent—were considered. We showed that in the case of a nearly incoherent source, the PDF has a longer tail

than in the partially coherent and fully coherent cases. PDF tail length dependence on the source coherence time can be justified using the concept of statistical granularity. If we have a nearly incoherent source, it means the number of uncorrelated modes or statistical granules is enormous. Therefore, the generated Stokes pulse is very noisy. The uncorrelated modes will compete for the energy supply from the pump. This will lead to selective amplification which causes the formation of ORWs.

Project 2: The formation of ORWs in near-resonance SRS with noisy pump pulses.

In this project, we have explored the role of coherence memory and source noise in the SRS process and also presented the differences between this case and noisy Stokes case. Gaussian Schell Model (GSM) pulses were employed as a generic model to simulate stochastic pulses at the source. We have demonstrated the crucial role that coherence memory plays in triggering heavy tailed statistics of the system in the situations when the input Stokes or pump pulses are noisy. However, the non-Gaussian statistics emergence has fundamentally different physical origins in the two cases. In our extensive simulations, we discovered that as the coherence memory increases, the probability of having an extreme value in the output increases dramatically. We also showed here that the non-Gaussian statistics and ORW excitation in SRS with noisy pump can be attributed to noise transfer from the pump to initially coherent Stokes pulses. We have developed the analytical theory of such noise transfer in the system in the initial stage of SRS, well described within the undepleted pump approximation (UPA). We also discussed the parameter regime in which the emergent extreme events can be quantitatively described under UPA.

Project 3: The formation of ORWs in self-similar regime of SRS with different source models.

In this project, we have demonstrated that RWs can be excited in a self-similar asymptotic regime of integrable turbulence and they appear as giant fluctuations away from the average (self-similar) evolution of the system. Although our results are based on numerical simulations of SRS in the transient regime, the conclusions are model independent; we can expect qualitatively similar findings in the TLA case. Indeed, the TLA and SRS in the integrable regime can be shown to be governed by the

same set of evolution equations with an appropriate choice of variables. Our results hold irrespective of a specific source correlation model, suggesting the universality of the proposed scenario.

Project 4: Liquid-filled PCFs and their nonlinear characteristics for slow light generation via stimulated Brillouin scattering (SBS).

In this project, slow light generation using stimulated Brillouin scattering (SBS) in a short highly nonlinear liquid-filled photonic crystal fiber (PCF) has been investigated. We designed a highly nonlinear carbon-disulfide-filled PCF with an effective area of 1.8 μm^2, nonlinear coefficient of more than 7700 $W^{-1}km^{-1}$ and a total loss lower than 0.3 dB/m over the C−band. Using the proposed PCF, we showed the possibility of slowing down group velocity of light to $c/50$ with a required power of only 25 mW via the SBS process. Relative to standard single mode fibers, the proposed fiber reduces a power × fiber length requirement for a given gain (delay) by nearly three orders of magnitude (830 times). We show that our PCF is about 7 times more efficient than the previously reported fiber designs.

Project 5: Possible dispersion engineering methods in a CS_2-PCF and wavelength conversion based on four-wave mixing (FWM).

In this project, we have analytically and numerically demonstrated widely tunable wavelength conversion based on four-wave mixing using a carbon-disulfide-filled photonic crystal fiber (CS-PCF). We designed a CS_2-PCF with a nonlinear coefficient of 7740 $W^{-1}km^{-1}$, nearly-zero dispersion of 0.00007 ps/(nm km) and a dispersion slope of 0.0000018 near 1550 nm. We have also showed that the proposed PCF has a good tolerance to fabrication imperfections near 1550 nm. A 2-meter-long CS_2-PCF is used as the nonlinear medium for all-optical wavelength conversion with a feasibility of high bit rates. A 3-dB tunable wavelength conversion bandwidth is about 108 nm and the conversion efficiency is about −10.6 dB when the pump power is only 14 dBm.

9.2 Future work

In this thesis, a comprehensive study of stochastic pulse propagation in SRS has been carried out with the aid of analytical and numerical methods to show the possibility of formation of ORWs. Furthermore, we show the possibility of designing highly nonlinear liquid-filled PCFs for different nonlinear applications, including slow light generation and wavelength conversion. The experimental tests of the our theoretical insights will be valuable as a future research step. Moreover, exploring alternative pulse propagation models such as backward propagation in SRS and also RW formation in TLA in the self-similar regime will be highly beneficial as future research directions.

Appendix A - Numerical Codes

Numerical codes for simulating propagation of noisy Stokes / noisy pump pulses in SRS:

```
%=====================================================
%Rogue waves formation in SRS inside a Gas-filled PCF
%=====================================================

%Initializing

clear
clc
tic
NN=0:100; %-- number of modes
IssV=0;
IPpV=0;

%constants

hbar=6.626e-34; %Planck constant
reff=1.55e-041; % Raman transition matrix element
epsilon0=8.854e-12;
C=3e+08; % speed of light in vaccum
np=1;
Aeff=30e-12; % Effective area of the PCF
Rs=354; %Raman shift of H2
wp1=2*pi*299.7e+12; %Pump wavelength
ws1=2*pi*2.6437e+14; %Stokes wavelength
Pen=100e-06; %Energy of the pump pulse
Wp=Pen;
k=1; %Hydrogen k
t0=10e-09; % pulse duration of pump and stokes
```

```
tp=t0;
ts=t0;
Gammarelax=5e-09; % Relaxation time of H_2
Nh2=1.82e+026; % Numbe density of H_2 molecule
Ps=100; % Stokes power = 100 W
Pp=Wp/tp
gammaPp=0.01*Pp;
Ws=0.1e-06; % Energy of Stokes pulse
Is00=Ps/Aeff;

%-----------------------------------------------

%time setup

dt=0.0025; %--time step
T=(-20:dt:20)';%(-5:dt:5)'; %-- dimensionless time vector
t=T;
nt=length(T)


%----------------------------------------

%Space setup

z=10;
nz=500;
dz=z/nz;   %--space step size
zz=0:dz:z; %-- dimensionless space vector
nplot=10;  %-- number of plots in Z
n1=round(nz/nplot)
%-----------------------------------------------
```

```
%Simulation parameters

L=1000; %--number of random realizations
zv=(0:nplot)*(z/nplot);
%----------------------------------------

%--initializing variables
Ut=zeros(length(t),length(zv));
Vt=zeros(length(t),length(zv));
Wt=zeros(length(t),length(zv));
Wwt=zeros(length(t),length(zv));
Gt=zeros(length(t),length(t),length(zv));
Asn=zeros(length(t),length(NN));


%----------------------------------------%
%Initial conditions
phi=((pi)*rand(L,length(NN)))-(pi/2); %-- random phase
   generation
%phi=((2*pi*rand(L,length(NN)))-pi); %-- random phase
   generation
%Is0av=Ps/(sqrt(pi)*Aeff); %<i_S0>
%Is0=exprnd(Is0av); % i_S0
ns=np;
Lsrs=(2*epsilon0*C)/(Nh2*reff*(sqrt(wp1*ws1))); % L_SRS
%As0n=sqrt((np*Is0)/(ns*Ip0)); % Amplitude of Stokes
T0=(reff*Pen)/(2*epsilon0*C*np*Aeff*hbar*sqrt(pi)); %-- T0
Tc=10*T0;
Tp=T0;
Ts=T0;
%Ap0=(exp((-T.^2)/(2*((T0).^2)))); % initial Pump pulse
```

```
%As0avgs=zeros(size(Ap0));
%Isavgs=zeros(size(Ap0));
As0const0=(np*Ps)/(ns*Pp)
As0const=sqrt(As0const0)
As0=(As0const.*(exp((-T.^2)/(2*((Ts).^2)))));
AREAs00=abs(sum(As0)*dt)
%figure (1)
%plot (T, As0)
%hold on
%fp=sqrt((1/(tp^2))+ (2/(tc^2)));
%fc=(tc*fp)/tp;
a=1/(2*Tp^2); %--modal weight coefficients
b=1/(2*Tc^2);
d=sqrt(a^2+2*a*b);
const2=gammaPp/Pp;
N=0:50;
H=hermx(t*(sqrt(2*d)),N);%--generating hermit function
for jn=1:length(NN)
    n=NN(jn);
lambda=(sqrt(pi)*Tp*const2)*((a+d)*(b^n))/((a+b+d)^(n+1))
   ;%-- modal weight generation
AAA=1; %-- initial pulse coefficient
Sai= AAA*(inv(sqrt((2^n)*(factorial(n)))))* ((2*d/pi)^0.25
    )*H(:,jn).*exp(-d*(t.^2));
%Depending on the source noise profile we can define
   different noises.
%Here as an example I just use a noise-free source.
Apn(:,jn)=0;
end
%----------------------------------------
% Monte Carlo method
for jL=1:L
```

```
jL
Ap0=zeros(length(t),1);
Apn;
phi;
for jN=1:length(NN)%-- generating the pump noisy pulses
Ap0=Ap0+(Apn(:,jN)*exp(1i*phi(jL,jN)));
end
Ap0=((Ap0))+((exp((-T.^2)/(2*((Tp).^2)))));
area_Ap0=abs(sum(Ap0)*dt);%-- pulse area at the source
Ip0=Pen/(sqrt(pi)*tp*Aeff) % I_P0
Tsrs=(2*hbar*epsilon0*C*np)/(reff*Ip0) % T_SRS
Trelative=t0/Tsrs;
Gammax=Tsrs*(1/Gammarelax); % Gamma = T_SRS * gamma^-1
%Gammax=0;
diffconst=(1/C)*(Lsrs/Tsrs);
%plot(T,As0)
%hold on
%title('Input Stokes Pulse')
%xlabel('T')
%ylabel('Amplitude')
%sigma0=zeros(length(t),1); % [ 0 0 0 0 ] zero matrix =
   sigma0
sigma=zeros(length(t),length(zv));%-- random pulse
Gamma=zeros(length(t),length(t),length(zv)); %-- mutual
   coherence
Ap=zeros(length(t),length(zv));
As=zeros(length(t),length(zv));
Ap1=zeros(length(t),length(zv));
As1=zeros(length(t),length(zv));
Is=zeros(length(t),length(zv));
derivAs=zeros(length(t),length(zv));
derivAp=zeros(length(t),length(zv));
```

```
Iz1=zeros(size(As(:,1)));
Iz10=zeros(size(As(:,10)));
%-- setting initial conditions
sigma0=0;
sigma(1,:)=sigma0;
Ap(:,1)=Ap0;
As(:,1)=As0;
%Gamma(:,:,1)=As0*(As0');
derivAp(:,1)=[diff(Ap0);0];
derivAs(:,1)=[diff(As0);0];
%blockf Function
y1=blc(sigma(:,1),Ap(:,1),zv,dz,dt,nt,Gammax,As(:,1),n1);
sigma(:,1)=y1(:,1);
%derivAp(1,:)=y1(:,3);
%derivAs(1,:)=y1(:,4);

%-- transmitting pulse realizations through SRS medium
for ii=1:nplot
    ii;
    y2=m4x(sigma(:,ii),zv,dz,Ap(:,ii),As(:,ii),n1,nt,dt,
       Gammax,derivAp(:,ii),derivAs(:,ii));
    sigma(:,ii+1)=y2(:,1);
    Ap(:,ii+1)=y2(:,2);
    As(:,ii+1)=y2(:,3);
    Gamma(:,:,ii+1)=As(:,ii+1)*(As(:,ii+1)');
end
%figure (2)
%plot(T,As(:,10))
%hold on
%title('Input Stokes Pulse')
%xlabel('T')
%ylabel('Amplitude')
```

```
%As0avgs=(As0avgs+As0);
Iss0=(As.^2);
Iss=abs(real(Iss0));
Iz1=Iz1+Iss(:,1);
Iz10=Iz10+Iss(:,10);
IPp=abs(Ap.^2);
IssV=(IssV+Iss);
IPpV=(IPpV+IPp);
%plot (T,100.*Iss(:,2),'color','r')
%hold on
%plot (T,IPp(:,2),'color','b')
%hold on
%figure (2) % plot input pump and stokes pulses over T
%areaas0=abs(sum(As0)*dt)
%plot (T,Iss(:,1), 'color','b')
%hold on
%plot(T, Iss(:,10), 'color','r')
%hold on
%plot(T,Ap(:,1), 'color','y')
%areas=abs(sum(As(:,10))*dt)
%plot (T,Iss(:,1), 'color', 'b')
%hold on
%plot(T,Iss(:,10))
%hold on
%plot (T,As(:,10))
%hold on
%plot(T,Iss(:,10),'color','r')
%hold on
%figure(2)
%subplot(2,1,1)
%hff=histogram(Iss(:,1),'Normalization','probability','
   facecolor','r','facealpha',0.2)
```

```
%hold on
%subplot(2,1,2)
%hff2=histogram(Iss(:,10),'Normalization','probability','
   facecolor','b','facealpha',0.2)
%hold on
%figure(2)
%subplot(2,1,1)
%hff=histogram(areaas0,'Normalization','probability','
   facecolor','r','facealpha',0.2)
%hold on
%subplot(2,1,2)
%hff2=histogram(areas,'Normalization','probability','
   facecolor','b','facealpha',0.2)
%hold on
end
%--performing ensemble averaging
%As0avgs=As0avgs.*(1/L);
%Iavg1=(1/L)*Iz1;
%Iavg10=(1/L)*Iz10;
%Iss=cdfplot(Iss0(800,:))
%pd=fitdist(Iss,'Normal');
%PDFIss=pdf(pd,zv)
%PDFIss=histogram(Iss)
%Fin=exppdf(Iss,2);
%---------------------------------
%y3=zeros(length(t),length(zv));
%for kji=1:length(zv)
%y3(:,kji) = pdf('Normal',zv,As)
%end
%Output%

%figure(3)
```

```
%plot(T,As0avgs)

%figure(4)
%subplot(2,1,1)
%plot(T,Asfavg)
Ivagh=Iss.*Ip0;
Pvagh=Ivagh.*Aeff;
Pnorm=Pvagh/100;

Ivpump=IPp.*Ip0;
Pvpump=Ivpump.*Aeff;
Ppumpnorm=Pvpump/100;

Pnorm2=10.*Pnorm;
Pnorm3=0.15.*Pnorm;
%plot (T,Pnorm(:,10))
%figure (1)
%plot(T,Iss(:,1))
%hold on
%plot (T,Pnorm2(:,1),T,Pnorm(:,10))
%hold on
IssA=IssV/L;
IPpA=IPpV/L;
%figure (1)
%subplot (2,1,1)
%plot (T,Pnorm(:,10),T,Pnorm(:,1))
%figure (2)
%subplot (2,1,2)
plot (T,IPp(:,10),T,Iss(:,10))
%figure (2)
%subplot (4,1,1)
%plot (T,IssA(:,1),'color','r')
```

```
%hold on
%plot (T,IPpA(:,1),'color','b')
%subplot (4,1,2)
%plot (T,IssA(:,3),'color','r')
%hold on
%plot (T,IPpA(:,3),'color','b')
%subplot (4,1,3)
%plot (T,IssA(:,5),'color','r')
%hold on
%plot (T,IPpA(:,5),'color','b')
%subplot (4,1,4)
%plot (T,IssA(:,10),'color','r')
%hold on
%plot (T,IPpA(:,10),'color','b')
%AREAp0=abs(sum(Ap0)*dt)
%AREAs0=abs(sum(As0)*dt)
AREAs=abs(sum(As(:,10))*dt)
AREAs=abs(sum(As(:,1))*dt)
%plot (T,Iss(:,10),T,IPp(:,10))
%hff=histogram(AREAs,'Normalization','probability','
   facecolor','r','facealpha',0.2)
%figure(2) %-- plot the pulse intensity over Z
%mesh(zv,T,abs(As), ...
 %    'MeshStyle', 'col', 'EdgeColor', 'black');
%set(gca,'YDir','reverse');
%hidden off;
%title('(a)','fontsize',24)
%xlabel ('Z','fontsize',20);
%ylabel('T','fontsize',20)
%zlabel ('Es(Z,T)','fontsize',20)
%figure (2)
%plot (T,10*Pnorm(:,1),T,1.2*Pnorm(:,10))
```

```
figure(3) %-- plot the pulse intensity over Z
mesh(zv,T,Pnorm, ...
    'MeshStyle', 'col', 'EdgeColor', 'black');
set(gca,'YDir','reverse');
hidden off;
%figure(4) %-- plot the pulse intensity over Z
%mesh(zv,T,Ppumpnorm, ...
 %   'MeshStyle', 'col', 'EdgeColor', 'black');
%set(gca,'YDir','reverse');
%hidden off;
%title('(a)','fontsize',24)
%xlabel ('z (m)','fontsize',20);
%ylabel('t (ns)','fontsize',20)
%zlabel ('P / <P>','fontsize',20)
%figure(1)
%hff=histogram(Iavg1,'Normalization','probability','
   facecolor','r','facealpha',1)
%hold on
%hff2=histogram(Iavg10,'Normalization','probability','
   facecolor','b','facealpha',0.3)
%hold on
%figure (7)
%plot (zv,max(Pnorm))

%============================
% Solving Maxwell equations
%============================

function y=m4x(sigma,zv,dz,Ap,As,n1,nt,dt,Gammax,derivAp,
   derivAs)
y=zeros(length(sigma),5);
nt=length(sigma);
```

```
r1=dz/1;
b1const=3.4e-03;
 for iz=1:n1
    dy1=(Ap)+(r1.*1i.*sigma.*As);
    dy2=(As)+(r1.*1i.*conj(sigma).*Ap);
    Ap=dy1;
    As=dy2;
    y1=blc(sigma,Ap,zv,dz,dt,nt,Gammax,As,n1);
    sigma=y1(:,1);


 end
y(:,1)=sigma;
y(:,2)=Ap;
y(:,3)=As;


%========================
%Solving Bloch equation
%========================

function y=blc(sigma,Ap,zv,dz,dt,nt,Gammax,As,n1)
y=zeros(length(sigma),1);
sigma(1)=0;
y(1,1)=sigma(1);


for i=1:nt-1 %-- numerical Runge Kutta method
          k1=diffx(sigma(i),Ap(i),As(i),Gammax);
          sigma1=sigma(i)+dt*k1/2;
          k2=diffx(sigma1,Ap(i),As(i),Gammax);
          sigma1=sigma(i)+dt*k2/2;
```

```
            k3=diffx(sigma1,Ap(i),As(i),Gammax);
            sigma1=sigma(i)+dt*k3;
            k4=diffx(sigma1,Ap(i),As(i),Gammax);
            nextstep=(dt*(k1+(2*k2)+(2*k3)+k4))/6;
            sigma(i+1)=sigma(i)+nextstep;



 end

y(:,1)=sigma;


%==========================================
%evaluating the Hermit function for each mode
%==========================================

function HH=hermx(t,N)

HH = zeros ( length(t), length(N) );

  HH(:,1) = 1.0; %--for N=0
  HH(:,2) = 2.0 *t; %--for N=1

  for jh = 2 : (length(N)-1)
    HH(:,jh+1) = 2.0 *t.* HH(:,jh) - 2.0 * ( jh - 1 ) * HH
       (:,jh-1);
  end
```

Appendix B - Statistical Ensemble Formulation for GSM and FBWN Sources

Gaussian correlated source

We first consider a pump source with a random component having an average Gaussian profile and Gaussian spectral correlations. This is the celebrated Gaussian Schell-model source that we employed in Ref. [1]. We briefly present it here for completeness. The corresponding mutual intensity, defined as

$$\Gamma(T_1, T_2, 0) \equiv \langle \Delta\mathcal{E}_p^*(T_1, 0)\Delta\mathcal{E}_p(T_2, 0)\rangle, \tag{1}$$

where the angle brackets denote ensemble averaging, can then be written as

$$\begin{aligned}\Gamma(T_1, T_2, 0) &= \left(\frac{\Delta P}{P_0}\right)\exp\left[-\frac{(T_1 - T_0)^2 + (T_2 - T_0)^2}{2T_*^2}\right] \\ &\quad \times \exp\left[-\frac{(T_1 - T_2)^2}{2T_c^2}\right].\end{aligned} \tag{2}$$

Here $\Delta P/P_0$ can be interpreted as a ratio of an average peak power of the random component to the coherent component peak power of the pump pulse at the source and T_c is a coherence time of the random component. It follows from Eq. (2) that the GSM source correlation spectrum is also Gaussian.

We can now represent the random component of the source using the Karhunen-Loève expansion [231, 120]

$$\Delta\mathcal{E}_p(T, 0) = 2^{-1/2}\left(\sum_n c_n\psi_n(T) + c.\ c.\right), \tag{3}$$

where c. c., stands for a complex conjugate. Note that Eq. (3) in this form guarantees that $\Delta\mathcal{E}_p(T, 0)$ is real which is the case for chirpless source pulses tuned to exact two-photon resonance to maximize the SRS efficiency. The random complex coefficients $\{c_n\}$ are statistically uncorrelated (orthogonal) such that

$$\langle c_n^* c_m\rangle = \lambda_n\delta_{mn}, \tag{4}$$

and the coherent modes are orthonormal, implying that

$$\int_{-\infty}^{\infty} dT\, \psi_n^*(T)\psi_m(T) = \delta_{mn}. \tag{5}$$

The mutual coherence function is then represented as a Mercer-type series in coherent modes as [232]

$$\Gamma(T_1, T_2, 0) = \sum_n \lambda_n \psi_n^*(T_1)\psi_n(T_2). \tag{6}$$

The coherent modes $\{\psi_n\}$ are determined by solving the following Fredholm integral equation

$$\int_{-\infty}^{\infty} dT_1\, \Gamma(T_1, T_2, 0)\psi_n(T_1) = \lambda_n \psi_n(T_2). \tag{7}$$

In the GSM case, Eq. (7) can be analytically solved and all modes and the eigenvalues $\{\lambda_n\}$ determined such that [232]

$$\psi_n(T) = \left(\frac{2\xi}{\pi}\right)^{1/4} \left(\frac{1}{2^n n!}\right)^{1/2} H_n[\sqrt{2\xi}(T - T_0)] e^{-\xi(T-T_0)^2}, \tag{8}$$

where $H_n(x)$ is a Hermite polynomial of the order n, and in our case,

$$\lambda_n = \sqrt{\pi} T_* \left(\frac{\Delta P}{P_0}\right) \frac{(\alpha + \xi)\beta^n}{(\alpha + \beta + \xi)^{n+1}}. \tag{9}$$

Here we introduced the notations

$$\alpha = \frac{1}{2T_*^2}, \quad \beta = \frac{1}{2T_c^2}, \tag{10}$$

and

$$\xi = \sqrt{\alpha^2 + 2\alpha\beta}. \tag{11}$$

We note that the mode powers, Eq. (9), are normalized so that they add up to the total power of the random component (relative to the coherent component power).

To complete the ensemble description, we must specify the random amplitude statistics to any order such that it is consistent with Eq. (4). We stipulate that the complex

amplitudes be independent Gaussian random variables. Expressing the complex random amplitudes $\{c_n\}$ in the polar form as

$$c_n = \sqrt{i_n} e^{i\phi_n}, \tag{12}$$

the powers i_n obey an exponential distribution,

$$\mathcal{P}(i_n) = \frac{1}{\lambda_n} e^{-i_n/\lambda_n}, \qquad i_n \geq 0, \tag{13}$$

and the phases are uniformly distributed in the interval $-\pi \leq \phi_n \leq \pi$. The overall field at the source is a superposition of uncorrelated mode fields. As each mode obeys Gaussian statistics, the overall source PDF is guaranteed to be Gaussian (thermal-like) for any source coherence time T_c. We stress that the central limit theorem alone is insufficient to guarantee Gaussian statistics because for sufficiently long T_c, there are only a few coherent modes effectively contributing to the expansion in Eq. (3) and the central limit theorem cannot be applied.

Band-limited white-light correlated source

We now consider a random component of the pulsed source that has uniform spectral correlations over a finite bandwidth B. We introduce the correlation time, $t_c = B^{-1}$. To construct the corresponding statistical ensemble, it will prove convenient to introduce the time and frequency scaled to the source coherence time t_c as

$$\bar{t} = t/t_c, \quad \overline{\omega} = \omega t_c. \tag{14}$$

Let us look at an auxiliary statistically stationary source, band-limited white light with a flat spectrum, $S(\overline{\omega}) \propto \mathrm{rect}(\overline{\omega})$. By virtue of the Wiener-Khintchine theorem [231], the source is *sinc*-correlated in time. Our pulsed source can be generated by amplitude modulating (time chopping) the band-limited white light. Assuming an optical modulator produces a pulse of intensity profile $I(\bar{t})$, we can express a field

realization of the resulting pulsed statistical source as

$$\Delta\mathcal{E}_p(\bar{t},0) = \sqrt{I(\bar{t})}U(\bar{t}). \tag{15}$$

Here the white light field $U(\bar{t})$ has the mutual intensity

$$\Gamma_U(\bar{t}_1 - \bar{t}_2) = \langle U^*(\bar{t}_1)U(\bar{t}_2)\rangle = \mathrm{sinc}(\bar{t}_1 - \bar{t}_2). \tag{16}$$

The mutual intensity of the pulse source can then be written as

$$\Gamma_{\Delta\mathcal{E}}(\bar{t}_1,\bar{t}_2,0) = \sqrt{I(\bar{t}_1)I(\bar{t}_2)}\Gamma_U(\bar{t}_1 - \bar{t}_2). \tag{17}$$

We note that the required amplitude modulation can be realized for nanosecond pulses of interest using the standard electro-optical modulators based on linear [6] or quadratic [7] electro-optical effects.

Unfortunately, it doesn't seem possible to analytically solve the Fredholm integral equation (7) for the mutual intensity $\Gamma_{\Delta\mathcal{E}}$ to explicitly determine coherent modes. We can however find non-orthogonal pseudo-modes. To this end, we use the following *sinc*-function representation [234]

$$\mathrm{sinc}(x-y) = \tfrac{\pi}{\sqrt{xy}} \textstyle\sum_{n=0}^{\infty}(n+1/2)J_{n+1/2}(x)J_{n+1/2}(y), \tag{18}$$

where $J_{n+1/2}(x)$ is a Bessel function of the first kind of a half-integer order. It follows from Eqs. (16) through (18) that the source mutual intensity can be expressed as

$$\Gamma_{\Delta\mathcal{E}}(\bar{t}_1,\bar{t}_2,0) = \sum_{n=0}^{\infty}(n+1/2)\Phi_n^*(\bar{t}_1)\Phi_n(\bar{t}_2), \tag{19}$$

where we introduced the mode functions

$$\Phi_n(x) = \sqrt{\pi I(x)/x}\, J_{n+1/2}(x). \tag{20}$$

These mode functions are neither orthogonal nor normalized, implying that the above

expansion is a pseudo-mode representation in the spirit of [235, 236]. One can introduce normalized pseudo-modes, though, viz.,

$$\Psi_n(\bar{t}) \equiv \sqrt{\mathcal{N}_n(\bar{t})I(\bar{t})/\bar{t}}\, J_{n+1/2}(\bar{t}), \tag{21}$$

so that

$$\int_0^\infty d\bar{t}\, |\Psi_n(\bar{t})|^2 = 1. \tag{22}$$

The normalization factor $\mathcal{N}_n$ is defined as

$$\mathcal{N}_n(\bar{t}) = \left[\int_0^\infty d\bar{t}\, J^2_{n+1/2}(\bar{t})I(\bar{t})/\bar{t}\right]^{-1}. \tag{23}$$

In terms of the normalized modes, the pseudo-mode representation reads

$$\Gamma_{\Delta\mathcal{E}}(\bar{t}_1, \bar{t}_2, 0) = \sum_{n=0}^{\infty} \lambda_n \Psi^*_n(\bar{t}_1)\Psi_n(\bar{t}_2), \tag{24}$$

where the physical eigenvalues, corresponding to the power carried by a given mode, can be expressed as

$$\lambda_n = \pi(n + 1/2) \int_0^\infty d\bar{t}\, J^2_{n+1/2}(\bar{t})I(\bar{t})/\bar{t}. \tag{25}$$

The sought ensemble representation, which yields Eq. (24) subject to (4), is then given by

$$\Delta\mathcal{E}_p(\bar{t}, 0) = 2^{-1/2}\left(\sum_n c_n \Psi_n(\bar{t}) + c.\ c.\right). \tag{26}$$

Finally, the random coefficients are governed by Eqs. (12) and (13) which completes the analytical description of the FBWN ensemble.

Bibliography

[1] Y. E. Monfared and S.A. Ponomarenko, Non-Gaussian statistics of extreme events in stimulated Raman scattering: The role of coherent memory and source noise, Phys. Rev. A, **96**, 043817 (2017).

[2] A. Papoulis, *Probability Random Variables, and Stochastic Processes* (McGraw Hill, New York, 1991) 3rd Ed.

[3] L. Mokhtarpour and S. A. Ponomarenko, Fluctuating pulse propagation in resonant nonlinear media: self-induced transparency random phase soliton formation, Opt. Express **23**, 30270 (2015).

[4] L. Mandel and E. Wolf, *Optical Coherence and Quantum Optics* (Cambridge University Press, Cambridge, 1995).

[5] S. A. Ponomarenko and E. Wolf, Universal structure of field correlations within a fluctuating medium, Phys. Rev. E., **65** , 016602 (2001).

[6] R. W. Boyd, *Nonlinear Optics,* (Academic Press, 2003), 2nd ed.

[7] M. Qasymeh, M. Cada and S. A. Ponomarenko, Quadratic Electro-Optic Kerr Effect: Applications to Photonic Devices, IEEE J. Quant. Electron., **44**, 740 (2008).

[8] A. P. Prudnikov, Yu. A. Brychkov, and O. I. Marichev, *Integrals and Series,* (Gordon, New York, 1992).

[9] S. A. Ponomarenko, Complex Gaussian representation of statistical pulses, Opt. Express, **19** 17086, (2011).

[10] S. Yang, S. A. Ponomarenko and Z. Chen, Coherent pseudo-mode decomposition of a new partially coherent source class, Opt. Lett., **40** 3081 (2015).

Appendix C - Copyright Permissions

[Feb 14, 2018]

Dear Optical Society of America,

I am preparing my PhD thesis for submission to the Faculty of Graduate Studies at Dalhousie University, Halifax, Nova Scotia, Canada. I am seeking your permission to include a manuscript version of the following paper as a chapter in the thesis:

Y. E. Monfared, and S. A. Ponomarenko, Non-Gaussian statistics and optical rogue waves in stimulated Raman scattering, Opt. Express 25, 5941-5950 (2017)

Canadian graduate theses are reproduced by the Library and Archives of Canada (formerly National Library of Canada) through a non-exclusive, world-wide license to reproduce, loan, distribute, or sell theses. I am also seeking your permission for the material described above to be reproduced and distributed by the LAC(NLC). Further details about the LAC(NLC) thesis program are available on the LAC(NLC) website (www.nlc-bnc.ca). Full publication details and a copy of this permission letter will be included in the thesis.

Yours sincerely, Yashar Esfahani Monfared

Dear Yashar Esfahani Monfared,

Thank you for contacting The Optical Society.

For the use of material from Yashar E. Monfared and Sergey A. Ponomarenko, Non-Gaussian statistics and optical rogue waves in stimulated Raman scattering, Opt. Express 25, 5941-5950 (2017):

As long as the copyrighted material is included within the body, section or chapter, of the thesis, and is not posted separate from the thesis, OSA considers your requested use of its copyrighted materials to be permissible within the author rights granted in

the Copyright Transfer Agreement submitted by the requester on acceptance for publication of his/her manuscript. If the entire article is being included, it is requested that the Author Accepted (or preprint) version be the version included within the thesis and that a complete citation of the original material be included in any publication. This permission assumes that the material was not reproduced from another source when published in the original publication.

The Author Accepted version is the preprint version of the article that was accepted for publication but not yet prepared and/or formatted by The Optical Society or its vendors.

While your publisher should be able to provide additional guidance, OSA prefers the below citation formats:

For citations in figure captions:

[Reprinted/Adapted] with permission from ref [x], [Publisher]. (with full citation in reference list)

For images without captions:

Journal Vol. first page (year published) An example: Opt. Express. 25, 5941 (2017)

Let me know if you have any questions.

Kind Regards,

Rebecca Robinson

Rebecca Robinson February 14, 2018 Authorized Agent, The Optical Society

---

The copyright statement for American physical society (APS) journals (*https* : *//journals.aps.org/c*

As the author of an APS-published article, may I include my article or a portion of my article in my thesis or dissertation?

Yes, the author has the right to use the article or a portion of the article in a thesis or dissertation without requesting permission from APS, provided the bibliographic citation and the APS copyright credit line are given on the appropriate pages.

Copyright for using a figure from one of the IEEE manuscripts.

Title: Fusion Splicing Photonic Crystal Fibers and Conventional Single-Mode Fibers: Microhole Collapse Effect

Author: Limin Xiao

Publication: Lightwave Technology, IEEE/OSA Journal of

Publisher: IEEE

Date: Nov. 2007

Copyright 2007, IEEE

Thesis / Dissertation Reuse

The IEEE does not require individuals working on a thesis to obtain a formal reuse license, however, you may print out this statement to be used as a permission grant:

Requirements to be followed when using any portion (e.g., figure, graph, table, or textual material) of an IEEE copyrighted paper in a thesis:

1) In the case of textual material (e.g., using short quotes or referring to the work within these papers) users must give full credit to the original source (author, paper, publication) followed by the IEEE copyright line 2011 IEEE. 2) In the case of illustrations or tabular material, we require that the copyright line [Year of original publication] IEEE appear prominently with each reprinted figure and/or table. 3) If a substantial portion of the original paper is to be used, and if you are not the senior author, also obtain the senior author's approval.

Requirements to be followed when using an entire IEEE copyrighted paper in a thesis:

1) The following IEEE copyright/ credit notice should be placed prominently in the references: [year of original publication] IEEE. Reprinted, with permission, from [author names, paper title, IEEE publication title, and month/year of publication] 2) Only the accepted version of an IEEE copyrighted paper can be used when posting the paper or your thesis on-line. 3) In placing the thesis on the author's university website, please display the following message in a prominent place on the website: In reference to IEEE copyrighted material which is used with permission in this thesis, the IEEE does not endorse any of [university/educational entity's name goes here]'s products or services. Internal or personal use of this material is permitted. If interested in reprinting/republishing IEEE copyrighted material for advertising or promotional purposes or for creating new collective works for resale or redistribution, please go to $http://www.ieee.org/publications_standards/publications/rights/rights_link.html$ to learn how to obtain a License from RightsLink.

If applicable, University Microfilms and/or ProQuest Library, or the Archives of Canada may supply single copies of the dissertation.

[Feb 14, 2018]

Dear Elsevier,

I am preparing my PhD thesis for submission to the Faculty of Graduate Studies at Dalhousie University, Halifax, Nova Scotia, Canada. I am seeking your permission to include a manuscript version of the following paper as a chapter in the thesis:

Y. E. Monfared and S. A. Ponomarenko, Slow light generation vis stimulated Brillouin scattering in liquid-filled photonic crystal fibers, Optik, 127, 5800 (2016).

Canadian graduate theses are reproduced by the Library and Archives of Canada (formerly National Library of Canada) through a non-exclusive, world-wide license to reproduce, loan, distribute, or sell theses. I am also seeking your permission for the material described above to be reproduced and distributed by the LAC(NLC). Further details about the LAC(NLC) thesis prog ram are available on the LAC(NLC)

website (www.nlc-bnc.ca). Full publication details and a copy of this permission letter will be included in the thesis.

Yours sincerely, Yashar Esfahani Monfared

Dear Yashar,

As an Elsevier journal author, you retain the right to Include the article in a thesis or dissertation (provided that this is not to be published commercially) whether in full or in part, subject to proper acknowledgment; see https://www.elsevier.com/about/our-business/policies/copyright/personal-use for more information. As this is a retained right, no written permission from Elsevier is necessary.

As outlined in our permissions licenses, this extends to the posting to your universitys digital repository of the thesis provided that if you include the published journal article (PJA) version, it is embedded in your thesis only and not separately downloadable:

19. Thesis/Dissertation: If your license is for use in a thesis/dissertation your thesis may be submitted to your institution in either print or electronic form. Should your thesis be published commercially, please reapply for permission. These requirements include permission for the Library and Archives of Canada to supply single copies, on demand, of the complete thesis and include permission for Proquest/UMI to supply single copies, on demand, of the complete thesis. Should your thesis be published commercially, please reapply for permission. Theses and dissertations which contain embedded PJAs as part of the formal submission can be posted publicly by the awarding institution with DOI links back to the formal publications on ScienceDirect.

Best of luck with your thesis and best regards,

Laura

Laura Stingelin Permissions Helpdesk Associate ELSEVIER — Global E-Operations Books +1 215-239-3867 office l.stingelin@elsevier.com Contact the Permissions Helpdesk +1 800-523-4069 x3808 — permissionshelpdesk@elsevier.com

Bibliography

[1] F. P. Schfer, F. P. W. Schmidt, and J. Volze, Organic dye solution laser, Appl. Phys. Lett. 9, 306309 (1966).

[2] M. Born and E. Wolf, Principles of Optics, 7th ed. (Cambridge University Press,1999).

[3] M. E. Fermann, A. Galvanauskas, and G. Sucha, Ultrafast Lasers. Technology and Applications, (Marcel Dekker, New York, 2003).

[4] L. Allen and J. H. Eberly, Optical Resonance and Two-level Atoms, (Dover Publications Inc., New York, 1975).

[5] A. Nazarkin, A. Abdolvand, A.V. Chugreev, and P. St.J. Russell, Direct Observation of Self-Similarity in Evolution of Transient Stimulated Raman Scattering in Gas-Filled Photonic Crystal Fibers, Phys. Rev. Lett. 105, 173902 (2010).

[6] P. Walczak, S. Randoux, and P. Surret, Optical Rogue Waves in Integrable Turbulence, Phys. Rev. Lett. 114, 143903 (2015).

[7] J. M.Dudley, F. Dias, M. Erkintalo and G. Genty, Instabilities, breathers, and rogue waves in optics, Nature Photon. 8, 755764 (2014).

[8] D. R. Solli, C. Ropers, P. Koonath and B. Jalali, Optical rogue waves, Nature (London) 450, 10541057 (2007).

[9] Yashar E. Monfared and Sergey A. Ponomarenko, Non-Gaussian statics and optical rogue waves in stimulated Raman scattering , Opt. Express 25, 5941-5950O, (2017).

[10] Yashar E. Monfared and Sergey A. Ponomarenko, Non-Gaussian statistics of extreme events in stimulated Raman scattering: The role of coherent memory and source noise, Phys. Rev. A, 96, 043817, (2017).

[11] Yashar E. Monfared and Sergey A. Ponomarenko, Rogue Waves, Self-similarity, Integrable Turbulence, Submitted to Phys. Rev. Lett., (2018).

[12] Yashar E. Monfared and Sergey A. Ponomarenko, Slow light generation in liquid-filled photonic crystal fibers via stimulated Brillouin scattering, Optik - Int. J. Light Electron Opt., 127 (15), pp. 5800-5805, (2016).

[13] Yashar E. Monfared and Sergey A. Ponomarenko, Design of a dispersion-flattened highly nonlinear carbon-disulfide-filled photonic crystal fiber for broadband wavelength conversion based on four-wave mixing, Submitted to Optik - Int. J. Light Electron Opt., (2018).

[14] F. P. Kapron, D. B. Keck and R. D. Maurer, Radiation losses in glass optical waveguides, Appl. Phys. Lett. 17, 423425 (1970).

[15] R. H. Stolen and A. Ashkin, Optical Kerr effect in glass waveguide, Appl. Phys. Lett. 22, 294296 (1973).

[16] S. Jiang, B. Bristiel, Y. Jaouen, P. Gallion, E. Pincemin, and S. Capouilliet, Full characterization of modern transmission fibers for Raman amplified-based communication systems, Opt. Express 15, 4883-4892 (2007).

[17] S. D. Dyer, M. G. Tanner, B. Baek, R. H. Hadfield, and S. . Nam, Analysis of a distributed fiber-optic temperature sensor using single-photon detectors, Opt. Express 20, 3456-3466 (2012).

[18] H. E Limodehi and F. Legare, Fiber optic humidity sensor using water vapor condensation, Opt. Express 25, 15313-15321 (2017).

[19] T. J. Muldoon, M. C. Pierce, D. L. Nida, M. D. Williams, A. Gillenwater, and R. Richards-Kortum, Subcellular-resolution molecular imaging within living tissue by fiber microendoscopy, Opt. Express 15, 16413-16423 (2007).

[20] Y. Wu, Y. Leng, J. Xi, and X. Li, Scanning all-fiber-optic endomicroscopy system for 3D nonlinear optical imaging of biological tissues, Opt. Express 17, 7907-7915 (2009).

[21] Y. Xu, L. Zhang, L. Chen, and X. Bao, Single-mode SOA-based 1kHz-linewidth dual-wavelength random fiber laser, Opt. Express 25, 15828-15837 (2017).

[22] N. M. Thang, Stimulated Raman Scattering in Gas Filled Hollow-Core Photonic Crystal Fibres, Max-Planck-Institut thesis, (2013).

[23] G. P. Agrawal, Nonlinear fiber optics: its history and recent progress [Invited], J. Opt. Soc. Am. B 28, A1-A10 (2011).

[24] P. Russell, Photonic-crystal fibers, J. Lightwave Technol, 24, 47294749, (2006).

[25] K. Saitoh, M. Koshiba, T. Hasegawa, and E. Sasaoka, Chromatic dispersion control in photonic crystal fibers: application to ultra-flattened dispersion, Opt. Express, 11, 843-852, (2003).

[26] R. Hubbard, Y. B. Ovchinnikov, J. Hayes, D. J. Richardson, Y. J. Fu, S.D. Lin, P. See, and A.G. Sinclair, Wide spectral range confocal microscope based on endlessly single-mode fiber, Opt. Express 18, 18811-18819 (2010).

[27] J. C. Knight and D. V. Skryabin, Nonlinear waveguide optics and photonic crystal fibers, Opt. Express 15, 15365-15376 (2007).

[28] F. Benabid, P. St. J. Russell, Hollow-core photonic crystal fibers: progress and prospects, Proc. SPIE, 5733, 5733-5733, (2005).

[29] R. Jamier, F. Gerome, G. Humbert, J. L. Auguste, J. M. Blondy and F. Benabid, Prospects on Hollow-core Photonic Crystal Fibers for unconventional fibered laser sources, 2011 13th International Conference on Transparent Optical Networks, Stockholm, 1-5, (2011).

[30] J. Kanka, Design of photonic crystal fibers with highly nonlinear glasses for four-wave-mixing based telecom applications, Opt. Express 16, 20395-20408 (2008).

[31] M. Koshiba and K. Saitoh, Structural dependence of effective area and mode field diameter for holey fibers, Opt. Express 11, 1746-1756 (2003).

[32] S. Yang, Y. Zhang, X. Peng, Y. Lu, S. Xie, J. Li, W. Chen, Z. Jiang, J. Peng, and H. Li, Theoretical study and experimental fabrication of high negative dispersion photonic crystal fiber with large area mode field, Opt. Express 14, 3015-3023 (2006).

[33] K. Saitoh and M. Koshiba, Empirical relations for simple design of photonic crystal fibers, Opt. Express 13, 267-274 (2005).

[34] J. Wang, C. Jiang, W. Hu, M. Gao, Modified design of photonic crystal fibers with flattened dispersion, Opt Laser Technol, 38, 169-172, (2006).

[35] M. F. Ferreira, Nonlinear effects in optical fibers, Wiley-OSA, US, (2011).

[36] F. Saltarelli, V. Kumar, D. Viola, F. Crisafi, F. Preda, G. Cerullo, and D. Polli, Broadband stimulated Raman scattering spectroscopy by a photonic time stretcher, Opt. Express 24, 21264-21275 (2016).

[37] A. G. Griffith, M. Yu, Y. Okawachi, J. Cardenas, A. Mohanty, A. L. Gaeta, and M. Lipson, Coherent mid-infrared frequency combs in silicon-microresonators in the presence of Raman effects, Opt. Express 24, 13044-13050 (2016).

[38] Y. Kida, T. Nagahara, S. Zaitsu, M. Matsuse, and T. Imasaka, Pulse compression based on coherent molecular motion induced by transient stimulated Raman scattering, Opt. Express 14, 3083-3092 (2006).

[39] S. Im, A. Husakou, and J. Herrmann, Guiding properties and dispersion control of kagome lattice hollow-core photonic crystal fibers, Opt. Express 17, 13050-13058 (2009).

[40] Y. Chen, Z. Wang, Z. Li, W. Huang, X. Xi, and Q. Lu, Ultra-efficient Raman amplifier in methane-filled hollow-core fiber operating at 1.5 m, Opt. Express 25, 20944-20949 (2017).

[41] C. Jauregui, J. Limpert, and A. Tunnermann, Derivation of Raman threshold formulas for CW double-clad fiber amplifiers, Opt. Express 17, 8476-8490 (2009).

[42] F. Benabid,G. Bouwmans, J. C. Knight, P. St. J. Russell,and F. Couny, Efficiency Laser Wavelength Conversion in a Gas-Filled Hollow Core Photonic Crystal Fiber by Pure Stimulated Rotational Raman Scattering in Molecular Hydrogen, Phys. Rev. Lett., 93, 12, 123903, (2004).

[43] F. Benabid, J. C. Knight, G. Antonopoulos, and P. St. J. Russell, Stimulated Raman Scattering in Hydrogen-Filled Hollow-Core Photonic Crystal Fiber, Science, 298, 5592, 399-402, (2002).

[44] W. Fu, F. Shu, Y. Zhang, C. Dong, C. Zou, and G. Guo, Integrated optical circulator by stimulated Brillouin scattering induced non-reciprocal phase shift, Opt. Express 23, 25118-25127 (2015).

[45] R. Pant, M. D. Stenner, M. A. Neifeld, and D. J. Gauthier, Optimal pump profile designs for broadband SBS slow-light systems, Opt. Express 16, 2764-2777 (2008).

[46] W. Gao, X. Hu, D. Sun, and J. Li, Simultaneous generation and Brillouin amplification of a dark hollow beam with a liquid-core optical fiber, Opt. Express 20, 20715-20720 (2012).

[47] A. Zadok, A. Eyal, and M. Tur, Stimulated Brillouin scattering slow light in optical fibers [Invited], Appl. Opt. 50, E38-E49 (2011).

[48] Y. Cao, P. Lu, Z. Yang, and W. Chen, An efficient method of all-optical buffering with ultra-small core photonic crystal fibers, Opt. Express 16, 14142-14150 (2008).

[49] L. Xing, L. Zhan, L. Yi, and Y. Xia, Storage capacity of slow-light tunable optical buffers based on fiber Brillouin amplifiers for real signal bit streams, Opt. Express 15, 10189-10195 (2007).

[50] R. Stolen, Phase-matched-stimulated four-photon mixing in silica-fiber waveguides, in IEEE Journal of Quantum Electronics, v11, 3, 100-103, (1975).

[51] R. Stolen and J. Bjorkholm, Parametric amplification and frequency conversion in optical fibers, in IEEE Journal of Quantum Electronics, 18, 7, 1062-1072, (1982).

[52] P. D. Rasmussen, J. Laesgaard, and O. Bang, Degenerate four wave mixing in solid core photonic bandgap fibers, Opt. Express 16, 4059-4068 (2008).

[53] A. Zhang and M. S. Demokan, Broadband wavelength converter based on four-wave mixing in a highly nonlinear photonic crystal fiber, Opt. Lett. 30, 2375-2377, (2005).

[54] K. K. Chow, K. Kikuchi, T. Nagashima, T. Hasegawa, S. Ohara, and N. Sugimoto, Four-wave mixing based widely tunable wavelength conversion using 1-m dispersion-shifted bismuth-oxide photonic crystal fiber, Opt. Express 15, 15418-15423 (2007).

[55] M. Ebnali-Heidari, C. Monat, C. Grillet, and M. K Moravvej-Farshi, A proposal for enhancing four-wave mixing in slow light engineered photonic crystal waveguides and its application to optical regeneration, Opt. Express 17, 18340-18353 (2009).

[56] J. M.Dudley, F. Dias, M. Erkintalo and G. Genty, Instabilities, breathers, and rogue waves in optics, Nature Photon. 8, 755764 (2014).

[57] C. Kharif, E. Pelinovsky, and A. Slunyaev, Rogue Waves in the Ocean, (Springer, Berlin, 2009).

[58] M. Onorato, S. Residori, U. Bertolozzo, A. Montina, and F. T. Arecchi, Rogue waves and their generating mechanisms in different physical contexts, Phys. Rep. 528, 47 (2013).

[59] K. Dysthe, H.E Krogstad and P. Muller, Oceanic rogue waves, Annu. Rev. Fluid Mech. 40, 287-310 (2008).

[60] A. Chabchoub, Tracking Breather Dynamics in Irregular Sea State Conditions, Phys. Rev. Lett., 117, 14, 144103, 2016.

[61] L. H. Holthuijsen, Waves in Oceanic and Coastal Waters, Cambridge University Press, 1st edition, UK, (2010).

[62] L. Cavaleri, L. Bertotti, L. Torrisi, E. Bitner-Gregersen, M. Serio, and M. Onorato, Rogue waves in crossing seas: The Louis Majesty accident, J. Geophys. Res., 117, C00J10, (2012).

[63] C. Kharif, and E. Pelinovsky, Physical mechanisms of the rogue wave phenomenon, Eur. J. Mech. B/Fluids 22, 603-634 (2003).

[64] N. Akhmediev, J. M. Dudley, D. R. Solli, and S. K. Turitsyn, Recent progress in invesitgating optical rogue waves, J. Opt. 15, 060201 (2013).

[65] N. Akhmediev, B. Kibler, F. Baronio, M. Belic, W-P Zhong, Y. Zhang, W. Chang, J. M. Soto-Crespo, P. Vouzas, P. Grelu, C. Lecaplain, K. Hammani, S. Rica, A. Picozzi, M. Tlidi, K. Panajotov, A. Mussot, A. Bendahmane, P. Szriftgiser, G. Genty, J. Dudley, A. Kudlinski, A. Demircan, U. Morgner, S. Amiranashvili, C. Bree, G. Steinmeyer, C. Masoller, N. G. R. Broderick, A. F. J. Runge, M. Erkintalo, S. Residori, U. Bortolozzo, F. T. Arecchi, S. Wabnitz, C. G. Tiofack, S. Coulibaly and M. Taki, Roadmap on optical rogue waves and extreme events, J. Opt. 18, 063001 (2016).

[66] A. I. Dyachenko and V. E. Zaklharov, Modulation instability of Stokes waves to freak wave, JETP Lett. 81, 255 (2005).

[67] V. E. Zakharov, A. I. Dyachenko, and A. O. Prokofiev, Freak waves as nonlinear stage of Stokes wave modulation instability, Eur. J. Mech. B 25, 677 (2006).

[68] S. Zhao, H. Yang, N. Chen and C. Zhao, Controlled generation of high-intensity optical rogue waves by induced modulation instability, Scientific Reports, 7, 39926, (2017).

[69] J. M. Dudley, G. Genty, G. and B. J. Eggleton, Harnessing and control of optical rogue waves in supercontinuum generation, Opt. Express, 16, 36443651 (2008).

[70] D. Buccoliero, H. Steffensen, H. Ebendorff-Heidepriem, T. M. Monro, O. Bang, Midinfrared optical rogue waves in soft glass photonic crystal fiber, Opt. Express 19, 1797317978 (2011).

[71] K. Hammani, B. Kibler, C. Finot, and A. Picozzi, Emergence of rogue waves from optical turbulence, Phys. Lett. A, 374, 35853589,(2010).

[72] A. Mathis, L. Froehly, S. Toenger, F. Dias, G. Genty and J. M. Dudley Caustics and rogue waves in an optical sea, Sci. Rep. 5, 12822 (2015).

[73] H. Yang, N. Chen, N., B. Wang, P. Tang, Q. Zeng, Supercontinuum and rogue soliton generation by induced modulation instability in photonic crystal fiber, Jour. of Mod. Opt. 63, 13701377 (2016).

[74] A. Montina, U. Bertolozzo, S. Residori, and F. T. Arecchi, Non-Gaussian statistics and extreme waves in a nonlinear optical cavity, Phys. Rev. Lett. 103, 173901 (2009).

[75] J.M. Soto-Crespo, Ph. Grelu and N. Akhmediev, Dissipative rogue waves: extreme pulses generated by passively mode-locked lasers, Phys. Rev. E 84, 016604 (2011).

[76] J. He, S. Xu and K. Porsezian, New types of rogue wave in an erbium-doped fiber system, J. Phys. Soc. Japan 81, 033002 (2012).

[77] R. Hohmann, U. Kuhl, H-J. Stockmann, L. Kaplan and E. J. Heller, Freak waves in the linear regime: a microwave study, Phys. Rev. Lett. 104, 093901 (2010).

[78] N. Akhmediev, V. Eleonskii, N. Kulagin, Exact first-order solutions of the nonlinear Schrdinger equation, Theoretical and Mathematical Physics, 72, 2, 809818, (1987).

[79] A. Chowdury, W. Krolikowski, and N. Akhmediev, Breather solutions of a fourth-order nonlinear Schrodinger equation in the degenerate, soliton, and rogue wave limits, Phys. Rev. E, 96, 4, 042209, (2017).

[80] P. Dubard, P. Gaillard, C. Klein, and V. B. Matveev, On multi-rogue wave solutions of the NLS equation and positon solutions of the KdV equation, Eur. Phys. J. Special Topics 185, 247-258 (2010).

[81] M. J. Ablowitz, D. J. Kaup, A. C. Newell, and H. Segur, Method for Solving the Sine-Gordon Equation, Phys. Rev. Lett., 30, 25, 1262-1264, (1973).

[82] N. Akhmediev, A. Ankiewicz, and M. Taki, Waves that appear from nowhere and disappear without a trace, Phys. Lett. A 373, 675-678 (2009).

[83] V. I. Shrira, and V. V. Geogjaev, What makes the Peregrine soliton so special as a prototype of freak waves? Journal of Engineering Mathematics, 67, 1, 11-22, (2010).

[84] S. Toenger, T. Godin, C. Billet, F. Dias, M. Erkintalo, G. Genty, G., and J. M. Dudley, Emergent rogue wave structures and statistics in spontaneous modulation instability, Scientific Reports, 5, 10380, (2015).

[85] H. Bailung, S. K. Sharma, and Y. Nakamura, Observation of Peregrine Solitons in a Multicomponent Plasma with Negative Ions, 107, 25, 255005, (2011).

[86] M. Eberhard, A. Savojardo, A. Maruta, and R. A. Rmer, Rogue wave generation by inelastic quasi-soliton collisions in optical fibres, Opt. Express 25, 28086-28099 (2017).

[87] L. Allen and J. H. Eberly, Optical resonance and two-level atoms, Dover Publications Inc., New York, (1975).

[88] Byoung S. Ham, Reversible quantum optical data storage based on resonant Raman optical field excited spin coherence, Opt. Express 16, 14304-14313 (2008).

[89] L. Mandel and E. Wolf, Optical Coherence and Quantum Optics, Cambridge University Press, (1995).

[90] J. W. Goodman , Statistical Optics, John Willy and Sons INC, (2000).

[91] J. M.Dudley, F. Dias, M. Erkintalo and G. Genty, Instabilities, breathers, and rogue waves in optics, Nature Photon., **8**, 755-764 (2014).

[92] A. Montina, U. Bertolozzo, S. Residori, and F. T. Arecchi, Non-Gaussian statistics and extreme waves in a nonlinear optical cavity, Phys. Rev. Lett., **103**, 173901 (2009).

[93] S. Residori, U. Bertolozzo, A. Montina, F. Lenzini and F. T. Arecchi, Rogue waves in spatially extended optical systems, Fluctuat. Noise Lett., **11**, 1240014 (2009).

[94] J.M. Soto-Crespo, Ph. Grelu and N. Akhmediev, Dissipative rogue waves: extreme pulses generated by passively mode-locked lasers, Phys. Rev. E, **84**, 016604, (2011).

[95] A. Zavyalov, O. Egorov, R. Iliew and F. Lederer, Rogue waves in mode-locked fiber lasers, Phys. Rev. A, **85**, 013828 (2012).

[96] A. F. J. Runge, N. G. R. Broderick, and M. Erkintalo, Observation of soliton explosions in a passively mode-locked fiber laser, Optica **2**, 36-39 (2015).

[97] J. He, S. Xu and K. Porsezian, New types of rogue wave in an erbium-doped fiber system, J. Phys. Soc. Japan, **81**, 033002 (2012).

[98] K. Hammani, C. Finot, J. M. Dudley and G. Millot, Optical rogue-wave-like extreme value fluctuations in fiber Raman amplifiers, Opt. Express **16**, 16467–16473 (2008).

[99] J. Kasparian, P. Béjot, J..-P. Wolf, and J. M. Dudley, Optical rogue wave statistics in laser filamentation, Opt. Express **17**, 12070-12075 (2009).

[100] D. Majus, V. Jukhna, G. Valiulis, D. Faccaio and A. Dubietis, Spatiotemporal rogue events in femtosecond filamentation, Phys. Rev A, **83**, 025802 (2011).

[101] K. Hammani, C. Finot and G. Millot, Emergence of extreme events in fiber-based parametric processes driven by a partially incoherent pump wave, Opt. Lett., **34**, 1138–1140 (2009).

[102] F. T. Arecchi, U. Bertolozzo, A. Montina and S. Residori, Granularity and inhomogeneity are joint generators of optical rogue waves, Phys. Rev. Lett., **106**, 153901 (2011).

[103] R. H ohmann, U. Kuhl, H-J. St ockmann, L. Kaplan and E. J. Heller, Freak waves in the linear regime: a microwave study, Phys. Rev. Lett., **104**, 093901 (2010).

[104] D. H. Peregine, "Water waves nonlinear Schr odinger equations and their solutions, J. Aust. Math. Soc. Ser. B, **25**, 16-43 (1983).

[105] N. Akhmediev, J. M. Soto-Crespo, and A. Ankiewicz, How to excite a rogue wave, Phys. Rev. A, **80**, 043818 (2009).

[106] V. I. Shrira and V. V. Geogjaev, What makes Peregrine soliton so special as a prototype of freak waves?, J. Eng. Math., **67**, 11-12 (2010).

[107] S. Toenger, T. Godin, C. Billet, F. Dias, M. Erkintalo, G. Genty, and J. M. Dudley, Emergent rogue wave structures and statistics in spontaneous modulation instability, Sci. Rep., **5**, 10380 (2015).

[108] B. Kibler, A. Chabchoub, A. Gelash, N. Akhmediev, and V. E. Zakharov, Superregular Breathers in Optics and Hydrodynamics: Omnipresent Modulation Instability beyond Simple Periodicity, Phys. Rev. X, **5**, 041026 (2015).

[109] B. Kibler, J. Fatome, C. Finot, G. Millot, F. Dias, G. Genty, N. Akhmediev, and J. M. Dudley, The Peregrine soliton in nonlinear fiber optics, Nat. Phys., **6**, 790-795 (2010).

[110] B. Kibler, J. Fatome, C. Finot, G. Millot, G. Genty, B. Wetzel, N. Akhmediev, F. Dias, and J. M. Dudley, Observation of Kuznetsov-Ma soliton dynamics in optical fiber, Sci. Rep., **2**, 463 (2012).

[111] A. Picozzi, J. Garnier, T. Hanson, P. Suret, S. Randoux, G. Millot, and D. N. Christodoulides,Optical wave turbulence: toward a unified thermodynamic formulation of statistical nonlinear optics, Phys. Rep. **542**, 1-132 (2014).

[112] P. Surret, R. El Koussaifi, A. Tikan, C. Evain, S. Randoux, C. Szwaj, and S. Bielawski, Single-shot observation of optical rogue waves in integrable turbulence using microscopy, Nat. Commun., **7**, 13136 (2016).

[113] J. M. Soto-Crespo, N. Devine, and N. Akhmediev, Integrable Turbulence and Rogue Waves: Breathers or Solitons? Phys. Rev. Lett., **116**, 103901 (2016).

[114] N. Akhmediev, J. M. Soto-Crespo, and N. Devine, Rogue waves, probability density functions and spectral features, Phys. Rev. E, **94**, 022212 (2016).

[115] D. Agafontsev and V. E. Zakharov, Integrable turbulence and formation of rogue waves, Nonlinearity, **28**, 2791 (2015).

[116] V. E. Zakharov, Turbulence in integrable systems, Stud. Appl. Math., **122**, 219-234 (2010).

[117] M. Taki, A. Mussot, A. Kudlinski, E. Louvergneaux, M. Kolobov, and M. Douay, Phys. Lett. A, "Third-order dispersion for generating optical solitons, **374**, 691-695 (2010).

[118] B. Kibler, K. Hammani, C. Michel, C. Finot, and A. Picozzi, Rogue waves, rational solitons and wave turbulence theory, Phys. Lett. A, **375**, 3149-3155 (2011).

[119] L. Allen and J. H. Eberly, *Optical resonance and two-level atoms,* (Dover Publications Inc., New York, 1975).

[120] L. Mokhtarpour and S. A. Ponomarenko, Fluctuating pulse propagation in resonant nonlinear media: self-induced transparency random phase soliton formation, Opt. Express **23**, 30270- 30282 (2015).

[121] A.Betlej, P. Schmitt, P. Sidereas, R. Tracy, C. G. Goedde, and J. R. Thompson, Increased Stokes pulse energy variation from amplified classical noise in a fiber Raman generator, Opt. Express, **13**, 2948–2960 (2005).

[122] E. Landahl, D. Baiocchi, and J. R. Thompson, A simple analytical model for noise shaping by an optical fiber generator, Opt. Commun., **150**, 339–347 (1998).

[123] A. S. Grabtchikov, A. I. Vodtchits, and V. A. Orlovich, Pulse-energy statistics in the linear regine of stimulated Raman scattering with a broad-band pump, Phys. Rev. A., **56**, 1666–1669 (1997).

[124] F. Benabid, G. Bouwmans, J. C. Knight, and P. St. J. Russell, Ultrahigh Efficiency Laser Wavelength Conversion in a Gas-Filled Hollow Core Photonic Crystal Fiber by Pure Stimulated Rotational Raman Scattering in Molecular Hydrogen, Phys. Rev. Lett. **93**, 123903 (2004).

[125] F. Belli, A. Abdolvand, W. Chang, J. C. Travers, and P. St.J. Russell, Vacuum-ultraviolet to infrared supercontinuum in hydrogen-filled photonic crystal fiber, Optica **2**, 292–300 (2015).

[126] F. Flora and L. Giudicotti, Complete calibration of a Thomson scattering spectrometer system by rotational Raman scattering in H_2, Appl. Opt. **26**, 4001–4008 (1987).

[127] L. Mandel and E. Wolf, *Optical Coherence and Quantum Optics* (Cambridge University Press, Cambridge, 1995).

[128] A. Papoulis, *Probability Random Variables, and Stochastic Processes* (McGraw Hill, New York, 1991) 3rd Ed.

[129] J. W. Goodman, *Statistical Optics* (Wiley, New York, 1985).

[130] M. Qasymeh, M. Cada and S. A. Ponomarenko, Quadratic Electro-Optical Kerr Effect: Application to Photonic Devices, IEEE J. Quant. Electron., **44**, 740–746 (2008).

[131] F. Y,. F. Chu and A. C. Scott, "Inverse scattering transform for wave-wave scattering, Phys. Rev. A, **12**, 2060–2064 (1975).

[132] C. R. Menyuk, Transient solitons in stimulated Raman scattering, Phys. Rev. Lett., **62**, 2937–2940 (1989).

[133] A.I. Dyachenko and V. E., Zaklharov, Modulation instability of Stokes waves $\Longrightarrow$ freak wave, JETP Lett., **81**, 255 (2005).

[134] C. Kharif, E. Pelinovsky, and A. Slunyaev, *Rogue waves in ocean* (Springer, 2009).

[135] M. Onorato, S. Residori, U. Bertolozzo, A. Montina and F. T. Arecchi, Rogue waves and their generating mechanisms in different physical contexts, Phys. Rep. **528**, 47 (2013).

[136] J. M.Dudley, F. Dias, M. Erkintalo and G. Genty, Instabilities, breathers, and rogue waves in optics, Nature Photon., **9**, 306 (2015).

[137]

[138] M. Erkintalo, G. Genty, and J. M. Dudley, Rogue-wave-like characteristics in femtosecond supercontinuum generation, Opt. Lett., **34** 2468 (2009).

[139] B. Kibler, C. Finot and J. M. Dudley, Soliton and rogue wave statistics in supercontinuum generation with two zero dispersion wavelengths, Eur. Phys. J., **173**, 289 (2009).

[140] A. Montina, U. Bertolozzo, S. Residori, and F. T. Arecchi, Non-Gaussian statistics and extreme waves in a nonlinear optical cavity, Phys. Rev. Lett., **103**, 173901 (2009).

[141] S. Residori, U. Bertolozzo, A. Montina, F. Lenzini and F. T. Arecchi, Rogue waves in spatially extended optical systems, Fluctuat. Noise Lett., **11**, 1240014 (2009).

[142] J.M. Soto-Crespo, Ph. Grelu and N. Akhmediev, Dissipative rogue waves: extreme pulses generated by passively mode-locked lasers, Phys. Rev. E, **84**, 016604, (2011).

[143] A. Zavyalov, O. Egorov, R. Iliew and F. Lederer, Rogue waves in mode-locked fiber lasers, Phys. Rev. A, **85**, 013828 (2012).

[144] A. F. J. Runge, N. G. R. Broderick, and M. Erkintalo, Observation of soliton explosions in a passively mode-locked fiber laser, Optica 2, 36 (2015).

[145] J. He, S. Xu and K. Porsezian, New types of rogue wave in an erbium-doped fiber system, J. Phys. Soc. Japan, **81**, 033002 (2012).

[146] K. Hammani, A. Picozzi, and C. Finot, Extreme statistics in Raman fiber amplifiers: From analytical description to experiments, Opt. Commun., **284**, 2594 (2011).

[147] J. Kasparian, P. Béjot, J..-P. Wolf, and J. M. Dudley, Optical rogue wave statistics in laser filamentation, Opt. Express **17**, 12070 (2009).

[148] D. Majus, V. Jukhna, G. Valiulis, D. Faccaio and A. Dubietis, Spatiotemporal rogue events in femtosecond filamentation, Phys. Rev A, **83** 2, (2011).

[149] P. M. Lushnikov and N. Vladimirova, Non-Gaussian statistics of multiple filamentation, Opt. Lett., **35**, 1965 (2010).

[150] F. T. Arecchi, U. Bertolozzo, A. Montina and S. Residori, Granularity and inhomogeneity are joint generators of optical rogue waves, Phys. Rev. Lett., **106**, 153901 (2011).

[151] A. Picozzi, J. Garnier, T. Hanson, P. Suret, S. Randoux, G. Millot, and D. N. Christodoulides, Optical wave turbulence: toward a unified thermodynamic formulation of statistical nonlinear optics, Phys. Rep. **542**, 1-132 (2014).

[152] S. Toenger, T. Godin, C. Billet, F. Dias, M. Erkintalo, G. Genty, and J. M. Dudley, Emergent rogue wave structures and statistics in spontaneous modulation instability, Sci. Rep., **5**, 10380 (2015).

[153] P. Surret, R. El Koussaifi, A. Tikan, C. Evain, S. Randoux, C. Szwaj, and S. Bielawski, Single-shot observation of optical rogue waves in integrable turbulence using microscopy, Nat. Commun., **7**, 13136 (2016).

[154] N. Akhmediev, J. M. Soto-Crespo, and N. Devine, Rogue waves, probability density functions and spectral features, Phys. Rev. E, **94**, 022212 (2016)

[155] F. Y,. F. Chu and A. C. Scott, Inverse scattering transform for wave-wave scattering, Phys. Rev. A, **12**, 2060 (1975).

[156] D. J. Kaup, Creation of a soluton out of dissipation, Physica D, **19**, 125 (1986).

[157] J. W. Goodman, *Statistical Optics* (Wiley, New York, 1985).

[158] F. Flora and L. Giudicotti, Complete calibration of a Thomson scattering spectrometer system by rotational Raman scattering in H_2, Appl. Opt. **26**, 4001 (1987).

[159] F. Benabid and P. J. Roberts, Linear and nonlinear properties of photonic crystal fibers, J. Mod. Opt., **58**, 87 (2011).

[160] M. G. Raymer and J. Mostowski, Stimulated Raman scattering: Unified theory of spontaneous initiation and spatial propagation, Phys. Rev. A, **24**, 1980 (1981).

[161] M. Qasymeh, M. Cada and S. A. Ponomarenko, Quadratic Electro-Optical Kerr Effect: Application to Photonic Devices, IEEE J. Quant. Electron., **44**, 740 (2008).

[162] A. Ablovind, A. Nazarkin, A.V. Chugreev, C. F. Kaminski, and P. St.J. Russell, Solitary Pulse Generation by Backward Raman Scattering in H_2-Filled Photonic Crystal Fibers, Phys. Rev.Lett., **103**, 183902 (2009).

[163] L. Mandel and E. Wolf, *Optical Coherence and Quantum Optics* (Cambridge University Press, Cambridge, 1995).

[164] M. H. Frosz, Validation of input-noise model for simulations of supercontinuum generation and rogue waves, Opt. Express, **18**, 14778 (2010).

[165] A. Papoulis, *Probability Random Variables, and Stochastic Processes* (McGraw Hill, New York, 1991) 3rd Ed.

[166] G.K.Batchelor, *The Theory of Homogeneous Turbulence,* (Cambridge University Press, Cambridge, 1986).

[167] M. Onorato, S. Residori, U. Bertolozzo, A. Montina and F. T. Arecchi, Rogue waves and their generating mechanisms in different physical contexts, Phys. Rep. **528**, 47 (2013).

[168] M. Shats and X. H. Punzmann, Capillary rogue waves, Phys. Rev. Lett., **104**, 104503 (2010).

[169] R. H ohmann U. Kuhl, H.-J.St ockmann, I. Kaplan and E. J. Heller, Freak waves in a linear regime: a microwave study, Phys. Rev. Lett., **104**, 093901 (2010).

[170] F. T. Arecchi, U. Bertolozzo, A. Montina and S. Residori, Granularity and inhomogeneity are joint generators of rogue waves, Phys. Rev. Lett., **106**, 153901 (2011).

[171] W.M. Moslem R. Sabry, S. K. El-Labany, and P. K. Shukla, Dust-acoustic rogue waves in nonextensive plasma, Phys. Rev. E, **84**, 066402 (2011).

[172] Y. Bludov, V. Konotop and N. Akhmediev, Matter rogue waves, Phys. Rev. A, **80**, 33610 (2009).

[173] M. Erkintalo, G. Genty and J. M. Dudley, Rogue-wave-like characteristics in supercontinuum generation, Opt. Lett., **34**, 2468 (2009).

[174] A. Montina U. Bertolozzo, S. Residori, and F. T. Arecchi, Non-Gaussian statistics and extreme waves in a nonlinear optical cavity, Phys. Rev. Lett., **103**, 173901 (2009).

[175] J.M. Soto-Crespo, Ph. Grelu, and N. Akhmediev, Dissipative rogue waves: extreme pulses generated by passively mode-locked lasers, Phys. Rev. E, **84**, 016604 (2011).

[176] A. F. J. Runge, N. G. R. Broederick, and M. Erkintalo, Observations of soliton explosions in a passively mode-locked fiber laser, Optica, **2**, 36 (2015).

[177] J. Kasparian, P. Béjot, J..-P. Wolf, and J. M. Dudley, Optical rogue wave statistics in laser filamentation, Opt. Express, **17**, 12070 (2009).

[178] A.Sauter, S.Pitsois, G. Millot, and A.Picozzi, Incoherent modulation instability in instantaneous nonlinear Kerr media, Opt. Lett., **30**, 2143 (2005).

[179] S.Toenger, T.Godin, C.Billet, F. Dias, M.Erkintalo, G.Genty, J.M. Dudley, Emergent rogue wave structures and statistics in spontaneous modulation instability, Sci. Rep., **5**, 10380 (2015).

[180] J.M. Soto-Crespo, N. Devine, and N. Akhmediev, Integrable Turbulence and Rogue Waves: Breathers or Solitons? Phys. Rev. Lett., **116**, 103901 (2016).

[181] P. Surret, R. El Koussaifi, A. Tikan, C. Evain, S. Randoux, C. Szwaj, and S. Bielawski, Single-shot observation of optical rogue waves in integrable turbulence using microscopy, Nat. Commun., **7**, 13136 (2016).

[182] L. Allen and J. H. Eberly, *Optical resonance and two-level atoms,* (Dover Publications Inc., New York, 1975).

[183] K. Sakai and A. Noguchi, Dark Soliton in Long and Short Wave Resonant Interaction, J. Phys. Soc. Jpn, **49**, 2009 (1980).

[184] G L.Lamb, Jr., *Elements of soliton theory* (Wiley, New York, 1976).

[185] F. Y,. F. Chu and A. C. Scott, Inverse scattering transform for wave-wave scattering, Phys. Rev. A, **12**, 2060 (1975).

[186] D. J. Kaup, Creation of a soluton out of dissipation, Physica D, **19**, 125 (1986).

[187] C. R. Menyuk, Transient solitons in stimulated Raman scattering, Phys. Rev. Lett., **62**, 2937–2940 (1989).

[188] J.N.Elgin and T.B.O'Hare, Saturation effects in transient stimulated Raman scattering, J. Phys. B, **12**, 159 (1979).

[189] C.R. Menyuk, D. Levi and P. Winternitz, Self-similarity in Transient Stimulated Raman Scattering, Phys. Rev. Lett., **69**, 3048 (1992).

[190] T. Baba,Slow light in photonic crystals, Nature Photonics 2, 465-473, (2008).

[191] R. Pant, M. D. Stenner, M. A. Neifeld, and D. J. Gauthier, Optimal pump profile designs for broadband SBS slow-light systems, Opt. Express 16, 2764-2777, (2008).

[192] D. Dahan and G. Eisenstein, Tunable all optical delay via slow and fast light propagation in a Raman assisted fiber optical parametric amplifier: a route to all optical buffering, Opt. Express 13, 6234-6249, (2005).

[193] A. Zadok, A. Eyal, and M. Tur, Stimulated Brillouin scattering slow light in optical fibers [Invited], Appl. Opt. 50, E38-E49, (2011).

[194] K. Y. Song, K.S. Abedin, K. Hotate, M. Gonz?lez Herr?ez, and L. Thaivenaz, Highly efficient Brillouin slow and fast light using As2Se3 chalcogenide fiber, Opt. Express 14, 5860-5865, (2006).

[195] Y. Okawachi, M. S. Bigelow, J. E. Sharping, Z. Zhu, A. Schweinsberg, D. J. Gauthier, R. W. Boyd, and A. L. Gaeta, Tunable all-optical delays via Brillouin slow light in an optical fiber, Phys. Rev. Lett. 94, 153902, (2005).

[196] C. Jauregui Misas, P. Petropoulos, and D. J. Richardson, Slowing of pulses to c=10 with subwatt power levels and low latency using Brillouin amplification in a bismuth-oxide optical fiber, J. Lightwave Technol. 25, 216-V221, (2007).

[197] K. Y. Song, K. S. Abedin, and K. Hotate, Gain-assisted superluminal propagation in tellurite glass fiber based on stimulated Brillouin scattering, Opt. Express 16, 225-230, (2008).

[198] S. G. Yang, H. W. Chen, C. Y. Qiu, M. Chen, M. Chen, S. Xie, J. Li, and W. Chen, Slow-light delay enhancement in small-core pure silica photonic crystal fiber based on Brillouin scatter- ing, Opt. Lett. 33, 95-V97, (2008).

[199] Y. E. Monfared, A. Mojtahedinia, A. R. Maleki Javan and A. R. Monajati Kashani, Highly Nonlinear EnhancedcorePhotonic Crystal Fiber with Low Dispersion for Wavelength Conversion Based on Four-Wave Mixing, Front.Optoelectron. 6, 3, 297-302, (2013).

[200] S. Yiou, P. Delaye, A. Rouvie, J. Chinaud, R. Frey, G. Roosen, P. Viale, S. Faivrier, P. Roy, J. Auguste, and J. Blondy, Stimulated Raman scattering in an ethanol core microstructured optical fiber, Opt. Express 13, 4786-4791, (2005).

[201] F. M. Cox, A. Argyros, and M. C. J. Large, Liquid-filled hollow core microstructured polymer optical fiber, Opt. Express 14, 4135-4140, (2006).

[202] D. Churin, T.N. Nguyen, K. Kieu, R. A. Norwood, and N. Peyghambarian, Mid-IR supercontinuum generation in an integrated liquid-core optical fiber filled with CS2, Opt. Mater. Express 3, 1358-1364, (2013).

[203] O. D. Herrera, L. Schneebeli, K. Kieu, R. A. Norwood, and N. Peyghambarian, Slow light based on stimulated Raman scattering in an integrated liquid-core optical fiber filled with CS2, Opt. Express 21, 8821-8830, (2013).

[204] F. Poletti, A. Camerlingo, P. Petropoulos, D. J. Richardson, Dispersion Management in Highly Nonlinear, Carbon Disulfide Filled Holey Fibers, IEEE Photonics Technology Letters 20, 17, 1449-1451, (2008).

[205] P. Russell, Photonic-crystal fibers, J. Lightwave Technol. 24, 4729-V4749, (2006).

[206] K. Saitoh and M. Koshiba, Numerical Modeling of Photonic Crystal Fibers, J. Lightwave Technol. 23, 3580, (2005).

[207] H. Taniyama, H. Sumikura, and M. Notomi, Finite-Difference Time-Domain Analysis of Photonic Crystal Slab Cavities with Two-Level Systems, Opt. Express 19, 23067-23077, (2011).

[208] T. Yang, E. Wang, H. Jiang, Z. Hu, and K. Xie, High birefringence photonic crystal fiber with high nonlinearity and low confinement loss, Opt. Express 23, 8329-8337, (2015).

[209] R. D. Boyd, Nonlinear Optics, Academic Press, (2003).

[210] Z. Zhu, D. J. Gauthier, Y. Okawachi, J. E. Sharping, A. L. Gaeta, R. W. Boyd, and Al. E. Willner, Numerical study of all-optical slow-light delays via stimulated Brillouin scattering in an optical fiber, J. Opt. Soc. Am. B 22, 2378-2384, (2005).

[211] V. I. Kovalev and R. G. Harrison, Threshold for stimulated Brillouin scattering in optical fiber, Opt. Express 15, 17625-17630, (2007).

[212] C. Meuer, C. Schmidt-Langhorst, H. Schmeckebier, G. Fiol, D. Arsenijevic, C. Schubert, and D. Bimberg, "40 Gb/s wavelength conversion via four-wave mixing in a quantum-dot semiconductor optical amplifier," Opt. Express vol. 19, no. 4, pp. 3788-3798, 2011.

[213] C. H. Kwok, S. H. Lee, K. K. Chow, C. Shu, C. Lin and A. Bjarklev, Widely tunable wavelength conversion with extinction ratio enhancement using PCF-based NOLM, in IEEE Photonics Technology Letters, vol. 17, no. 12, pp. 2655-2657, 2005.

[214] K. Inoue and H. Toba, Wavelength conversion experiment using fiber four-wave mixing, IEEE Photon. Technol. Lett. vol. 4, no. 1, pp. 69-72, 1992.

[215] Q. Xu, R. Miao, Y. Zhang, Highly nonlinear low-dispersion photonic crystal fiber with high birefringence for four-wave mixing, Opt. Materials, vol. 35, no. 2, pp. 217-221, 2012.

[216] I. Abdelaziz, F. AbdelMalek, S. Haxha, H. Ademgil and H. Bouchriha, Photonic Crystal Fiber With an Ultrahigh Birefringence and Flattened Dispersion by Using Genetic Algorithms, in Journal of Lightwave Technology, vol. 31, no. 2, pp. 343-348, 2013.

[217] D. Lu, X. Li, G. Zeng and J. Liu, Dispersion Engineering in Single-Polarization Single-Mode Photonic Crystal Fibers for a Nearly Zero Flattened Profile, in IEEE Photonics Journal, vol. 9, no. 5, pp. 1-8, 2017.

[218] J. Liao, J. Sun, M. Du and Y. Qin, Highly Nonlinear Dispersion-Flattened Slotted Spiral Photonic Crystal Fibers, in IEEE Photonics Technology Letters, vol. 26, no. 4, pp. 380-383, 2014.

[219] F. Shi, Y. Wu, M. Li, Y. Zhao and L. Zhao, Highly Birefringent Two-Mode Photonic Crystal Fibers With Near-Zero Flattened Dispersion, in IEEE Photonics Journal, vol. 3, no. 6, pp. 1181-1188, 2011.

[220] R. R. Mahmud, M. A. G. Khan and S. M. A. Razzak, Design and Comparison of SF57 Over SiO2 on Same Structured PCF for Residual Dispersion Compensation, in IEEE Photonics Journal, vol. 8, no. 6, pp. 1-10, 2016.

[221] M. I. Hasan, S. M. A. Razzak, G. K. M. Hasanuzzaman and M. S. Habib, Ultra-Low Material Loss and Dispersion Flattened Fiber for THz Transmission, in IEEE Photonics Technology Letters, vol. 26, no. 23, pp. 2372-2375, 2014.

[222] M. E. Heidari, F. Dehghan, H. Saghaei, F. K. Kamali and M. M. Farshi, Dispersion engineering of photonic crystal fibers by means of fluidic infiltration, J. Mod. Opt., 59, pp. 1384-1390, 2012.

[223] Z. Zhu and T. G. Brown, Full-vectorial finite-difference analysis of microstructured optical fibers, Opt. Express, vol. 10, pp. 853-864, 2002.

[224] T. Yang, E. Wang, H. Jiang, Z. Hu, and K. Xie, High birefringence photonic crystal fiber with high nonlinearity and low confinement loss, Opt. Express, vol. 23, pp. 8329-8337, 2015.

[225] R. A. Ganeev *et. al.*, Nonlinear refraction in CS2," Appl. Phys. B, vol. 78, no. 3-4, pp. 433-438, 2004.

[226] M. Reichert *et. al.*, Temporal, spectral, and polarization dependence of the nonlinear optical response of carbon disulfide, Optica, vol. 1, no. 6, pp. 436-445, 2014.

[227] R. V. J. Raja, A.Husakou, J. Hermann, and K. Porsezian, Supercontinuum generation in liquid-filled photonic crystal fiber with slow nonlinear response, J. Opt. Soc. Am. B, vol. 27, no. 9, pp. 1763-1768, 2010.

[228] Schott company, http://www.schott.com.

[229] V. I. Kovalev, R. G. Harrison, Threshold for stimulated Brillouin scattering in optical fiber, Opt. Express, vol. 15, no. 26, pp. 1762517630, 2007.

[230] Optiwave Systems Inc., http://www.optiwave.com.

[231] A. Papoulis, *Probability Random Variables, and Stochastic Processes* (McGraw Hill, New York, 1991) 3rd Ed.

[232] L. Mandel and E. Wolf, *Optical Coherence and Quantum Optics* (Cambridge University Press, Cambridge, 1995).

[233] S. A. Ponomarenko and E. Wolf, Universal structure of field correlations within a fluctuating medium, Phys. Rev. E., **65** , 016602 (2001).

[234] A. P. Prudnikov, Yu. A. Brychkov, and O. I. Marichev, *Integrals and Series,* (Gordon, New York, 1992).

[235] S. A. Ponomarenko, Complex Gaussian representation of statistical pulses, Opt. Express, **19** 17086, (2011).

[236] S. Yang, S. A. Ponomarenko and Z. Chen, Coherent pseudo-mode decomposition of a new partially coherent source class, Opt. Lett., **40** 3081 (2015).

[237] S. A. Ponomarenko and E. Wolf, The spectral degree of coherence of fully spatially coherent electromagnetic beams, Opt. Commun., 227, 73 (2003).

[238] S. A. Ponomarenko and E. Wolf, Correlations in an open quantum system and associated uncertainty relations, Phys. Rev. A, 63, 062106, (2001).

[239] S. A. Ponomarenko and G. P. Agrawal, Asymmetric incoherent vector solitons, Phys. Rev. E, 69, 036604 (2004).

[240] Y. Chen S. A. Ponomarenko, and Y. Cai, Experimental generation of optical coherence lattices, Appl. Phys. Lett., 109, 061107 (2016).